Identification and Characterization of MicroRNAs Modulating Cardiac Hypertrophy

Thesis

Identification and characterization of microRNAs modulating cardiac hypertrophy

Luca Braga

A Thesis submitted in fulfilment of the requirements of the Open University (UK) for the degree of Doctor of Philosophy

The Open University (UK)

International Centre for Genetic Engineering and Biotechnology (ICGEB), Trieste, Italy

Director of the studies: Prof. Mauro Giacca

External supervisor: Prof. Thierry Pedrazzini

Submitted May, 2017

TABLE OF CONTENTS

Acknowledgment

I'm really grateful to Prof. Mauro Giacca, for the opportunity to work in the Molecular Medicine group and for the great scientific support over the last years.

I thank Dr. Thierry Pedrazzini, my external supervisor, for all the fruitful discussions that we had.

I thank Dr. Miguel Mano and Dr. Ana Eulalio for sharing with me the data of the original screening and for the great technical and theoretical support.

I would like to thank Dr. Matteo Dal Ferro, for taking care of all the surgical experimental procedures; your contribution was fundamental.

I would like to thank Dr. Lorena Zentilin and Marina Dapas for the help in generating the AAV preparations.

I would like to thank Dr. Danilo Licastro for the bioinformatic analysis.

A special thanks goes to all the past and present colleagues at ICGEB. In particular, Rudy Ippodrino, Giulia de Sabbata, Nadja Ring, Alessandro Carrer, Giulia Ruozi, Silvia Moimas, Hashim Ali, Edoardo Schneider, Serena Zacchigna and Giulia Bortolussi.

I would like to thank ICGEB for the stimulating environment and the financial support.

Contributions

The HTS screening was performed at the HTS-Facility of ICGEB in collaboration with Miguel Mano, PhD and Ana Eulalio, PhD. All the surgical experimental procedures were carried out by Matteo dal Ferro, MD and mRNA seq data analysis was performed by Danilo Licastro, PhD. All the other experiments were performed by the candidate, Luca Braga.

ABBREVIATIONS

AAV	adeno associated virus
AC	adenylate cyclase
ADR	adrenalin
AJ	adherent junction
ANGII	angiotensin II
AT1	angiotensin receptor 1
BSA	bovine serum albumin
caPI3K	constitutively active phosphatidylinositol-3-kinases
CM	Cardiomyocytes
COPD	chronic obstructive pulmonary disease
CSA	cyclosporine A
CVD	cardiovascular disease
dHF	diastolic heart failure
ECM	extracellular matrix
EF	ejection fraction
ENDPR	end-diastolic pressure volume relationship
ET	endhotelin
FBS	foetal bovine serum
FN	fibronectin
GH	growth hormone
GJ	gap junction
GPCR G	protein coupled receptor
GSK3	glycogen synthase kinase-3
HAT	histone acetyl transferase
HDAC	histone deacetylase
HF	heart failure
HFpEF	heart failure with preserve ejection fraction
HFrEF	heart failure with reduced ejection fraction
HSPG	Heparan sulfate proteoglycan
ID	intercalated disc
Ig	immunoglobulin
IGF-1	insulin like growth factor 1
IGF1R	insulin like growth factor 1
LV	left ventricle
LVAW	left ventricular anterior wall
LVEF	left ventricular ejection fraction
LVID	left ventricular internal diameter
MAPK	mitogen-activated protein kinase
MC1	microRNA control 1 (cel-miR-67)
MC4	microRNA control 4 (cel-miR-231)

mRNA	messenger RNA
miRNA	microRNA
NE	Norepinephrine
NLS	nuclear localization signal
PAS	periodic acid-shiff
PBS	phosphate buffer saline
pDNA	plasmidic DNA
PE	Phenylephrine
PFA	paraformaldehyde
PI3K	phosphatidylinositol-3-kinases
PKA	protein kinase A
PKC	protein kinase C
PKD	protein kinase D
PLC	phospholipase C
PTX	pertussis toxin
rAAV	recombinant adeno associate virus
RISC RNA	induced silencing complex
sHF	systolic heart failure
TAC	thoracic aortic constriction
TRE	thyroid hormone response element
TRα1	thyroid hormone receptor alpha-1
β-AdR	beta adrenergic receptor
vPLA2	viral phospholipase A2
wt	wild type

ABSTRACT

The adult heart is capable of remodelling in response to different pathological stimuli; in most cases, a phase of compensated hypertrophy evolves into frank dysfunction and heart failure. To identify microRNAs able to prevent cardiac hypertrophy and preserve cardiac function, we performed a high-content microscopy, high-throughput functional screening for human microRNAs able to reduce neonatal cardiomyocyte (CM) cell size using a whole-genome microRNA library. The most effective anti-hypertrophic microRNA was hsa-miR-665. In a model of transverse abdominal aortic constriction (TAC) in 8 weeks old CD1 mice (n=14 per group), AAV9-mediated delivery of miR-665 showed remarkable capacity to protect against pathological cardiac hypertrophy and preserve function over time. This effect was observed when the vectors were delivered either before (LVEF at 60 day after TAC: 51.3% ±5.8% in treated vs 34.82% ±0.77% in controls; $P<0.005$) or after hypertrophy onset (LVEF at 60 days after TAC: 57.5%±5.60% in treated vs 28.4%±15% in controls; $P<0.001$). Global mRNA changes in hearts treated with miR-665 were evaluated by mRNA deep sequencing. All the 43 genes, for which siRNA were available, out of the 67 genes that were found to be significantly expressed ≤2 fold over control were individually down-regulated by specific siRNAs and tested for being direct miR-665 targets. This approach identified three sarcomeric proteins as direct mediators of miR-665 activity, namely Enah, Fhl1 and Xirp2, which are known to be involved in sarcomeric mechanotransduction and myofibrillar remodelling. In conclusion, miR-665 represents an important tool to decipher the molecular mechanisms of hypertrophy and offers a potential lead for the development of new biotherapeutics.

INTRODUCTION

1.1 The heart

The heart and its study has fascinated artists, philosophers and scientists since antiquity. Historians mutually agree that the start of modern cardiovascular medicine took place with the work of William Harvey and the discovery of blood circulation.

"The heart . . is the beginning of life; the sun of the microcosm . . for it is the heart by whose virtue and pulse the blood is moved, perfected, made apt to nourish, and is preserved from corruption and coagulation; it is the household divinity which, discharging its function, nourishes, cherishes, quickens the whole body, and is indeed the foundation of life, the source of all action." William Harvey, 1628.

Taber's Medical Dictionary defines the heart as a hollow, muscular organ that pumps blood through the circulatory system [1]. Blood is fundamental in providing the body with nutrients and oxygen whilst collecting and transporting metabolic waste from the periphery to kidneys and lungs where it is respectively filtered and oxygenated.

The heart is the first organ to form and function during embryogenesis in vertebrates [2]. In mammals and birds four chambers form the heart: upper left and right atria; and lower left and right ventricles [3]. The wall delimiting each chamber has a structure composed of three layers: an outer part called epicardium, the middle part called myocardium (the cardiac muscle) and the inner part called endocardium, which lines the chambers and covers the valves. The heart is then enclosed in the pericardium, a fibro-serous sac that surrounds the organ generating an anatomical structure called pericardial cavity, which contains serous fluid to prevent friction as the heart beats. [4] (**Figure 1**).

1.2 The cardiomyocyte

The contractile portion of the heart is the myocardium. It is mainly composed of cardiomyocytes (CMs), which are the building blocks of cardiac striated muscle. In light phase contrast microscopy, the shape of isolated adult CMs is rectangular and characterised by a typical cross-striated pattern [5]. Adjacent CMs are joined together at their extremities, on the longitudinal axis, by a complex structure termed as the intercalated disc (ID). IDs are composed mainly by three main structures: the desmosome, which functions as a cell anchor, the adherens junction (AJ), which provides cell strength, and the gap junction (GJ), which couples cells electrically and

metabolically. These structures closely connect the cytoskeleton of adjacent CMs and are fundamental for the proper cardiac function ensuring the fast propagation of the electrical signal that initiates contraction thus generating a coordinated mechanical syncytium [6]. The lateral membrane of CMs is characterized by different structures such as costamers and focal adhesions, which are responsible for linking sarcomeres to the extracellular matrix (ECM) [6] (**Figure 1**).

1.3 The sarcomere

The motor function of CMs is based on sarcomeres, which confer to the CM cytoplasm its characteristic cross-striated appearance. Sarcomeres can be defined as highly ordered arrays of myosin (thick) and actin (thin) filaments. The scaffold of these arrays is titin: a giant protein (1 mm length) mostly composed of immunoglobulin (Ig) and fibronectin-like (Fn) domains, which serves as a molecular ruler for sarcomere assembly; the phosphorylation state of specific domains of titin is responsible for the elasticity of cardiac muscle [7]. The N-terminus of titin is bound to the Z-disk, a complex protein structure that defines the sarcomere extremities [7]. Thin filaments, which are composed of actin, tropomyosin and troponin are also bound to the Z-disk. Another important protein that co-ocalizes within the Z-disk is α-actinin, which binds both titin and actin [5] .

Thick filaments are bipolar and they are joined together by myomesin in correspondence to the M-line [5]. They span along titin from the M-line towards the extremities of the sarcomere so defining the A-band, which corresponds to the entire length of a thick filament [7]. The region that surrounds the M-line is termed the H-zone and is characterized by the prevalence of thick filaments that are not superimposed by thin filaments [7]. In comparison, the I-band is the region that surrounds Z-lines and is characterized by the prevalence of thin filaments, which are not overlapped by thick filaments [7]. Cardiac muscle contraction relies on the possibility of thin filaments to slide on thick filaments, thus shortening muscle fibers. The frequency of subsequent cycles of contraction and relaxation is paced by the level of cytoplasmic calcium (Ca^{2+}), which interacts with the troponin/tropmoyosin complex inducing conformational changes that expose the myosin's binding site on actin filaments allowing the globular head of myosin to bind thin filaments [8]. During contraction, the myosin globular domain moves thin filaments towards the centre of the sarcomere. This sliding induces a conformational change that moves Z-lines together, thus shortening H- and I-bands whereas the A-band length remains unchanged [5] (**Figure 1**).

1.4 The problem

Despite recent advances in cardiovascular surgery and therapy, cardiovascular diseases (CVDs) are responsible of over 17 million deaths each year, corresponding to 31% of all deaths worldwide (http://www.who.int/cardiovascular_diseases/en/). The burden of CVD is no longer restricted to the high-income population, since 80% of these deaths occur in middle- and low-income countries. Since the adult heart is a dynamic organ, capable of significant remodelling in response to different extrinsic and intrinsic stimuli, the majority of the pathological stimuli first induce a phase of cardiac hypertrophy, which consists of the growth of the heart primarily through an increase in CM area [9]. The individual CM growth in length and/or width leads to an increase in cardiac pump function and a decrease in ventricular wall tension, initially leading to a state of compensated hypertrophy [10]. However, in the long term, myocardial hypertrophy often evolves in a form of decompensated hypertrophy, which predisposes individuals to heart failure, arrhythmia and sudden death [11, 12]. Therefore, cardiac hypertrophy and heart failure represent interesting targets for the development of novel biotherapeutics able to interfere with this processes.

1.5 Cardiac hypertrophy

During the foetal phases of heart development, CMs rapidly proliferate. However, immediately after birth proliferation stops, often after a final cycle of acytokinetic mytosis (karyokinesis without cytokinesis), which leaves a fraction of adult CMs binucleated [13]. Thus, the predominant form of heart postnatal growth is due to CM hypertrophy, a process that is mainly activated by the functional pressure overload that the heart walls are forced to face immediately after birth and is further stimulated by high levels of pro-hypertrophic circulating hormones, such as insulin-like growth factor-1 (IGF-1) and growth hormone (GH) [14]. The same happens to the mother's heart during pregnancy, and to the hearts of athletes as a result of extreme and/or repetitive exercise [15] [16]. In all the abovementioned cases, hypertrophy can be defined as physiological. Physiological hypertrophy is an adaptive process aimed at the decrease of the ventricular wall stress by increasing the thickness of ventricular wall. The phenotype of physiological hypertrophy is mild (≤10-20% of increase in total heart mass), coupled with a preserved or increased cardiac function, induces a net increase in ventricular angiogenesis and is reversible. At a morphological level, exercise-induced hypertrophy is typically not accompanied by an accumulation of collagen in the myocardium [17].

In contrast, pathological hypertrophy is generally induced by a prolonged wall stress caused by disorders such as systemic or pulmonary hypertension, myocardial infarction, coronary artery disease, genetic mutations, diabetic and metabolic cardiomyopathy, viral and bacterial myocarditis, valvular insufficiency and congenital heart defects. Pathological hypertrophy characteristically evokes a specific molecular signature, which is characterized by the re-activation of the so-called foetal cardiac gene program [17]. This program includes the induction of mRNAs for atrial natriuretic peptide (ANP), β-myosin-heavy-chain (βMHC), α-skeletal actin (sk-α actin) and brain natriuretic peptide (BNP). Moreover, genes encoding for calcium-handling proteins (Serca2a and Ryr) are usually down-regulated [17].

On the contrary, in models of physiological hypertrophy (exercised rats), this condition is characterized by increased expression of α-myosin-heavy-chain (αMHC) [18] and SERCA2a [19] and no reactivation of the foetal gene program. Furthermore, pathological hypertrophy triggers a metabolic transition in the heart from an oxidative toward a more glycolytic metabolism [20]. This metabolic switch in substrate utilization may be a protective response, improving the ratio between ATP production and oxygen consumption [20]. This scenario is reminiscent of what occurs during foetal cardiac development both in terms of metabolism and gene expression. At the morphological level, pathological heart hypertrophy, is typically associated with loss of myocytes and fibrotic replacement, cardiac dysfunction, and increased risk of heart failure and sudden death [11].

1.5.1 Concentric and eccentric cardiac hypertrophy

The mechanism by which cardiac hypertrophy can be considered adaptive follows the Laplace's law, which defines wall tension as an inverse function of wall thickness (tension = (pressure x radius)/(2 x wall thickness)). Cardiac hypertrophy can be classified as either eccentric or concentric, based on the geometry of the heart and the sarcomere's organization of individual CMs. Concentric hypertrophy refers to an increase in relative wall thickness and cardiac mass, with a small reduction or no change in chamber volume and is characterized by a parallel pattern of sarcomeres addition leading to an increase in myocyte cell width [11] (**Figure 2**). Conversely, eccentric hypertrophy consists in an increase in cardiac mass, depending on the addition of sarcomeres in series, with increased chamber volume and a wall thickness that may be normal, decreased, or increased [11].

Both phenotypes can develop as a consequence of physiological and pathological stimuli. For instance, a pathological stimulus causing pressure overload produces an increase in systolic wall stress, which results in concentric hypertrophy [11]. Conversely, a stimulus causing volume overload produces an increase in diastolic wall stress and results in eccentric hypertrophy [11](**Figure 2**). During pregnancy and in athletes used to prolonged aerobic exercise (also referred to as endurance training, isotonic or dynamic exercise e.g. long-distance running, swimming), the heart underwent to eccentric hypertrophy characterized by chamber enlargement and a proportional change in wall thickness, whilst eccentric hypertrophy in pathological conditions (myocardial infarction or dilated cardiomyopathy) is generally associated with thinning of the ventricular walls with preferential lengthening of CMs. Strength training (also referred to as isometric or static exercise, e.g. weight lifting, wrestling, throwing heavy objects) results in a pressure load on the heart rather than volume load and concentric hypertrophy [21] [11]. The heart can transition from a normal state to a state of physiological hypertrophy and back, although pathological hypertrophy that produces heart failure may be less reversible (**Figure 2**).

1.5.2 Molecular mechanisms of cardiac hypertrophy

Cardiac hypertrophy is primarily triggered at the CM level by a defined number of hypertrophic stimuli. Depending on the kind of stimulus, the transduced signals will converge on a specific subset of intracellular pathways that finally determine specific changes in gene expression. These changes in gene expression define the molecular signature of both physiological and pathological hypertrophy (The main pathways involved in either pathological an physiological hypertrophy are summarized in Figure 3).

1.5.2.1 Signalling pathways involved in pathological hypertrophy

1.5.2.1.1 G protein-coupled receptors

G protein-coupled receptors (GPCRs) play a pivotal role in the regulation of cardiac function and adaptation to changes in hemodynamic load. The most important myocardial GPCRs include adrenergic (α- and β-adrenergic) and muscarinic receptors. These receptors are respectively coupled with three main classes of hetero-trimeric GTP-binding proteins, Gs, Gαq/Gα11 and Gi, which are responsible for the transduction of agonist- or antagonist-induced signals [17]. It is important to underline that β-adrenergic receptors are homogenously expressed in all cardiac cell type (i.e. cardiac

smooth muscle cells and cardiac fibroblast) and in a cell-type dependent manner they exert distinct effects.

Gq/G11 signalling

Pathological stimuli such as pressure overload, hormones and vasoactive factors (angiotensin 2 (Ang II), endothelin 1 (ET-1) and phenylephrine (PE)) interacts with alpha adrenergic receptors and activates both Gαq/Gα11 and its downstream signalling proteins, including phospholipase C (PLC), MAPKs (Ras-MEKK-MEK-ERK1/2), protein kinase C (PKC), protein kinase A (PKA) and Ca^{2+}/calmodulin-dependent protein kinase [22]. It has been shown that in animal models harbouring a double heart specific knockout for Gαq/Gα11, the cardiac hypertrophic phenotype or activation of the foetal gene program in response to aortic banding is completely blunted [23], supporting the cardinal role of this pathway in the development of pressure overload-induced cardiac hypertrophy. Consequently, agonist stimulation of all these three receptors is sufficient to induce strong CM hypertrophy [24].

ANGII is the principal vasoactive peptide of the renin-angiotensin system. It exerts multiple pathophysiological effects in the cardiovascular system, at both endocrine and paracrine level, including vasoconstriction, aldosterone release and regulation of cell growth [25]. ANGII acts through two specific and different alpha adrenergic receptors, namely AT1 (two isoforms are present in rodents AT1A and AT1B) and AT2 [26]. Both receptors are expressed in the heart; nevertheless, only AT1 transgenic mice developed pathological hypertrophy and die prematurely of heart failure, whilst AT2 transgenic mice do not show any specific cardiac phenotype [27] [28]. Conversely, both cardiac specific AT1- and AT2- KO mice showed a blunted hypertrophic phenotype in pressure overload-induced hypertrophy. Furthermore, Zou et al. [29] have shown that AT1 receptors can sense and transduce mechanical stress even in absence of ANGII thus underlying the involvement of Gαq/Gα11 and MAPKs in mechanotransduction. In addition, it has been shown that both ANGII and Mechanical stretch activates PKC [30] [31] and that specific PKC isozymes are increased in several in vivo models of cardiac hypertrophy [32] [33]. The heart expresses different PKC isozymes, namely α-, β-, δ-, ε-, η-, and ζ-PKCs [34]. In particular, εPKC and δPKC have been reported to be activated in response to hypertrophic stimuli in cultured myocytes and their overexpression and activation in vivo induced a physiological form of cardiac hypertrophy, thus suggesting a common role in regulating adaptive CMs-hypertrophy [33]. Conversely, mice treated

with a εPKC - selective inhibitor showed LV-dilation, heart failure and death [33]. The expression β PKC is characteristics of the foetal stages of heart development and its expression is augmented during pathological cardiac remodelling and heart failure. Accordingly, β PKC overexpression and activation leads to pathological cardiac hypertrophy and fibrosis with increased expression of ANP and βMHC, known markers of detrimental cardiac remodelling [34]. Even though specific inhibitors of βPKC prevented hypertrophy in mouse model of constitutively active β PKC, pressure overload induced hypertrophy was not blunted in a mouse model of β PKC knock out, thus suggesting that β PKC is not a key-player in pressure-overload induced cardiac hypertrophy.

Phenylephrine (PE) is an α_1-adrenergic receptor agonist, which elicits hypertrophic effects in CMs via Gαq/Gα11 activation [35]. The hypertrophic phenotype induced by PE on NRVCs and ARVCs is mainly sustained by the overall increase in protein synthesis [35]. This effect is due to the activation of Erk, which phosphorylates the ribosomal S6 kinase 1 (S6K1) and the eukaryotic translation initiation factor 4E-binding protein 1 (4E-BP1) [35]. Phosphorylated S6K1 promotes the translation of mRNAs for components of the translation machinery while phosphorylated 4E-BP1 cannot sequester eIF4E thus promoting the formation eIF4E/eIF4G complex with the recruitment of ribosomes to the mRNA [35]. The effects of PE on S6K1 and 4E-BP1 are completely blunted by MEK inhibitors and partially inhibited by rapamycin (an mTOR blocker), this implying a convergence between mTOR and MEK-dependent signalling pathways [35].

Gs signalling

β-adrenergic receptor stimulation by catecholamines, namely adrenalin and noradrenalin, represents the most important regulatory mechanism for cardiac performance, and it works through a Gs subunit.

In particular, after an acute- (myocardial infraction) or a chronic- (hypertension) insult to the myocardium, there is an increase in sympathetic nervous system activation and consequent increase in catecholamine production, which may promote pathological cardiac remodelling and lead to heart failure, arrhythmia and eventually death [36]. Reduction of an excessive and prolonged activation of β -adrenergic receptors by β -blockers improves cardiac function and stands as one of the most effective therapeutic interventions in patients with HF [37, 38]. Moreover, β -blockers exert other beneficial effects, including reduction of heart rate, decrease of blood pressure, inhibition of the renin-angiotensin system and reduction of atrial and ventricular arrhythmias [38].

The human heart expresses three β-adrenergic receptor (β-AdR) subtypes: β1, β2 and β3. In the healthy human heart, the stimulation of β1- and β2-AdRs leads to inotropic and chronotropic effect on CMs whilst the effect of β3-adrenergic activation is reported to decrease cardiac contractility. The role of the β3-AdR, however, still remains not completely understood.

β1- and β2-AdRs are the most abundant in the heart and are expressed at a ratio of 7:3. In humans, both β1 and β2 subtypes are both coupled to a Gs-type of G protein, which in turn activates adenylate-cyclase (AC) and, consequently, PKA. Activated PKA phosphorylates key proteins for cardiac function, namely L-type calcium channels, phospholamban, troponin-I (TPNI), ryanodine receptor2 (RYR2), myosin binding protein-C (MyBP-C) and protein phosphatase inhibitor-I [39]. This influences CM contractile activity by augmenting Ca2+ influx and reuptake into the sarcoplasmic reticulum, and modulating myofilament Ca2+ sensitivity [39]. In contrast, GS activation by β2-agonist in vascular smooth muscle cells (vSMCs), leads to vSMCs relaxation due to the cAMP-dependent inhibition of myosin light chain kinase that is responsible for the phosphorylation of smooth muscle myosin [40]. It is also important to underline that Cardiac fibroblast (CFs) contain G protein-coupled signalling systems that are distinct from those of cardiac myocytes [41]. In particular, β2receptors links Gs with a peculiar Gq/Gs cross talk phenomenon associated with little or no coupling to G_i, thus distinguising the signaling in CFs from that in myocytes [41].

However, β2-AdR-induced production of cAMP has been characterized in CMs, depending on species, as undetectable or highly localized in contrast to β1-AdR-induced-production that homogenously elevates cAMP in all the cells [39, 42, 43]. Not only cAMP production is highly localized under β2-AdR stimulation, but also the β2-AdRs themselves show a different sub-cellular compartmentalization compared to β1-AdRs.

In CMs, β2-AdRs are localized in the sub-sarcolemmal region in close proximity to L-type calcium channels and tend to be embedded into CM's caveolae together with their effectors AC and PKA [44]. These compartments function as a separate signalosome, thus defining the spatial activation of β2-AdRs [44]. This evidence is in general agreement with the observation that, in frog CMs, in which the β2-AdR subtype is predominant, stimulation by the β2-AdR agonist isoproterenol applied to one extremity of the cell is not effective on remote L-type calcium channels [45].

Considering the fact that both PKA active subunits and cAMP are readily diffusible, another mechanism must be involved in the local control of the β2-AdR/PKA axis, such as transduction pathways that inhibit cAMP/PKA activity. In accordance, it has been shown that treatment of ventricular rat CMs with pertussis toxin (PTX), a potent inhibitor of Gi subunits, significantly potentiate β2 -AdR-mediated inotropic effects closely resembling the β1 -AdR effect [46]. These results collectively indicate that β2 -AdR/Gi coupling improves the functional compartmentalization of β2 -AdR/Gs-PKA signalling in ventricular rat CMs.

Accordingly, the transgenic overexpression of the β1-AdR in mice is detrimental, since it determines an increase in cardiac contractility at a young age that evolves into a marked CMs hypertrophy associated with progressive HF with functional and histological abnormalities [47].

Conversely, the effect of the overexpression of β2 -receptor is closely related to the amount of receptor produced; on the one hand, low-level (30-fold over expression) of β2-receptor improves cardiac contractility in transgenic mice overexpressing Gq/G11 (Tg-Gq/G11); on the other hand, high-level (350-fold over expression) are detrimental in pressure-overload hypertrophy and Tg-Gq/G11 mice, whilst beneficial in restoring cardiac contractility in a mouse model of myocardial infarction. On the contrary, two large-scale retrospective analyses regarding the effect on the use of β2 -agonists in patients with chronic obstructive pulmonary disease (COPD) reported increased rate of hospitalizations for HF as well as increased risk of mortality in patients with left ventricular dysfunction [48] [49]. This can be also partially explained by the fact that apart from the effect on cardiac contractility, β -AdR-stimulation induces also a remarkable CMs hypertrophy both in vitro and in vivo. By studying of the effect of the β-AdR-agonist isoproterenol (ISO), emerged that the ISO-induced stimulation of β-AdRs evokes the Raf1-MEK1-ERK1/2 pathway. In particular, the pre-treatment of cells with specific PKA inhibitors (Gs signalling) as well as PTX (Gi inhibitors) completely blunts the activation of ERK1/2 by ISO, thus suggesting that the pro-hypertrophic effect dependent on β -AdRs agonist is dependent on activation of ERK1/2 by both Gs/cAMP/PKA an Gi/Src/Ras pathways.

Gi signalling

Both cardiac muscarinic and β2 -adrenergic receptors couple with inhibitory signal-transducing G protein-i (Gi) to inhibit AC and directly oppose Gs-dependent signalling (reviewed in [17]). In human ventricular myocardium, Giα2 and Giα3 (Giα splice variants)

mRNA are the predominant Giα mRNA subtypes [50]. In CMs, settings of induced Gi correlate with reduced PKA activity and with constitutively active phospholamban, leading to prolonged inhibition of the sarcoplasmic reticulum calcium pump (SERCA2a), so contributing to impaired ventricular pump function [51, 52]. Moreover, NRVCMs treated with ISO showed a pro-hypertrophic phenotype characterized by the activation of the Raf1-MEK1-ERK1/2 pathway in a Gi dependent manner; the βγ subunit of Gi protein activates ERKs through the Src/Ras tyrosine kinases pathway. Of note, both Giα2 and Giα3 mRNA levels were found up-regulated in left ventricular myocardium from failing hearts and Inhibitory signal-transducing Gi was also found to play an important role in the development of severe arrhythmia and heart failure [51].

1.5.2.1.2 Calcineurin-NFAT pathway

The calcineurin-NFAT pathway plays a crucial role in the pro-hypertrophic signalling. The serine-threonine phosphatase calcineurin is expressed in multiple tissues and consists of two subunits: CnA, which is the catalytic domain (it exists in three different isoforms, CnAα, CnAβ and CnAγ) and CnB, which is regulatory [53]. In the presence of high levels of Ca^{2+}, calcineurin binds with calmodulin and dephosphorylates transcription factors of the NFAT (nuclear factor of activated T-cells) family, thus allowing translocation of these factors into the nucleus [53] [54]. Activated NFAT3 interacts with the cardiac zinc-finger nucleases GATA4, resulting in increased expression of genes associated with cardiac hypertrophy [55]. Due to its dependence on Ca^{2+} levels, the calcineurin-NFAT pathway is activated also under ANGII and PE stimulation, which both activate PLC leading to an increase of Ca^{2+} cytosolic levels [55].

Accordingly, the calcineurin inhibitors cyclosporine A (CsA) and FK 506, which form cytoplasmic immunophilin complexes that are potent calcineurin inhibitors, completely blunted hypertrophy induced by both PE and ANGII in neonatal rat ventricular CMs [55].

The effect of CsA and FK 506 was further validated as an effective treatment in preventing cardiac hypertrophy in Tg mice carrying a constitutive form of CnA, which are known to develop a massive cardiac hypertrophy [55].

Moreover CsA and FK 506 were shown to counteract hypertrophy in different Tg models such as cardiac specific overexpression of tropomodulin (TOT mice), cardiac specific mutant form of myosin light chain 2v (MLC2v), cardiac specific overexpression of β-tropomyosin as well as in a rat model of pressure overload [56].

Collectively, this evidence suggests that calcineurin might be involved in most, if not all, aetiologies of pathological cardiac hypertrophy, thereby representing an attractive therapeutic target for prevention, and perhaps treatment, of this pathological condition.

1.5.2.1.3 MEF2/HDAC and chromatin remodelling

Chromatin remodelling plays an important role in the alteration of gene expression during cardiac hypertrophy, mainly thanks to the activity of histone deacetylases (HDACs) and histone acetyl transferase (HATs) (reviewed in [57]).

In particular, HATs promote gene activation by acetylating nucleosomal histones, thereby relaxing chromatin structure [58]. On the contrary, HDACs, which deacetylate histones, induce chromatin condensation and consequent transcriptional repression [58]. In physiological conditions, class II HDACs (HDAC4, HDAC5 and HDAC9) were shown to inhibit activity of MEF2, a transcription factor known to be involved in the transduction of pro-hypertrophic stimuli and the cosequent cell growth [59]. Under pro-hypertrophic stimuli such as pressure overload and calcineurin activation, class II HDACs are phosphorylated by specific kinases, which inhibit their association to MEF2A and thus blunt the protective effect of HDACs against cardiac hypertrophy [59]. Accordingly, Tg mice with a double cardiac specific KO of HDAC9 (the class II HDAC most expressed in cardiac tissue) showed an age-dependent hypertrophic cardiac phenotype and increased sensitivity to cardiac pressure overload [59]. The identities of cardiac HDAC kinases have remained unclear; nevertheless it has been shown that phosphorylation of HDAC5 by protein kinase D (PKD), a downstream effector of PKC, drives nuclear export of class II HDAC5 in CMs [60]. Accordingly, inhibition of PKC and PKD prevents nucleo-cytoplasmic shuttling of HDAC5 in response to a subset of hypertrophic agonists [61]. These findings collectively support a novel function for the PKC/PKD axis in coupling extracellular cues to chromatin modifications that control cellular growth.

In contrast, pharmacological treatment of mice with non selective (trichostatin A and valproic acid) or HDACI-selective (SK-7041) inhibitors almost completely block cardiac hypertrophy induced by isoproterenol, ANGII and pressure overload after 2 weeks of pressure overload [62]. Even if the inhibition of type II HDACs promotes cardiac hypertrophy, the overall effect, observed in pharmacological non selective inhibition of HDACs, reflects the higher activity of type I HDACs compared to type II HDACs [62].

1.5.2.2 Signalling pathways involved in physiological hypertrophy

1.5.2.2.1 PI3K-Akt

Insulin-like growth factor 1 (IGF1) receptor signalling

Insulin-like growth factor 1 (IGF-1) plays an essential role in normal foetal and postnatal growth and development [63]. IGF1 is also produced by the heart and binds to a cell surface receptor, insulin-like growth factor 1 receptor (IGF1R), a tyrosine kinase receptor that in turn activates the phosphatidylinositol-3-kinases (PI3Ks). PI3Ks are a family of enzymes that have been linked to a diverse group of cellular functions, particularly cell growth, survival, differentiation, proliferation and cell trafficking [64].

Transgenic mice expressing human IGF1 under the α-skeletal actin promoter (SIS2 mice) developed cardiac hypertrophy, which was associated with a short-term increase in cardiac function [65]. However, the prolonged cardiac specific overexpression of IGF1 was associated with systolic dysfunction [65]. Due to the cardiac specific overexpression of IGF1, SIS2 mice showed low serum levels of IGF1 but long-term expression was associated with increases in gut, liver and spleen weight, suggesting undesired systemic effects related to IGF1 over-expression.

In 2004, McMullen et al. [66] generated a transgenic mouse model that overexpressed IFG1R under the control of α MHC. Interestingly, these IGF1R-Tg mice showed cardiac hypertrophy (proportional increase of all chambers and ventricular wall thickness), increased CM area, and enhanced systolic function up to 16 month of age, overall displaying a phenotype similar to Tg-mice expressing a constitutive active variant of PI3k (caPI3K) [66] [67]. Furthermore, these animals did not show any sign of cardiomyopathy, such as necrosis, fibrosis, or myocyte disarray at histological analysis [66].

At the molecular level, the PI3K pathway was increased in IGF1R-Tg mice, while no activation of the MAPK pathway or calcineurin was detected [66]. In addition, IGF1R-Tg mice developed less interstitial fibrosis in the TAC model, suggesting a protective effect of IGF1 in a setting of pressure overload-induced hypertrophy [66]. Notably, these features of physiological hypertrophy were completely blunted in the dominant-negative-PI3K mutant, suggesting a model in which IGF1 induces compensated hypertrophy in a PI3K-dependent manner [66]. Moreover, this evidence was confirmed in two additional, more recent studies using mice with muscle-specific knockout of the p85α/p55α/p50α and p85β(global) regulatory subunits of PI3K [68] or cardiac-specific

ablation of p110α [69]. These mice showed a decrease in heart weight-to-body weight ratio of approximately 20% and 16%, respectively [68, 69], similar to what reported by Shioi T. et al. [67]. In addition, similar to what was observed in the CM-specific knockout of IGF1R [70], dnPI3K mice also exhibited a reduced hypertrophic response to exercise.

A well characterized target of PI3K is Akt, a serine/threonine kinase (also known as protein kinase B), which belongs to a family of proteins, including 3 different isoforms (Akt1, Akt2 and Akt3), each encoded by a different gene [71]. Only Akt1 is highly expressed in the heart [71]. Akt knockout mice revealed that Akt1 is required for physiological, rather than pathological, heart growth, as these mice showed a reduced hypertrophic response to exercise but not to pressure overload [72], also in agreement with the phenotype of mice with reduced PI3K [73]. It is now generally accepted that Akt1 mediates cardiac cell growth, whereas Akt2 is important for cardiac metabolism [74] [72]. In mice, the selective cardiac overexpression of a constitutively active mutant of Akt (E40K mutant) under the control of the αMHC promoter produced a concentric LV hypertrophy with a significant increase in CM cell size whilst inducing a remarkable inotropic effect [75]. Moreover, it was shown that Akt induces cardiac hypertrophy in vivo by activating the glycogen synthase kinase-3 (GSK3)-GATA4 pathway [75].

GSK3 also exists in different isoforms (GSK3α and GSK3β), which are both expressed in the heart, where they play different roles. Phosphorylation of GSK3α induces a compensatory response reducing hypertrophy through the inhibition of ERK, as shown by knock-in mice harbouring a mutated GSK3α insensitive to Akt phosphorylation, which exhibit severe cardiac dysfunction and heart failure [76]. In contrast, phosphorylation of GSK3β is essential for the development of pathological hypertrophy, as GSK3β knock-in mice, similarly expressing a mutated protein insensitive to Akt phosphorylation, maintain LV function after TAC, despite suppression of hypertrophy [77].

1.5.2.2.2 Thyroid hormone receptor signalling

The thyroid gland secretes two biologically active hormones: T3 (3,5,3′-triiodothyronine) and T4 (3,5,3′,5′- tetraiodothyronine; also known as thyroxine), although T4 is often converted into cells in T3, which is the molecular active molecule, by the enzyme 5′-deiodinases (reviewed in [78]).

Thyroid hormone exerts a large number of activities in the cardiovascular system involving both cardiac contractile effects and cardiac remodelling (reviewed in [78]).

These effects are exerted mainly through three ways: by directly binding its cognate nuclear receptor in cardiac cells (thyroid hormone receptor-α is highly expressed in the heart) and consequent up-regulation of target genes mediated by binding of the activated receptor to the thyroid hormone response element (TREs); by regulating ion channels in the CM cell membrane; and through systemic effects of T3 and T4, which determine modulation of cardiovascular haemodynamic and cardiac filling (reviewed in [78]).

In CMs, the speed of relaxation is mainly dependent on the reuptake of calcium into the sarcoplasmic reticulum by SERCA2a, the calcium ATPase of the sarcoplasmic reticulum, the activity of which is negatively regulated by phospholamban [79]. Thanks to three TREs present in its promoter, the transcription of the Serca-2a gene is regulated by thyroid hormone [80]. The expression of phospholamban is also dependent on the levels of thyroid hormone, as shown by its up-regulation in patients with hypothyroidism [81]. Taking this evidence together, thyroid hormones regulate CMs contraction rate by the regulation of the Ca^{2+}-ATPase/phospholamban pump ratio.

An additional cardiac effect of the thyroid hormone occurs immediately after birth, when it switches on transcription of the myosin heavy chain α (αMHC) and inhibits the expression of βMHC [82].

The pro-hypertrophic effect of T3 in cultured CMs is mainly driven by the PI3K-AKT-S6K cascade [83]. Accordingly, the effect of T3 hormone on cultured CMs is completely inhibited by PI3K inhibitors as Wortmannin or LY294002 [83]. Furthermore, co-immuno-precipitation studies have shown a direct interaction between the cytosol-localized thyroid hormone receptor alpha-1 (TRα1) and the p85α subunits of PI3k [83], thus supporting the existence of a non-genomic response to T3 hormone based on cytosolic-localized TRα1 [83].

1.5.3 Murine models of cardiac hypertrophy

There is a wide range of different genetic and non-genetic animal models of cardiac hypertrophy. The most relevant genetic models, including transgenic, knock-in, knockout and dominant negative (dn) animals, are described in section 1.5.1 in the context of the description of the main pathways involved in cardiac hypertrophy. In addition, pharmacological modulation of known intracellular signalling pathways involved in pathological cardiac hypertrophy is widely used in order to obtain a more tunable phenotype and to avoid embryonic lethality, which may occur in transgenic

models. Among all pharmacological models it is worth to mention the mouse and rat model of ANGII-induced cardiac hypertrophy. It has been shown in adult rat that a continuous infusion of ANGII (200ng/kg/min) produced a clear hypertrophic phenotype, characterized by reactivation of the foetal genes, increase in LV-mass, and cardiac fibrosis [84]. Moreover, as mentioned in section 1.5.2.1.1, AT1 receptor plays also a pivotal role in the stretch-dependent hypertrophic response in a mouse model of pressure-overload, thus eliciting the ANGII-induced cardiac hypertrophy model as an alternative and less-invasive model then TAC-induced pressure overload. Big efforts have been done in the last years to elucidate the direct effects of ANGII on cardiac myocytes and cardiac fibroblast independent of secondary hemodynamic and neuro-humoral effects due to renin-angiotensin system (RAS) activation. On the one hand, ANGII exerts its trophic effect by activating MEK/ERK/p70S6 cascade thus inducing an increase in protein synthesis and a consequent increase in CMs cell size. Accordingly, the hypertrophic response of CMs exposed to ANGII and treated with PD98059, a selective inhibition of ERK1/2 activity, was completely blunted [85]. On the other hand, ANGII upregulates TGF-β1 expression via activation of the angiotensin type 1 (AT1) receptor in cardiac myocytes and cardiac fibroblasts, thus leading to cardiac fibroblast proliferation, increased collagen deposition [86].

In addition to these genetic models, physical procedures can be applied to induce physiological or pathological hypertrophy, such as exercise and aortic banding (transverse aortic constriction).

1.5.3.1 Transverse aortic constriction

Transverse aortic constriction (TAC) as a mouse model of pressure overload induced hypertrophy, was first described by Rockman H. A. et al. [87].

Aortic banding is a widely used method to induce left ventricular (LV) hypertrophy in mice and mimics human aortic stenosis with development of pressure-overload-induced LV hypertrophy [87]. Alternative sites for aortic constriction include the ascending and abdominal aorta. On the one hand ascending aortic constriction provides a stronger LV-overload. On the other hand, abdominal aortic constriction leaves intact a larger portion of the circulation as a means of possible compensation (reviewed in [88]). The ascending aortic banding is usually preferred providing a more direct and rapid source of pressure overload on the LV with a significant degree of

hypertrophy already after 48 h (reviewed in [88]). In order to reproduce this artificial stenosis, a wire with a snare on the end is passed under the aorta between the origin of the right innominate and the left common carotid arteries. A silk suture is snared with the wire and pulled back around the aorta (reviewed in [88]). Then a gauge needle is placed next to the aortic arch, the suture is snugly tied around the needle and the aorta, and following ligation the needle is quickly removed (reviewed in [88]).

As mentioned in section 1.5.2.1, angiotensin type 1 (AT1) receptors and the associated Gαq/Gα11 proteins play a critical role in transducing stretch-associated stress signals in pressure overload-induced hypertrophy; accordingly, a double heart specific knockout for Gαq/Gα11 completely blunts aortic banding induced hypertrophy [23]. Interestingly, the work of Kebir S. et al. reports a massive mis-localization of intercalated disk (ID)-associated proteins in mice submitted to pressure overload-induced [89]. This finding suggests that TAC-induced hypertrophy not only induces the activation of pro-hypertrophic genes at the transcriptional level via the AT1 receptor but also induces massive remodelling of IDs, thus impairing the myocardial functional syncytium.

1.5.3.2 Exercise induced hypertrophy

Exercise-induced cardiac hypertrophy occurs following aerobic endurance exercise and is considered a physiologically beneficial adaptation [90]. A robust experimental model to mimic the training response in humans is the model of exercise training in laboratory animals. The exercise can follow different protocols: treadmill, voluntary and swim training. Different treadmill protocols have been developed involving different duration, intensity, frequency, speed and with different range of treadmill inclination [90]. Interval treadmill training program, involving high-intensity running bouts and progressive increased exercise load, has been shown to induce observable hypertrophy within 4 weeks and resulted in 25-35% increased ventricular weight with increased CM dimension [90]. This protocol was reported to be the most effective among the treadmill variants.

Voluntary wheel program has also been reported to induce robust physiological hypertrophy, leading to a complete hypertrophic phenotype in 3-4 weeks of training.

The swim program appears to be equally effective as treadmill or voluntary wheel to induce physiological hypertrophy [90]. The duration of swim applied varies considerably, from 1-6 hours/day and 1-24 months; it is now accepted that the duration and magnitude of response are not directly proportional [90].

1.6 Heart failure

The American Heart Association/American College of Cardiology guidelines define HF as a complex clinical syndrome that can result from any structural or functional cardiac disorder that impairs the ability of the ventricle to fill or eject blood" [91] [92]. This syndrome scores more than 26 million cases worldwide, of whom 74% suffer at least 1 comorbidity, which is considerably worsened by HF [93]. Due to the complexity of the HF pathophysiology together with the high number of causes that can lead to the development of this condition, a standard criteria used to distinguish between systolic- and diastolic-HF is the Left Ventricular Ejection Fraction that can respectively be preserved in the case of systolic-HF (EF≥40%; HFpEF) or reduced in the case of diastolic-HF (EF≤40%; HFrEF). Current therapies for HFrEF are effective and can count on several classes of chemical compound, including angiotensin aldosterone system-inhibitors, beta-blockers, statins and, very recently, LCZ696 (neprilysin pathway inhibitor) [94].

Clinical trials based the above-mentioned drugs for the treatment of HFpEF have insted been ineffective in showing benefit, with the exception of a small study evaluating statins effect on 185 patients; however, a working-mechanism for statins in this condition is still missing [95]. The number of patients with HFpEF is growing year by year thus inevitably raising the claim for the development of novel therapeutic approaches for compensated HF.

1.6.1 Heart failure with preserved ejection fraction (HFpEF)

HFpEF currently accounts for 50% of all cases of HF with a higher incidence in women then man; the prevalence of this form relative to HFrEF is growing by 10% per decade [96, 97]. This trend is sustained by the increasing rate of HFpEF-associated comorbidities (hypertension, obesity, average increased life-span) together with the availability of effective therapies for patients with HFrEF, as reported above [94].

HFpEF pathophysiology is complex and several stages become apparent in the range between asymptomatic and symptomatic HFpEF, including systemic inflammation, LV hypertrophy, slow LV relaxation, LV diastolic stiffness, decreased LV systolic performance, left atrial remodeling, peripheral vascular resistance, impaired epithelial function, increased pulmonary arterial and venous resistance, neurohormonal activation and ventricular-arterial coupling [98]. Although there is not a widely accepted definition of HFpEF yet, a combination of three main conditions are considered as required to diagnose HFpEF: 1) signs and symptoms of HF, 2) conserved

or slightly reduced EF with no LV dilation; 3) relevant LV remodeling associated with hypertrophy and diastolic dysfunction [99].

Up to now, there are two main pathophysiologic theories about the progressive maladaptive process leading to HFpEF. One theory, originally suggested by Borlaug and Kass, attributes a pivotal role to an increase in LV-stiffness, which impairs LV-relaxation and contributes to a dramatic increase in LV-filling pressure, eventually evolving into diastolic dysfunction and incident HFpEF. An alternative theory by Paulus and Tschope suggests that multiple comorbidities (obesity, diabetes, hypertension) induce a pro-inflammatory state; this shifts the paradigm of HFpEF-onset from pathological LV-overload to coronary micro vascular inflammation [100].

In accordance with the model proposed by Borlaug and Kass, the passive force of single CMs, isolated from patients with diastolic-HF (dHF), is higher compared to patients with systolic-HF (sHF), suggesting an increased CMs stiffness.

The major known regulator of CM stiffness is Titin. This very large protein exists in three major isoforms, which are the result of different spicing events: 1) the adult N2B is the shortest form and results in the highest stiffness; 2) the N2BA is longer and provides a medium level of stiffness; 3) N2BA foetal form is the longest and most compliant. Titin elasticity can be regulated both by isoform relative expression (increased N2B/N2BA ratio results in increased stiffness) and phosphorylation (hypo-phosphorylation of the N2B domain results in increased stiffness) [101] [102]. N2B has also been described to bind the scaffolding protein four and half lim domain 1 (FHL1) [103]. FHL1 senses cell stretch via the N2B domain and is responsible for Gq-induced activation of the MAPK cascade in pressure-overload-induced hypertrophy [103]. Furthermore, FHL1 double KO mice showed increased LV-diastolic-compliance in TAC-induced hypertrophy [103]. These observations suggest the critical importance of a better understanding in the role of Gq/MAPK-FHL1-Titin axis in diastolic heart failure.

1.6.2 Murine models of HFpEF

The major contributor to HFpEF development is hypertension, which also represents a major risk factor for coronary heart disease [97]. Dahl-salt-sensitive rats are an inbred strain that develops hypertension (systolic blood pressure ≥175 mm Hg) when fed with a high-salt diet (8% NaCl), leading to LV-hypertrophy and HF [104]. These rats if started on a high-salt diet at 7 weeks eventually develop HFpEF by 19 weeks [105] and present signs of HFpEF including tachypnea, lack of activity and pulmonary oedema (confirmed

post mortem by increased lung weight) [105]. Conversely, Klots S. et al. reports that Dahl-salt-sensitive rats show only a slight increase in end-diastolic pressure volume relationship (ENDPR), which become undistinguishable when LV-dilation appears [106].

Obese diabetic Zucker rats, which do not develop increased LV-mass whereas diastolic dysfunction is evident, have recently been crossed with Dahl-salt-sensitive rats generating the Dahl/SS/obese rats, which show LV-hypertrophy, LV-diastolic-dysfunction and cardiac fibrosis [107]. This model is of particular interest since diabetes is one of the most frequent comorbidities In patients with HFpEF.

HFpEF can also be effectively induced in mice. C57bl6 mice treated for 4 weeks with subcutaneous infusion of ANGII develop diastolic dysfunction with conserved EF (decreased E/A ratio, decrease dP/dTmax and prolonged LV-relaxation time), whereas no evidence of increased lung weight has been reported [108] [109].

1.7 MicroRNAs in cardiac remodelling

1.7.1 Biology of microRNAs

MicroRNAs are small, highly conserved, approximately 21-mer RNA molecules that regulate the expression of genes by binding the 3'-untranslated regions (3'-UTR) of specific mRNAs in the process of RNA interference (RNAi) (reviewed in ref. [110]). These regulatory molecules are produced by the processing of long RNA transcripts, referred to as primary microRNAs (pri-microRNAs), which form stem-loop structures [110]. These are further processed in the nucleus by the Microprocessor, containing Drosha (RNase III enzyme) and DGCR8 (dsRNA-binding protein), allowing formation of pre-microRNAs, short stem-loop structures of 65–75 nt. Finally, after export into the cytoplasm by the exportin V protein, a further complex including the RNase III Dicer produces the mature microRNA [110]. The leading strand of the microRNA is loaded onto the RNA-induced silencing complex (RISC) in order to silence the target mRNA through sequestration, translational repression or mRNA degradation [111] (**Figure 4**). Unlike the process involving siRNAs, microRNAs do not require perfect pairing to induce silencing, and are therefore expected each to control expression of several tens or hundred different cellular genes.

Several thousand microRNAs have been identified and sequenced so far; to date, the largest searchable online repository for published microRNA sequences and associated annotations is miRBASE. The latest release of this database (miRBASE version 21)

contains 28,645 entries representing hairpin precursor microRNAs, expressing 35,828 mature microRNA products, in 223 species (see www.mirbase.org).

The sequences of many microRNAs are homologous among organisms, suggesting that microRNAs represent a relatively old and relevant regulatory pathway (reviewed in ref. [112]). Taken together these evidences , it is becoming evident that the role of microRNAs in regulating gene expression in higher eukaryotes could be as important as that of transcription factors, with the advantage that they are relatively limited in number, thus facilitating any screening strategy.

1.7.2. microRNA-mediated mechanisms of mRNA degradation

MicroRNAs control post-transcriptional gene expression by three main mechanisms:

1) triggering an endonuclease cleavage;
2) accelerating mRNA decapping, thus increasing mRNA decay;
3) promoting translation repression.

A perfect base pairing between microRNA and targeted mRNA generally improves endonuclease cleavage even though it is not per se sufficient, and some mismatches are still allowed for an efficient cleavage of the targeted transcript. This shows that there are additional requirements for a RISC complex to catalyse endonucleolytic cleavage [113, 114]. The microRNA determined endonuclease cleavage is generally referred to as "slicer" activity and was first described in mammal cells by Tuschl et al. in 1999 [115] and further confirmed in both plants and metazoans [113, 116]. Even though the complete picture of the determinant requirements for "slicer" activity is still missing, it has been shown that Argonaute-2 (AGO2), a protein which is part of the RISC complex, is the only one of the four mammalian Argonaute (AGO) proteins capable of directing cleavage[117]. The requirement for a specific AGO protein for endonuclease cleavage suggests that a specific microRNA, which preferentially assembles with an alternative AGO protein, might be unable to direct cleavage, even if the microRNA/mRNA base-pairing is perfect.

In addition, several experimental evidences suggest the possibility that microRNAs also target mRNAs for increased decay by a "slicer-independent" mechanism [118]. Accordingly, all four versions of the mammalian AGO proteins co-immunoprecipitate with the decapping enzyme DCP1 [119], and in both mammals and nematodes these

proteins are mainly concentrated in specific cytoplasmic foci known as P-bodies, which can be considered hot-spots of mRNA decapping and degradation [120].

A third way that microRNAs silence mRNAs is by interfering with their translation. The first evidence was reported in 1993 by the fact that the lin-4 microRNA reduced the lin-14 protein with no changes in lin-14 mRNA levels [121]. There are now several examples where protein-silencing by a microRNA is observed with either no change in the mRNA level, or only a slight decrease in mRNA levels [122-124]. The ability to repress translation is thought to be common to all members of the AGO family of proteins. For example, tethering of either human AGO2 or AGO4 to a target mRNA can lead to translational repression[125], even though translational repression in response to microRNAs remains intact only in AGO2-null cells, thus suggesting a more direct involvement of the other members of AGO2 family in microRNA-mediated translational repression.

Different approaches have been employed so far to identify microRNA targets such as bioinformatic-based prediction algorithms, mRNA sequencing (mRNA-Seq), RNA cross-linking and AGO2-IP followed by mRNA sequencing (RIP-Seq) and quantitative proteomics (SILAC). All these approaches lead to the identification of several hits that must be further validated with both 3'UTR-reporter assay, using mutated or WT variants of the predicted binding sites, and WB analysis against the targeted proteins.

The bioinformatic-based approach is fast and cheap, however it generates too many false-positive predictions of microRNA targets. On the one hand the major limitations of transcriptomics-based methodologies is that changes in protein abundance are missed; on the other hand quantitative proteomics can be considered a complementary technology to integrate the information generated by mRNA-Seq analysis after microRNA over-expression or inhibition (reviewed in [126]).

1.7.3. Heart biology and microRNAs

The crucial role of different microRNAs in cardiac development, hypertrophy and heart failure has been extensively investigated (reviewed in ref. [127]). In particular, it was shown that microRNAs are fundamental for the correct cardiac development and the ablation of the whole microRNAs network by the knock-out of DICER, in both the developing and adult heart, leads to severe heart failure and death [128]. Furthermore,

many studies of gain- and loss-of-function have highlighted microRNA families or single microRNAs involved in pathological cardiac remodelling, raising the possibility to use these microRNAs as either biomarkers or targets for novel therapies [129], [130]). Several microRNAs have been described that regulate specific processes in cardiac biology, including CM proliferation (miR-1 [131], miR-133a [132], miR-199a-3p [133]), CM hypertrophy (miR-1[134], miR-133 [135], miR-195 [136], miR-199b [137], miR-212/132 family [138], miR-378 [139], miR-23a [140]), cardiac fibrosis (miR-29 [141], miR-21 [142] and CMs contractility (miR-208a [143]).

To date, no one microRNA for the treatment of any cardiac disease has undergone human clinical investigation. Furthermore, the only microRNA suggested for the treatment of heart failure, miR-208, is still blocked at a preclinical stage, more than 6 years after the first evidences of its effectiveness in small animal models [144]. A detailed description of the most relevant microRNAs in the context of cardiac hypertrophy is reported in the following sections.

1.7.3.1 Anti-hypertrophic microRNAs

1.7.3.1.1 The bicistronic cluster of miR-1 and miR-133

The miR-1-1 and miR-1-2 are among the most abundantly expressed microRNAs in the human heart and play an important role in CM morphology and function [131]. In terms of sequence, miR-1-1 and miR-1-2 are identical [145]. Twinfilin1 (Twf1), a cytoskeletal regulatory protein that binds actin monomers, preventing their assembly into filaments, was reported to be up-regulated by hypertrophic stimuli as aortic banding and alpha-adrenergic stimulation by phenylephrine (PE) [134]. Li Q. and co-workers reported that twinfilin1 is down-regulated in the adult heart by miR-1, suggesting that the increased levels of this protein during hypertrophy is a consequence of the down-regulation of miR-1 [134]. miR-1 also negatively regulates the expression of the key calcium-signalling components calmodulin (CaM); in a consistent manner, reduction of miR-1 expression correlates with activation of the Calcineurin-NFAT pathway [146].

Calcineurin is also negatively regulated by miR-133, the other member of the bicistronic cluster miR-133/miR-1 [147]. The miR-133 also targets NFATc4, one of the four calcineurin-activated NFAT family members, the overexpression of which is sufficient to promote cardiac hypertrophy in vivo [55]. In different rodent models of cardiac hypertrophy, both physiological and pathological, miR-1 and miR-133 are down-

regulated [135], similar to what observed in patients with mitral stenosis and dilated atria [135]. On the other hand, overexpression of miR-133 in Akt Tg mice significant decreases both size of left ventricular CMs and expression of foetal genes, except for α-skeletal actin [135]. Interestingly, the down-regulation of miR-133a can be detected only 8 week after aortic banding, whereas no change occurs at an earlier stage of hypertrophy (2 weeks), suggesting an involvement of miR-133a in late, maladaptive hypertrophic growth of the heart [148].

1.7.3.1.3 miR-9

NFATc3 is another calcineurin-activated NFAT family members, regulating the expression of myocardin, a transcriptional co-activator that promotes cardiac hypertrophic responses [149] [150]. miR-9 was demonstrated to be a negative regulator of cardiac hypertrophy targeting NFATc3 [150] and, consistently, administration of a miR-9 mimic in models of isoproterenol-induced hypertrophy led to inhibition of hypertrophy and decreased myocardin level [150].

1.7.4.1 Pro-hypertrophic microRNAs

1.7.4.1.1 miR-195, a member of the miR-15 family

MicroRNA-195 is a member of the miR-15 family that was shown to be up-regulated in cardiac tissue from both mice in response to TAC or expression of activated calcineurin [136]. Moreover, the over-expression of miR-195 in neonatal primary rat CMs evoked hypertrophic growth as well as cardiac overexpression of miR-195 in vivo was sufficient to drive cardiac hypertrophy, which rapidly transitioned to heart failure [136]. Interestingly, the miR-15 family (miR-15a, miR-15b, miR-16-1, miR-16-2, miR-195 and miR-497) was reported by Porrello et al. to be up-regulated in mouse hearts between 7 and 14 days of age. In particular, mir-195 targets the expression of Check1 a cell cycle check-point gene that is implicated in the regulation of mitosis, coordinates progression through the G2/M and spindle checkpoints and regulates chromosome segregation and cytokinesis [151]. Taken together, this evidence suggests a role of pro-hypertrophic miR-195 in regulating the switch between proliferation and hypertrophy, which is the predominant form of heart postnatal growth, which occurs immediately after birth.

1.7.4.1.2 miR-199b

The miR-199b was described as a direct downstream target of calcineurin/NFAT signalling [137]. miR-199b targets the dual specificity tyrosine-phosphorylation-

regulated kinase 1a (Dyrk1a), an NFAT kinase [137]. Accordingly, decreased levels of Dyrk1a were found in patients with HF together with increased levels of miR-199b [137]. Moreover, mice treated with a miR-199b antagomir subjected to pressure overload showed normalized levels of Dyrk1A expression, no activation of the foetal gene program, attenuated levels of interstitial fibrosis and reduced CM size [137].

1.7.4.1.3 miR-23a

MircroRNA-23a was found to be the most induced microRNA in the rat heart after two weeks of pressure overload [152]. miR-23a is a member of the microRNA-23a~27a~24-2 cluster and was found up-regulated in neonatal rat CMs upon treatment with either isoproterenol or aldosterone [140]. The expression of miR-23a is regulated by NFATc3, which directly binds the promoter region of the microRNA-23a~27a~24-2 cluster gene locus. In fact, cyclosporine A, an inhibitor of calcineurin, blunts both isoproterenol-induced myocyte growth and miR-23a expression [140]. Luciferase activity assay identified the muscle-specific ring finger protein1 (Murf1) as a down-stream target of miR-23a, and overexpression of Murf1 in CMs was able to inhibit the hypertrophic response elicited by miR-23a [140].

1.7.3.1.4 miR-212 /132

The miR212/132 family is an evolutionary conserved family of microRNAs, which are known to promote cardiac hypertrophy both in vitro and in vivo [138]. In particular, miR-212/132 family promotes CMs hypertrophic growth via direct downregulation of FoxO3 expression [138]. FoxO3 exerts its anti-hypertrophic effect mainly activating atrogin-1, which induces the ubiquitination and consequent degradation of Calcineurin-A [138]. Therefore, increased calcineurin phosphatase activity and increased NFAT activity were detected in the heart of transgenic mice over-expressing miR-212/132 (miR-212/132-Tg) under the control of α MHC promoter [138]. Moreover, the analysis of cardiac functional parameters in miR-212/132-Tg mice depicted a severe status of pathological cardiac hypertrophy resulting in HF development [138]. On the other hand, miR-212/132 -/- mice were protected from TAC-induced hypertrophy as well as wt mice, submitted to TAC surgery and injected intravenously with antagomirs targeting both miR-212 and miR-132 [138].

1.8 Adeno-Associated Viral Vectors (AAVs)

The Adeno-associated viruses (AAV) are small, with a diameter of 18-25 nm. They are single stranded (ss) DNA virus, and are non-enveloped. AAV belong to the family Parvoviridae and the genus Dependovirus. The main feature that differentiates AAV from the other genus (erythroviruses) of the Parvoviridae family is the inability of autonomous replication. In particular, the infectivity of AAV depends on the super-infection with another virus [153]. The first factor identified as a successful helper in the generation of AAV particles was Adenovirus, hence the name Adeno-associated [153]. Moreover, wt AAV2 can integrate into chromosome 19q13.4 [154]. Hundreds of naturally occurring AAV serotypes have been identified to date and each serotype has a specific tropism for different tissues, mainly determined by its ability to bind specific cell surface primary receptors.

1.8.1 Genome organization

AAVs have a linear ssDNA genome with a length of approximately 4.7 kb. The AAV genome contains two long inverted terminal repeats (ITRs) flanking two open reading frames, corresponding to the genes *rep* and *cap* [155]. An additional gene, AAP, is nested within the *cap* gene and codes for a recently discovered protein assisting virion assembly [156] (**Figure 5** panel **A**). The *rep* region encodes for replication-related proteins while the *cap* region encodes for the three structural proteins VP1, VP2, and VP3 that together form the viral capsid [155]. Two different promoters, p5 and p19, drive expression of the viral *rep* gene, resulting in the expression of four protein isoforms, namely Rep78, 68, 52 and 40. All four of these Rep proteins have helicase and ATPase activity but only Rep78 and Rep 68 have strand- and site-specific endonuclease and site-specific DNA binding activities.

In particular, Rep78 and Rep68 bind specific sites within the ITRs, and are required for both viral DNA replication and site-specific integration whilst Rep52 and Rep40 are involved in the generation of single-stranded viral genomes for packaging into AAV capsids [155]. On the other hand, transcripts encoding for VP1, VP2 and VP3 are transcribed from the *cap* gene from the p40 promoter, but using three different start sites for translation. Sixty units of VP1, VP2 and VP3 assemble together with the ratio of 1:1:18, thus generating a capsid shell with icosahedral symmetry and a diameter of 18-25 nm [157]. Each viral particle contains the viral genome: a single stranded DNA molecule having either positive or negative polarity [157]. The VP1 protein also contains

a phospholipase A2 (PLA2) motif, fundamental for AAV escape from the endosomes [158].

The coding region of the viral genome is flanked at both ends by two identical long inverted terminal repeats (ITRs). The ITRs are of 125 nt containing a palindromic sequence, which forms a T-shaped hairpin structure [159]. The ITRs, due to their structure, provide a free 3' hydroxyl group that is essential for the initiation of viral DNA replication by the cellular polymerase in a primase independent manner [160] [154]. Due to their importance in AAV biology, the ITRs are the only sequences maintained during the generation of recombinant AAV vectors (**Figure 5** panel **B**).

1.8.2 AAV infection

1.8.2.1 Docking to the cell membrane

During the early phases of AAV infection, the virus binds to specific receptors, which mediate its internalization. In particular, AAV interacts with primary receptors, which differ across serotypes, but after virus binding the interaction with a secondary receptor is necessary for the internalization of the virus. Heparan sulfate proteoglycan (HSPG) is the primary receptor for AAV2, AAV3 [161]; sialic acid for AAV1, AAV4, AAV5, AAV6; the 37/67 kDa laminin receptor for AAV8; and N-linked glycans with terminal galactosyl residues for AAV9. Up to now, five co-receptors are known for AAV2 including $\alpha_v\beta_5$ integrins [162], fibroblast growth factor receptor 1 FGFR1 [163], hepatocyte growth factor (c-Met) [164], $\alpha_v\beta_1$ integrin [165], 37/67 kDa laminin receptor [166].

1.8.2.2 Endocytosis and cytoplasmatic trafficking

The next phase in AAV viral entry is internalization and it can involve different pathways of endocytosis; however, the events that characterize AAV-entry and post-entry trafficking are still not completely described. To successfully infect cells, AAV viral particles need to escape from the endocytosis pathway, thus avoiding degradation. Escape from endosomes is mainly due to the activity of the viral phospholipase A2 (vPLA2) motif (HDXXY), which is present at the N-terminal of VP1; accordingly, mutations into this domain impair AAV infectivity [158]. Due to the lowering of endosomal pH during vesicle maturation, VP1 undergoes a conformational change that mediates the exposure of the N-terminal ends of VP1, which contains the vPLA2 domain as well as nuclear localization signals (NLS) [158, 167]. The PLA2 domain was reported to

induce pore formation in the endocytic vesicles, thus allowing the virus to escape and, thanks to the exposed NLS, to translocate into the nucleus [168] [167].

1.8.2.3 Nuclear entry and viral uncoating

Little is still known on the processes that control the nuclear translocation of the virus across the nuclear membrane. Previous reports suggested a passive diffusion model across nuclear pores [169] as well as a pore-independent mechanism of AAV nuclear entry [170]. However, it was recently shown that nuclear entry of rAAV2 is mainly dependent on the canonical nuclear import pathway, involving an active importin-β mechanism [167]. A study by Sessiseberger et al. reports the presence of GFP-labeled AAV viral capsids into the nucleus, thus suggesting that viral uncoating occurs after nuclear entry [171]. On the other hand, Lux et al. originally showed that viral uncoating occurs before and during nuclear entry [172]. A more recent study, however, has demonstrated that AAV2 virions enters the nucleus and accumulate in the nucleolus [173], thus confirming that viral uncoating occurs into the nucleus. In accordance, the nuclear injection of antibody against intact capsids considerably reduces AAV-infectivity [174].

1.8.2.4 Genome processing

To be transcribed, AAV genomes have to be converted from ssDNA to dsDNA. The mechanism by which this conversion occurs is still debated; nevertheless it is generally accepted that: 1) a cellular polymerase is needed for second-strand synthesis [154]; 2) DNA damaging agents (for example, ultraviolet- or γ-radiation) as well as agents that blocs DNA synthesis (for example, hydroxyurea or topoisomerase inhibitors) increase rAAV2 transduction in vitro [175]; 3) self-annealing of complementary AAV (+) and (-) single-stranded genomes contributes to the generation of double-stranded AAV genomes [176].

1.8.3 Recombinant AAV

The first attempts to use AAV as a tool for the expression of exogenous genes in mammalian cells took place in the 1980s, thus funding the basis of recombinant-AAV (rAAV) biology [177]. In rAAV vectors, the *rep* and *cap* genes are removed and the expression cassette is cloned in between of the two145 bp ITRs, which are the only sequences of the WT virus required as cis-elements for successful expression of the

cDNA (**Figure 5** panel **B**). Any kind of promoter is suitable for the expression of the insert, whose size is restricted to a maximum of 4 - 4.5 kb. In the absence of the *rep* gene, rAAV vectors persist inside the cells mainly as extra-chromosomal DNA, thus allowing a long-term expression in non-dividing cells [178]. Since AAV2 is still the best-characterized AAV serotype, its genome has been combined with different capsid serotypes in order to generate the most suitable rAAV vector for each tissue. Up to date, the most exploited strategy for the production of rAAV preparation in a helper-free method is based on the transfection of HEK293cells with three plasmids: 1) an AAV2-ITR-containing plasmid carrying the gene of interest; (2) a plasmid carrying the Rep-Cap for the desired serotype; (3) a plasmid expressing the helper genes (E4, VA, E2A) from adenovirus (**Figure 5** panel **C**). In particular, rAAV vectors have been shown to be very efficient in transducing post-mitotic tissues such as brain (neurons; rAAV9), heart (CMs; rAAV9 [179], rAAV6 [180]), retina (photoreceptors; rAAV5, rAAV8 [181]) skeletal muscle (myofibers; rAAV1, rAAV6 and rAAV7 [182] [183]), liver (hepatocytes; rAAV8 and rAAV9 [184]) and pancreas (endocrine/exocrine pancreas; rAAV8, rAAV6 [185]).

1.8.4. Clinical applications of gene transfer using rAAV

The two most used vectors for the treatment of genetic disorders using gene therapy are lentiviruses, for *ex vivo* gene transfer into haematopoietic and other stem cells, and rAAV for *in vivo* gene transfer into post mitotic tissues for which the vector has tropism. Both viral based- approaches present different drawbacks: on the one hand, lentiviruses raise a major safety issue related to insertional mutagenesis, while, on the other hand, pre-existing or acquired neutralizing antibody activity against AAV capsid is a major limitation for efficient in vivo gene transfer using AAV vectors.

According to the Wiley Gene Therapy database updated on April 2017 (http://www.abedia.com/wiley/), 183 clinical trials have been conducted so far using rAAV vectors. Of these studies, it is worth mentioning the successful gene transfer to the subretinal space of the retinal pigment epithelium-specific 65 kDa protein (RPE65) in patients with Leber Congenital Amaurosis (LCA) caused by mutations in the RPE65 gene, which is currently in Phase III (NCT00999609). Due to the immune-privileged injection site, the immune response against the vector and the transgene were minimal in this trial, thus providing the groundwork for trials for a host of more common inherited retinal degenerative disorders, such as Leber's hereditary optic neuropathy

(ClinicalTrials.gov identifier: NCT02161380), choroideraemia (ClinicalTrials.gov identifier: NCT02553135; NCT02341807; NCT02407678), X-linked retinoschisis (ClinicalTrials.gov identifier: NCT00055029) and age-related macular degeneration (ClinicalTrials.gov identifier: NCT01024998).

Another attractive tissue for gene transfer is the skeletal muscle, which can be targeted with treatments aimed not only at correcting neuromuscular diseases but also exploited for the production of recombinant proteins that are missing in inherited protein deficiencies such as haemophilia, α1-antitrypsin deficiency and lipoprotein lipase (LPL) deficiency. The most widely used administration route to the skeletal muscle is direct intramuscular injection and the most efficient AAV serotypes for muscle transduction are AAV1 and AAV2 (reviewed in [186]). This delivery route is procedurally simple, the vector dissemination to other organs is minimal and pre-existing anti-capsid antibody does not block transduction [187]. Conversely, the skeletal muscle has been shown to be an organ that develops strong anti-transgene immune response [188]. In addition, in disease such as Duchenne muscular dystrophy, the transduction of most muscle groups, such as the diaphragm for which a clinically available procedure is not yet established, represents an important limit to the therapeutic efficacy of this approach. Interestingly, the first gene therapy approved in the Western world is Glybera (alipogen tiparvovec, AAV1-LPL), which consists of an AAV1 encoding for the human LPL. The therapy consists of *LPL*, encoded by an AAV1 virus vector, administered in a one-time series of up to 60 intramuscular injections in combination with immunosuppressive regimen is recommended from three days prior to and for 12 weeks following Glybera administration [189]. Recently, however, Glybera was withdrawn from the market mainly due to marketing considerations, especially related to its disproportionately high price (over 1 million Euro per patient) compared to the prevalence of the disease.

So far all clinical trials conducted for the gene transfer to the cardiac tissues were aimed at the over-expression of the sarco/endoplasmic reticulum Ca2+-ATPase (Serca2a) in patients with chronic heart failure. In particular, the Serca2a upregulation by intra-coronary administration using an adeno-associated virus type 1/sarcoplasmic reticulum Ca(2+)-ATPase in patients with heart failure (CUPID ClinicalTrials.gov identifier: NCT00454818) demonstrated safety and suggested benefit of the treatment, supporting larger confirmatory trials [190]. Following this was the CUPID2 trial (ClinicalTrials.gov identifier: NCT01643330)[191], a placebo-controlled phase 2b trial with 250 enrolled patients, which despite earlier promise in the CUPID trial failed to

reach the primary end point. A composite of HF hospitalization or ambulatory treatment for worsening heart failure at 12 months was 0.93 (95% CI 0.53-1.65, P=0.81) [192]. Unfortunately, a Phase III follow up clinical trial (AGENT-HF) has not confirmed this preliminary positive outcome [191].

Materials and methods

All the laboratory reagents used in this research project were purchased from standard suppliers. All the solutions and buffers were prepared with MilliQ (Millipore) quality water and, depending to the protocol, solutions were sterile filtered (0.22µm pores) before use. Table 1 reports a detailed description of all the reagents used.

2.1 Cellular biology protocols

2.1.1 Cell line culture

2.1.1.1 HeLa cells

HeLa cells were incubated in D-MEM 1gr/l glucose medium with 10% fetal bovine serum and penicillin/streptomycin 100 U/mL. Cells were passaged every 3 days.

2.1.2 Isolation and culture of primary neonatal rat/mouse ventricular cardiomyocytes

Wistar rats were purchased from Charles River Laboratories Italia Srl. Animal care and treatments were conducted in conformity with institutional guidelines in compliance with national and international laws and policies (EEC Council Directive 86/609, OJL 358, December 12, 1987).

Ventricular CMs from neonatal rats/mice have been separated from the atria, cut into smaller pieces and then digested, at room temperature using CBFHH buffer (calcium and bicarbonate-free Hanks with HEPES) supplemented with 1.75mg/ml trypsin (BD Difco) and 10 µ g/ml DNaseI (SIGMA). The collected supernatant was centrifuged to separate the cells, which were then re-suspended in DMEM, high glucose supplemented with vitamin B12 (Sigma), 5% of foetal bovine serum (FBS, Life Technologies) and with 100U/ml of penicillin and 100 µg/ml of streptomycin (Pen-Strep, Sigma). The collected cells were strained in a cell strainer (40µm, BD Falcon) and then seeded on uncoated 100 mm dishes (DB Falcon) for 2 hours at 37°C in 5% C02. The cardiomycytes are now mainly in the supernatant, which was then collected, counted and plated at the desired density in primary or collagen coated plates.

2.1.3 Transfection protocols

2.1.3.1 Transfection of rat CMs with human microRNAs:

The microRNAs mimics were transfected into neonatal rat CMs using a standard or reverse transfection protocol, at a final microRNA concentration of 25 nM.

- **Reverse transfection:** 7.5 µ l of each microRNA 500nM concentrated were spotted into each well (final reaction volume 150 µl). The transfection reagent (Lipofectamine RNAiMAX, Life Technologies) was diluted in OPTI-MEM (Life Technologies) and incubated for 5 minutes (final volume was calculated considering 0.2 µl of RNAiMAX and 25 µl of OPTI-MEM for each well). The mixture of transfection reagent and OPTI-MEM was added to the microRNAs previously spotted into each well and incubated for 30 minutes. Immediately after 1.0×10^4 cells/well were seeded. Here below it follows a detailed description of the transfection procedure optimized for different well format:
    - **MicroRNA transfection protocol 96 well plates format, mix per well:**

      - 7.5 µl of microRNA 500nM

      - 25 µl of OPTI-MEM

      - 0,2 µl of RNAiMAX

    - **Procedure :**

    1. Incubate RNAiMAX and Opti-MEM medium (Gibco) for 5 minutes at RT
    2. Dispense 25µl/well of transfection MIX on plates spotted with the microRNA; incubate for 30 minutes at RT
    3. Dispense 1.0 × 10^4 rat CMs (118µl total volume) into each well
    4. Change medium 24 hours after transfection
    5. Incubate for 48 hours
    6. Wash the cells 3 times in PBS (100µl/well), fixed in 4% PFA (50µl/well)

- **Forward transfection:** The transfection reagent (Lipofectamine RNAiMAX, Life Technologies) was diluted in OPTI-MEM (Life Technologies) and incubated for 5 minutes (final volume was calculated considering 0.2 µl of RNAiMAX and 25ul of OPTI-MEM for each well). 25 µl of transfection mixture were added to 1.5ml Eppendorf Tubes containing 7.5 µl of each microRNA (500 nM concentrated) and incubated for 30 minutes. Immediately after 32.5 µ l of mixture was transferred

into each well, where 1.0×10^4 cells had been seeded 24 hours before (final volume 150µl /well).

- **MicroRNA Transfection protocol 96 well plates format, mix per well:**
  - 7.5 µl of microRNA 500nM
  - 25 µl of OPTI-MEM
  - 0,2 µl of RNAiMAX
- **Procedure :**

1. Incubate RNAiMAX and Opti-MEM medium (Gibco) for 5 minutes at RT
2. Dispense 25µl/well of transfection MIX into 1.5ml eppendorf tube containing the 7.5 µ l /well of microRNA (500nM); incubate for 30 minutes at RT
3. Dispense 32.5 µl of mix/well on top of previously seeded rat CMs 1.0×10^4 cells/well (150 µl final volume).
4. Change medium 24 hours after transfection
5. Incubate for 48 hours
6. Wash the cells 3 times in PBS (100µl/well)
7. Fix the cells in 4% PFA (50µl/well)

2.1.3.2 Forward Transfection of rat cardiomyocytes with human microRNAs in 35mm dishes

The transfection reagent (Lipofectamine RNAiMAX, Life Technologies) was diluted in OPTI-MEM (Life Technologies) and incubated for 5 minutes (final volume was calculated considering 4 µ l of RNAiMAX and 500 µ l of OPTI-MEM for each dish). 500 µ l of transfection mixture were added to 1.5ml Eppendorf Tubes containing 15 µ l of each microRNA (5µM concentrated) and incubated for 30 minutes. Immediately after 515 µl of mixture was transferred into each well, where 2×10^6 cells were seeded 24 hours before (final volume 3ml /dish).

- **MicroRNA Transfection protocol 35mm dish format, mix per well**:
  - 15 µl of microRNA 5uM
  - 500 µl of optimum
  - 4 µl of RNAiMAX
- **Procedure**:

1. Incubate RNAiMAX and Opti-MEM medium (Gibco) for 5 minutes at RT
2. Dispense 500µl/well of transfection MIX into 1.5ml eppendorf tube containing the 7.5 µl /well of microRNA (500nM); incubate for 30 minutes at RT
3. Dispense 500 µ l of mix/well on top of previously seeded rat CMs 2.0 × 10^6 cells/well (2.5 ml final volume).
4. Incubate cells for 72 hours.

2.1.3.3 Transfection of mouse cardiomyocytes with human microRNAs

Human microRNAs transfection in mouse CMs follows the same protocol for rat CMs described in section 2.1.3.1 and 2.1.3.2. The only difference is the final concentration of microRNAs that was optimized at 50 nM for mouse CMs instead of 25 nM for rat CMs.

2.1.3.4 pDNA and microRNA transfection in HeLa cells

2.1.3.4.1 MicroRNA transfection

HeLa (human cervical cancer) cells were transfected with MC1 or hsa-miR-665 at a final concentration of 50 nM in 96-well plates, through a standard reverse transfection protocol similar to that described in section 2.1.3.1.

2.1.3.4.2 Plasmidic DNA transfection

HeLa cells were transfected with 100 ng per well (96 well plate) of pDNA using FuGENE HD as transfection reagent (Promega). The optimized ratio of pDNA:lipids is 1:3.

- **pDNA Transfection protocol 96 well plate format, mix per well**:
  - 100 ng of pDNA
  - 30 µl of OPTI-MEM
  - 0.3 µl of FugeneHD
- **Procedure**:

1. Dilute pDNA into OPTI-MEM
2. Prepare the transfection mix adding 0.3 µl of Fugene HD each 100 ng of pDNA, vortex and incubate for 20 minutes at RT
3. Dispense 20 µ l of transfection mix/well on top of 1.2×10^4 HeLa cells seeded 24 hours before.
4. Incubate cells for 72 hours.

2.1.4 Human microRNA screening in rat cardiomyocytes

The microRNA mimics (miRDIAN microRNA mimics; Dharmacon) library corresponding to the all human mature microRNAs (988 microRNAs, 875 unique sequences miRBase release 13.0 (2009), http://mirbase.org;) were obtained by Dharmacon, Fhisher Thermo Scientific. The library of microRNAs was robotically (Hamilton StarLab) replicated from stock library plates to Primaria 96-well plates (BD Falcon); 7.5 µl of each microRNA 500nM concentrated were spotted into each well leaving columns 1 and 12 empty for addition of controls (buffer, MC1, MC4). MicroRNAs were transfected into neonatal rat CMs using a standard reverse transfection protocol, at a final microRNA concentration of 25 nM (final volume 150 µl). Briefly, the transfection reagent (Lipofectamine RNAiMAX, Life Technologies) was diluted in OPTI-MEM (Life Technologies) and incubated for 5 minutes (final volume was calculated considering 0.2 µl of RNAiMAX and 25 µl of OPTI-MEM for each well). The mixture of transfection reagent and OPTI-MEM was robotically added to the microRNAs arrayed on 96-well plates, using the Multidrop™ reagent dispenser (Thermo Fisher SCIENTIFIC). Transfection mix and microRNA were incubated for 30 minutes and immediately after 1.0×10^4 cells/well were robotically seeded using the Multidrop™ reagent dispenser (Thermo Fisher SCIENTIFIC). Twenty-four hours after transfection, culture medium was replaced by fresh medium; 28 h later, that is, 52 h after plating, the culture medium was replaced with medium containing 5 µM 5-ethynyl-2′-deoxyuridine (EdU, Life Technologies) for 20 h. Cells were fixed at 72 h after plating using 4% PFA and processed for immunofluorescence. The screenings were performed at the ICGEB High-Throughput Screening Facility (http://www.icgeb.org/high-throughput-screening.html).

2.1.5 Mouse siRNAs screening in mouse cardiomyocytes

For the transfection experiments in mouse CMs, the selected siRNAs (list reported in Table 3) were "cherry-picked" from siRNA library stock plates and robotically re-arrayed into collagen-coated black clear-bottom 384-well plates (PerkinElmer) using the Starlab Liquid handler (Hamilton). Transfection was performed as described in section 2.1.3.3, in particular 7.5×10^4 cells were seeded per well and a final microRNA concentration of 50 nM was used. The screenings were performed at the ICGEB High-Throughput Screening Facility (http://www.icgeb.org/high-throughput-screening.html).

2.2 Molecular biology protocols

2.2.1 UTR-luciferase reporter: construct generation

Portions of the 3'-UTR of Enah, Fhl1 and the 5'-UTR of Xlrp2 were obtained by gene synthesis (gBlocks) from IDT (Integrated DNA Technology) and sub-cloned into psiCHECK2 vector (Promega). The extremities of gBlocks were implemented with restriction sites for XhoI and NotI in addition to flanking regions of stuffer-DNA to increase cut efficiency.

The gBlocks were then digested with XhoI (New England Biolabs) and Not-HF (New England Biolabs) according to the following protocol:

- **GBlocks digestion protocol**:
  - Prepare the following digestion mix and incubate at 37° for 2 hours
    I. 500 ng of gBlock
    II. 0.1µl of XhoI (10000U/ml)
    III. 0.1µl of NotI-HF (10000U/ml)
    IV. 2µl of 10x Buffer 2.1 (New England Biolabs)
    V. H20 to final volume of 20 µl

The psiCHECK2 vector was linearized with XhoI (New England Biolabs) and Not-HF (New England Biolabs) according to the following protocol:

- **PsiCHECK2-Vector preparation:**

- Prepare the following digestion mix and incubate at 37° for 2 hours
  I. 2 µg of the vector
  II. 0.5µl of XhoI (10000U/ml)
  III. 0.5µl of NotI-HF (10000U/ml)
  IV. 3µl of 10x Buffer 2.1 (New England Biolabs
  V. H20 to final volume of 30 µl
- The digestion reaction was heat inactivated (15' at 65°C) and submitted to DNA gel electrophoresis. 1% agarose gel was prepared place into an electrophoresis chamber and rinsed in TBE (Tris-Borate-EDTA buffer; SIGMA). The samples were loaded into pre-cast wells and when placed in an electric field, due to the negatively uniform mass/charge ratio of nucleic acids, DNA fragments migrate according to their molecular weight and secondary structure. The linearized vector was then excised

and purified by gel using Wizard SV Gel and PCR Clean-Up System (Promega) according to manufacture's instruction.

Linearized vector and digested gBlocks were ligated and transformed into into XL10 Gold (Stratagene) recombination deficient bacteria. Colonies were screened for ampicillin resistance as well as insert size by restriction enzyme digestion.

- **Cloning of gBlocks into PsiCHECK2-Vector:**

  The vector ligated with the inserts with the following reaction 60' at room temperature:

  I. 50ng of purified vector
  II. 50ng of gBlocks
  III. 1 µl of the DNA ligase T4 (New England Biolabs)
  IV. 2 µl of DNA ligase T4 10x Buffer (New England Biolabs)
  V. H_20 to final volume of 20 µl

  – The ligation reaction was heat inactivated (15 minutes at 65°C) and transformed into XL10 Gold (Stratagene) recombination deficient bacteria by heat shock, following manufacture's instruction. The cells were then plated on Ampicillin selective agar.
  – Single colonies were picked and plasmidic DNA purification performed using the Wizard SV MiniPrep system (Promega) according to manufacture's instruction.
  – The so obtained DNA was digested with XhoI and NotI restriction enzymes following the aforementioned protocol; only positive clones show right size insert excision.
  – The digestion reaction was heat inactivated (15' at 65°C) and submitted to DNA gel electrophoresis. 2 % agarose gel was prepared place into an electrophoresis chamber and rinsed in TBE (Tris-Borate-EDTA buffer; SIGMA). The samples were loaded into pre-cast wells and when placed in an electric field, due to the negatively uniform mass/charge ratio of nucleic acids, DNA fragments migrate according to their molecular weight and secondary structure. 100bp and 1kb ladder (New England Bioloabs) were used.

2.2.2 UTR-luciferase reporter: Assay

HeLa cells were reverse transfected with MC1, hsa-miR-665 at a final concentration of 50 nM in 96-well plates. Twenty-four hours after microRNAs transfection, cells were transfected with 100 ng per well of the reporter constructs or psiCHECK2 vector (control) using FuGENE HD transfection reagent (Promega) (transfection protocols described section 2.1.3.4). Firefly and Renilla luciferase activities were measured (Envision plate reader (PerkinElmer), 1second integration signal), 36 hours after plasmid transfection using Dual-Glo® Luciferase Assay System, according to the manufacturer's instructions.

2.2.3 Total RNA isolation from total heart and cultured cardiomyocytes

In the case of RNA extraction from whole hearts, hearts were removed by gross dissection from the body, washed in PBS and snap frozen in liquid nitrogen. Once frozen the samples were stored at -80°C for further processing. The same day of RNA extraction 1 ml of TRIzol reagent (Invitrogen, Carlsbad, CA, USA) was added to each heart samples and efficiently disrupted using the MagNA Lyser Instrument (ROCHE). In the case of cultured rat or mouse CMs, cells were washed in PBS and directly lysed using TRIzol reagent (1ml for ≅250 thousands CMs) (Invitrogen, Carlsbad, CA, USA). After either tissue homogenization or cell lysis supernatant containing nucleic acids were recovered and submitted to RNA extraction using the miRneasy mini kit (Quiagen), according to the manufacturer's instructions.

2.2.4 Quantitation of nucleic acids by real-time PCR

Total RNA from isolated CMs was reverse-transcribed using hexameric random primers (Invitrogen), starting from 250 ng of RNA. The cDNA was used as a template for real-time PCR amplification to detect the expression levels of selected genes. The housekeeping gene GAPDH was used to normalize the results. Quantification of gene expression was performed by quantitative real-time PCR, using TaqMan® assays (Applied Biosystems) reported in Table 2.

TaqMan assays employ a sequence-specific, fluorescently labelled oligonucleotide probe called the TaqMan probe, in addition to the sequence-specific primers. Also known as the 5'-nuclease assay, the TaqMan assay exploits the 5'-exonuclease activity of thermophilus aquaticus polymerase (Taq). The probe contains a fluorescent reporter at the 5' end and a quencher at the 3' end. When intact, the fluorescence of the reporter is

quenched due to its proximity to the quencher. During the combined annealing/extension step of the amplification reaction, the probe hybridizes to the target and the dsDNA-specific 5' to 3' exonuclease activity of Taq cleaves off the reporter. As a result, the reporter is separated from the quencher, and the resulting fluorescence signal is proportional to the amount of amplified product in the sample. One commonly used fluorescent reporter- quencher pair is fluorescein (FAM, which emits green fluorescence) and Black Hole Quencher 1. The main advantages of using TaqMan probes include high specificity and a high signal-to-noise ratio.

2.2.4.1 Assay settings

The adopted settings reported here below have been tested to ensure a reaction efficiency of 2.

- Each reaction was composed in 20 µl:
    - i) 10µl 2X PCR Master Mix (Biorad)*;*
    - ii) 1µl 20X primers and probe fluorofore FAM
    - iii) 1µl cDNA
    - iv) H2O to final volume.
- The adopted protocol was:
    - i) 95° 5 minutes
    - ii) 44 cycles:
        1. 95° 10 seconds
        2. 60° 30 seconds
        3. Read
    - i) Melting curve 60° to 95°- 0,5° increments

2.2.4.2 Normalization method: The 2−ΔΔCT (Livak) Method

The 2−ΔΔCT method for relative gene expression analysis is widely used and easy to perform.

1) First, normalize the CT of the target gene to that of the reference (ref) gene, for both the test sample and the calibrator sample:
    a) ΔCT(test) = CT(target, test) – CT(ref, test)
    b) ΔCT(calibrator) = CT(target, calibrator) – CT(ref, calibrator)
2) Second, normalize the ΔCT of the test sample to the ΔCT of the calibrator:

a) $\Delta\Delta CT = \Delta CT(test) - \Delta CT(calibrator)$

3) Finally, calculate the expression ratio:

a) $2^{-\Delta\Delta CT}$ = Normalized expression ratio

The result obtained is the fold increase (or decrease) of the target gene in the test sample relative to the calibrator sample and is normalized to the expression of a reference gene. Normalizing the expression of the target gene to that of the reference gene compensates for any difference in the amount of sample.

2.2.5 mRNA sequencing

Left ventricle of hearts extracted from 8 weeks old TAC-operated CD1 mice injected with AAV9-hsa-miR-665 (N°=3) and AAV9-Control (N°=3) or 8 weeks old sham operated mice (N°=3) were processed for total RNA extraction (see protocol described in section 3.2.3). Deep-sequencing was performed by IGA Technology Services. Samples were processed using TruSeq RNA-seq sample prep kit from Illumina. Briefly, the poly-A containing mRNA molecules were purified using poly-T oligo-attached magnetic beads, fragmented into small pieces using divalent cations under elevated temperature, cDNA was synthesized by reverse transcription and standard blunt-ending plus added 'A' was performed. Then, Illumina TruSeq adapters with indexes were ligated to the ends of the cDNA fragments. After ligation and separation of non-ligated adapters, only the fragments captured by complementary adapter oligonucleotides, which are covalently bound to Illumina flow cells, were extended and brigde-amplified to create milions of clusters, each of which contains thousands copies of a single template molecule. The clusters were sequenced at ultra-highthroughput on the Illumina HiSeq2000, obtaining 30–57 millions of single-reads per sample, 50 bp long.

Raw data were subjected to quality control using FASTQC tool (http://www.bioinformatics.bbsrc.ac.uk/projects/fastqc) and, in order to estimate gene expression levels, only QC passing reads were subsequently mapped to the *Mus musculus* reference genome (University of California at Santa Cruz, UCSC, mm10) by using the ultrafast universal RNA-seq aligner STAR [193] and the Mouse Genecode release M12 (GRCm38.p5) as gene annotation file. Mapped reads for all transcript variants of a gene were combined into a single value to perform differential gene expression analysis.

The Bioconductor packages DESeq2 version 1.12.4 [194] and EdgeR [195] version 3.6.2 in the framework of R software version 3.3.1 were used to perform the differential gene expression analysis of mRNAseq data. Both packages are based on the negative binomial distribution (NB) to model the gene reads counts and shrinkage estimator to estimate the per-gene NB dispersion parameters. Specifically, we used rounded gene counts as input and we estimated the per-gene NB dispersion parameter using the function DESeq for DESEQ2 while for edgeR we used the function calcNormFactors with the default parameters for the estimation of the biological coefficient of variation (BCV). Estimated p-values for each gene was adjusted using the Benjamini-Hochberg method [196] and adjusted $P<0.05$ was selected as statistical threshold. Using the number of replicas and the BCV as starting data for rnapower function [197] we estimated as optimal non statistical thresholds: 10 normalized counts and 1 absolute Logarithmic base 2 fold change.

2.2.6 Immunofluorescence on culture rat and mouse cardiomyocytes

2.2.6.1 Immunofluorescence in 96/384 well plate

Cells were fixed with 4% paraformaldehyde (PFA) for 15 min (40µl/20µl), permeabilized with 0.5% Triton X-100 in phosphate buffered saline (PBS) solution for 10 min (40µl/20µl), followed by 30 min blocking in 1% bovine serum albumin (BSA, Roche) (40µl/20µl). Cells were then stained overnight at 4°C with the following primary antibodies diluted in blocking solution (BSA 1% in PBS): mouse monoclonal antibody against sarcomeric α-actinin 1:400 (Abcam), mouse monoclonal antibody against atrial natriuretic peptide 1:400 (ANP) (Millipore). Cells were washed with PBS (100µl/60µl) and incubated for 2 hours, at room temperature, with the selected secondary antibody labelled with Alexa Fluor-488 (green) or Alexa Fluor-594 (red). Cell nuclei were further stained with Hoechst 33342 (Life Technologies) diluted 1:5000 in PBS (100µl/50µl).

2.2.6.2 EdU Staining in 96/384 well plate

When indicated, cells were further processed using the Click-IT EdU 594 Imaging kit to reveal EdU incorporation, according to the manufacturer's instructions. Cell nuclei were further stained with Hoechst 33342 (Life Technologies) diluted 1:5000 in PBS (100µl/50µl).

2.2.7 Histology

At the end of the studies, animals were sacrificed by injection of 10% KCl, to stop the heart at diastole. Heart and tibia were removed by gross dissection from the body. Heart weight and tibia length were taken after the hearts were washed in PBS and chambers and tibias were cleaned of cartilaginous tissue. The heart was fixed in 10% formalin at room temperature, embedded in paraffin and further processed for histology

2.2.7.1 Masson's trichrome stain

Masson's trichrome stain is a tri-color stain that produces red keratin and muscle fibers, blue collagen and bone, pink cytoplasm, and dark brown to black cell nuclei. This peculiar stain is achieved by the combination of four different stains: Weigert's iron hematoxylin for nuclei, picric acid for erythrocytes, a mixture of acid dyes (acid fuchsin-"ponceau de xylidine") for cytoplasm and aniline blue for connective tissue.

After fixation in formalin, hearts were embedded in paraffin and processed for slides preparation. Sections were deparaffinised (65°C for 12 hours), rehydrated (5'-100% EtOh; 5'-95% EtOh, 5'-75% EtOh, 5'-50% EtOh, H_20) and processed using a commercially available kit for Masson's trichrome stain (BioOptica), according to the manufacturer's instructions. After the staining the slides were dehydrated (5'-50% EtOh; 5'-75% EtOh, 5'-95% EtOh, 5'-100% EtOh, H_20) and mounted in Eukitt mounting medium by Sigma.

2.2.7.2 Periodic acid-Shiff (PAS) stain

The Periodic acid-Shiff (PAS) stain specifically detects glycogen, glycoproteins, glycolipids and mucins in tissues. Periodic acid oxidises glycols to aldehydes. These aldehydes then react with the Schiff reagent and releases a pararosaniline adduct, which stains the glycol-containing cellular elements in purple. Slides were deparaffinised (65°C for 12 hours), rehydrated (5'-100% EtOh; 5'-95% EtOh, 5'-75% EtOh, 5'-50% EtOh, H_20) and processed using the PAS staining kit (SigmaAldrich) to detects fibres border, according to the manufacturer's instructions. After the staining the slides were dehydrated (5'-50% EtOh; 5'-75% EtOh, 5'-95% EtOh, 5'-100% EtOh, H_20) and mounted in Eukitt mounting medium by Sigma.

2.2.7.3 Immunofluorescence on heart section

After excision, the heart was fixed in 10% formalin at room temperature, embedded in paraffin and further processed for immunofluorescence. Sections were deparaffinised (65°C for 12 hours), rehydrated (5'-100% EtOh; 5'-95% EtOh, 5'-75% EtOh, 5'-50% EtOh, H_20) and then underwent antigen retrieval by boiling in sodium citrate solution for 30 min. Slides were processed for sarcomeric α -actinin, wheat germ agglutinin (WGA)staining).

2.3 *In vivo* experiment protocol

CD1 mice were purchased from Charles River Laboratories Italia Srl. Animal care and treatments were conducted in conformity with institutional guidelines in compliance with national and international laws and policies (EEC Council Directive 86/609, OJL 358, December 12, 1987).

2.3.1 Aortic Banding and simultaneous intra-cardiac injection of AAV vectors

Aortic banding was produced in adult female CD1 mice (10 weeks old), by permanent Aortic Arch constriction as described previously by deAlmeida and colleagues [198]. Our technique contains slight modifications to allow simultaneous intra-cardiac AAV injection. Briefly, mice were anesthetized with an i.p. injection of ketamine and xylazine, endotracheally intubated and placed on a rodent ventilator. Body temperature was maintained at 37°C on a heating pad. The Aortic Arch and beating heart was accessed via superior median sternotomy prolonged until 4th intercostal space. A chest dilatator was used to optimize heart and vessels visualization. After gentle separation of the thymus fat tissue from the vessels of interest, constriction of Aortic Arch was performed against a 2 gauge needle with 7.0 silk suture knots. Immediately post-ligation, recombinant AAV vectors, at a dose of 1×1011 vg per animal, were injected in left ventricle anterior wall (single injection) about 1 mm under the left atrium, using an insulin syringe with incorporated 30-gauge needle. Two groups of animals were studied, receiving AAV9-control and AAV9-hsa-miR-665. The chest was closed, and the animals moved to a prone position until the occurrence of spontaneous breathing. Echocardiography analysis was performed at days 12, 30 and 60 days after banding, and hearts were collected at 30 (n=8 animals per group) and 60 (n=8 animals per group) days after banding.

2.3.2 Aortic Banding and subsequent intra-cardiac injection of AAV vectors

This model was designed in order to assess whether has-miR-665 was able to revert an already established hypertrophic phenotype. For this purpose, aortic banding was produced (same procedure in 3.3.1) and immediately post ligation the chest was closed and the animals moved to a prone position until the occurrence of spontaneous breathing. All the animals underwent echocardiography 15 days after banding to assess the severity of the hypertrophic phenotype and then divided into two homogenous groups. Both control and treated groups underwent intra-cardiac injection (same procedure in 3.3.1) respectively with AAV9-control and AAV9-miR-665. Echocardiography analysis was performed at days 15, 30 and 60 days after AAV9 injection, and hearts were collected at 30 (n=8 animals per group) and 60 (n=8 animals per group) days after banding.

2.3.3 Echocardiography analysis

To evaluate left ventricular function and dimensions, transthoracic two-dimensional echocardiography was performed on mice sedated with 5% isofluorane at 15, 30 and 60 days after aortic banding, using a Visual Sonics Vevo 770 Ultrasound (Visual Sonics) equipped with a 30 MHz linear array transducer. M-mode tracings in parasternal short axis view were used to measure left ventricular anterior and posterior wall thickness and left ventricular internal diameter at end-systole and end-diastole, which were used to calculate left ventricular ejection fraction.

2.4 Statistics

The Prism package (GraphPad Software, La Jolla, CA) was used to analyse the data. All the results are expressed as mean ± s.d. Values of $p<0.05$ were considered statistically significant. Depending on the experimental design, Student's *t*-test, one-way ANOVA or two-way ANOVA with Tukey's post-hoc comparison tests were used, as indicated in the legends to the figures and text. Correlation analyses were done using the Pearson coefficient to assess the linearity between two variables and calculate two-tailed p-value (95% of confidence interval).

RESULTS

3.1 High-content, fluorescence-microscopy-based, high-throughput screen identifies microRNAs able to modify cardiomyocytes area

A high-content, fluorescence-microscopy-based, high-throughput screen was performed in neonatal rat CMs using a library of 875 microRNA mimics (988 mature microRNAs, 875 unique sequences, miRBase release 13.0 (2009), http://mirbase.org). MicroRNA mimics were introduced into cultures of neonatal rat ventricular CMs by reverse transfection. To assess efficiency of the procedure, several wells were transfected with a toxic siRNA against the UBC component of the ubiquitin-proteasome pathway, followed by nuclear count. By this approach, efficiency of transfection was estimated ≥ 92% (**Figure 6** panels **B** and **C**).

After 72 h from reverse transfection, cells were stained for sarcomeric α -actinin to specifically measure CM cell size and number and for uptake of 5-ethynyl-29-deoxyuridine (EdU), a uridine analogue that is incorporated into newly synthesized DNA (experimental scheme in **Figure 6**, panel **A**). Image segmentation and analysis was performed to selectively quantify CM size and number of proliferating CMs (**Figure 6**, panel **G**). **Figure 6** panel **E** reports correlation between CM size and percentage of proliferating cells following treatment with the 875 microRNAs. The screening was performed in duplicate; the replicates showed very good reproducibility (Spearman coefficient 0.84; Fig. **6D**). On average, approximately 2,500 cells were analysed per experimental condition and replicate. Representative images of microRNAs able to strongly reduce or increase CM cell size are shown in panel **G**, and include hsa-miR-665 and hsa-miR-664-5p.

Next we decided to individually study each of those microRNAs unable to promote EdU incorporation but able to influence CM cell size. According to these parameters, 11 microRNAs were selected: 4 of these induced CM hypertrophy and 7 instead reduced cell size (**Figure 6,** panel F).

3.2 Validation of the screening hits

Based on the screening results, we decided to validate and characterize the effect of the selected top microRNAs under both anti-hypertrophic and pro-hypertrophic conditions, in order to assess the ability of each microRNA to counteract or induce the hypertrophic phenotype.

First, we investigated the effect of each microRNA on the expression of a set of genes previously associated with either pathological hypertrophy (foetal cardiac gene program: NPPA, NPPB, MYH7 and ACTA-1) (reviewed in ref. [11]) or to physiological hypertrophy (ATP2a2, MYH6 and RYR) (**Figure 7**, panel **B**). In particular, to examine the effect of microRNAs able to decrease CM cell size, we stimulated the cells with phenylephrine (PE), a known pro-hypertrophic stimulus, and simultaneously transfected them with individual microRNAs. In parallel, to test the effect of microRNAs able to increase CM cell size, the cells were starved (0.1% FBS) and transfected with the individual microRNAs. In all cases, total RNA was extracted 72 hours after transfection and analysed by qRT-PCR using TaqMan probes specific for the abovementioned subset of genes (experimental scheme **Figure 7**, panel **A**).

The pure effect of PE (40 μM) on rat CMs cultured in 0.1% FBS was evaluated after 72 hours of treatment, in the absence of microRNAs, by both qRT-PCR (**Figure 7**, panel C) and immunofluorescence (α-actinin, ANP) (**Figure 7**, panel B). PE strongly upregulated the subset of genes typical of the foetal cardiac gene program (NPPA, NPPB and ACtA1) and significantly increased CM size compared to the control. All the anti-hypertrophic microRNAs were able to revert the signature of pathological hypertrophy induced by PE by reducing the levels of ANP and BMP. However, only hsa-miR-1255, hsa-miR-1288, hsa-miR-509-3p and hsa-miR-665 were simultaneously able to significantly upregulate Myh6, Serca2a, and RyR, two known markers of good contractility (**Figure 7**, panel **B** and **C**)[18, 19]. The validation experiments confirmed that all the pro-hypertrophic microRNAs were able to increase CM cell size (**Figure 7**, panels **E, F**). In addition, all the selected microRNAs, with the exclusion of hsa-miR-29b, did not induce reactivation of the foetal gene program (**Figure 7**, panels **E, F**). On the other hand, overexpression of hsa-miR-29b remarkably increased both cell area and ANP when compared to the control (**Figure 7**, panel **E**). Accordingly, the qRT-PCR results showed a strong activation of the foetal gene program (increased ANP, BNP and skeletal α-actin) and reduced levels of SERCA2a and RYR, thereby displaying the typical molecular signature of pathological hypertrophy (**Figure 7**, panel **F**).

Due to the epidemiological relevance of cardiac hypertrophy as a landmark of cardiac pathology, we decided to focus the subsequent research on anti-hypertrophic microRNAs and, in particular, to explore their capability to block and/or revert pathological hypertrophy.

To understand whether the identified microRNAs also modulate cell size of CMs from another species, thus increasing the probability of the conservation of their functional effect in human cells, we re-tested the selected 6 anti-hypertrophic microRNAs in neonatal mouse CMs. For these experiments, we evaluated the effect of selected anti-hypertrophic microRNAs against the pro-hypertrophic effect of foetal bovine serum (FBS). As reported by Bass et al. [199], FBS, which contains a wide range of different growth factors, induces the largest increase in CM cell area compared to other pro-hypertrophic stimuli such as insuin growth factor 1, isoproterenol and PE. As reported in **Figure 8** panel **A**, we transfected mouse primary CMs after 24 hours of starvation and simultaneously treated the cells with 5% FBS. Seventy-two hours after transfection, cells were fixed and immuno-stained for α-actinin and ANP. Image segmentation and analysis was performed to selectively quantify cell size and number of ANP-positive CMs. As displayed in **Figure 8** panel **B** and **C**, hsa-miR-665 scored the best in reducing CM cell area and significantly decreasing the percentage of ANP-positive CMs compared to CMs transfected with MC4.

Based on these results, next we decided to individually test the effect of hsa-miR-665 *in vivo* in a model of hypertrophic response to transverse aortic constriction-induced (TAC-induced) pressure overload.

3.3 Hsa-miR-665 counteracts the onset of hypertrophy and preserves cardiac function after transverse aortic constriction

To evaluate the anti-hypertrophic effect of hsa-miR-665 in vivo, we chose to investigate whether this microRNA was able to prevent development of hypertrophy in a TAC model of chronic cardiac pressure overload. Eight-week-old CD1 mice were subjected to TAC or sham surgery and, simultaneously, the mice were injected in the left ventricle anterior wall (LVAW), using AAV9 vectors expressing hsa-miR-665 or a control vector expressing an empty cassette (AAV9-Control) (1×10^{11} vg/animal; n=10 per group; **Figure 9,** panel **A**). Our previous experience indicates that this procedure results in efficient myocardial transduction and month-long expression of the transgene [133]. As reported in **Figure 9** panel **B**, gross anatomic differences are appreciable across treatments. In particular, the overexpression of hsa-miR-665 successfully counteracted, at both 30 and 60 days, the hypertrophic remodelling of the heart thus maintaining the heart mass at physiological levels (30 days after TAC heart mass (gr) normalized on tibia

length (mm) was 0.09±0.020; compared with 0.13±0.019 for the animals that received the control vector, *P*<0.001; at 60 day after TAC, 0.010±0.0006 for AAV9-miR-665 injected animals and 0.015±0.0008 for the animals that received the AAV9-Control *P*<0,.01. (**Figure 9**, panel **C**).

Periodic Acid-Schiff (PAS) staining revealed a marked reduction in CM cross sectional area at 30 days after TAC (242.26±76.02 μm ^{2} for AAV9-miR-665 injected animals; compared with 487.26±104.27 μm ^{2} for the animals that received the AAV9-Control, *P*<0.001), different from what observed at 60 days after TAC where no significant differences between treated and control were measured (**Figure 9,** panel **D**).

Masson's trichrome staining, at day 30 and 60, revealed both a marked reduction in in tissue fibrosis in AAV9-miR-665 injected animals compared to AAV9-Control treated animals (**Figure 9,** panel **E**).

As evaluated by echocardiography (echo) at 15, 30 and 60 days after TAC, LVAW thickness was significantly decreased in the treated mice with respect to controls at both 30 and 60 days. At 30 days after TAC, AAV9-miR-665-injected animals showed a LVAW thickness-s of 1.01±0.05 mm; compared with 1.36±0.65 mm for the animals that received the AAV9-Control, *P*<0.01 and the effect was maintained up to 60 day after TAC, 1.02±0.15 mm for AAV9-miR-665 and 1.44±0.8 mm for control treated animals (**Figure 9**, panel **F**). Even more interestingly, at 30 and 60 days after TAC, left ventricular ejection fraction (LVEF) was also markedly preserved in constricted mice treated with AAV9-miR-665 compared to control animals. (**Figure 9**, panel **G**) (30 days after TAC LVEF of AAV9-miR-665 injected animals scored 56.5±5.4 compared to 42.54±5.90% in AAV9-Control treated animals, *P*<0.05; at 60 days after TAC LVEF of AAV9-miR-665 injected animals scored 51.3±5.8 compared to 34.82±0.77% in AAV9-Control treated animals, *P*<0.01). Besides, no significant differences were observed in left ventricular internal diameter (LVID) measurements between treated and control groups (**Figure 9**, panel **H**).

Taken together, these results indicate that the over-expression of hsa-miR-665 after aortic banding exerts a beneficial effect in reducing cardiac hypertrophy and preserving cardiac function in a chronic cardiac overload model, consistent with the effect that this microRNA had shown in vitro.

3.4 miR-665 delays cardiac dilatation and dysfunction in hypertrophic hearts

Focusing on a possible translational application of these results, next we decided to verify whether hsa-miR-665 was able to revert established cardiac hypertrophy to normal phenotype and function. In this rescue experiment, mice were injected in the LVAW 2 weeks after TAC surgery with AAV9-hsa-miR-665 (1×10^{11} vg/animal; 10 weeks old female CD1 mice, n=8 per group). Using echo to determine LWAV thickness at 15 days after TAC, animals were homogeneously grouped and then followed at day 30, 45 and 60 (experimental scheme in **Figure 10**, panel **A**). While no significant rescue of the mild hypertrophic phenotype was observed during follow up (at day 15/30 post AAV injection - 45 and 60 post TAC, LVAW thickness: 0.88±1.13/0.91± 0.08 mm for AAV9-miR-665 treated animals, compared to AAV9-Contol injected mice with 0.8±0.11/0.96±0.33 mm), LV diastolic diameter and ejection fraction was strongly maintained in normal ranges in the treated animals in respect to controls (LVEF at final time point: 57.5%±5.60 vs. 28.4%±15 in treated and control animals respectively, $P<0.001$; LVID at final time: 4.05±0.16mm 4.8±0.69mm in treated and control animals respectively, $P<0.001$) (**Figure 10** panel **F**,**G** and **H**).

Consistently, hsa-miR-665-treated mice showed the highest survival curve during the 2 months follow up (data not shown). At day 60 after TAC, mice were sacrificed and the hearts examined. Gross anatomy examination revealed a marked myocardial fibrosis with left ventricular dilatation and wall thinning in animals, which had received the control vector (**Figure 10**, panel **B** and **E**). It has to be acknowledged that thinned fibrotic segments may be responsible of partially unreliable M-Mode measurement of LVAW thickness. In fact, analysis of PAS-stained heart cross sections in non fibrotic areas revealed no significant differences in CM cross sectional area between treated versus control animals (**Figure 10**, panels **C** and **D**).

Comprehensively, these results are consistent with a beneficial effect of the tested microRNA: LV dimensions and function were maintained in normal ranges in treated mice despite the harsh surgical model characterized by high mortality and detrimental LV remodeling in AAV9-control treated mice.

3.5 The transcriptomic signature of AAV9-miR665 overexpression in a transverse aortic constriction (TAC) model of chronic cardiac pressure overload.

To identify the relevant targets of has-miR-665, we assessed global transcriptome changes by in vivo deep-sequencing of total heart RNA after TAC and transduction with AAV9-hsa-miR-665 or AAV9-Control (**Figure 11**, panel **A**). We calculated, using EdgeR, the biological coefficient of variation across replicates, which represents the extent of variability in relation to the mean of the distribution.

The BCV plot in **Figure 11** panel **A** reports the results of the analysis, which showed a coefficient of biological variation across the replicates of 0.2 (this value indicates that the true abundance for each gene can vary up or down by 20% between replicates).

We assumed the following conditions as starting data for rnapower function [197]: 1) Number of 3 replicates per condition (AAV9-miR665 upon TAC, AAV-CTRL upon TAC and sham-operated animals); 2) Coefficient of Variation= 0.2 ; 3) P-Value≤0.05. We estimated as optimal non statistical thresholds 10 normalized FPKM/gene (Fragments Per Kilobase Of Exon Per Million Fragments Mapped) and 1 absolute Logarithmic base 2 fold change fo down/up regulation (**Figure 11**, panel **B**).

RNAseq data were also processed with pvclust (**Figure6**, panel **C**), which is an R package for assessing the uncertainty in hierarchical cluster analysis. For each cluster in hierarchical clustering, quantities called p-values are calculated via multiscale bootstrap resampling. The p-value of a cluster is a value between 0 and 1, which indicates how robustly the cluster is supported by the data. This analysis provides two types of p-values: **AU** (Approximately Unbiased) p-value and **BP** (Bootstrap Probability) value. Clusters with AU larger than 95% are highlighted by red rectangles, showing that these are strongly supported by data. As reported in **Figure 11** panel **C**, the group of TAC-mice injected with AAV9-hsa-miR665 clustered together with sham-operated animals. This evidence strongly supports the fact that the overexpression of hsa-miR-665 massively counteracts TAC-induced hypertrophy, leading to an mRNA signature not statistically significantly different to that of a healthy heart.

This analysis identified 67 down-regulated transcripts (FPKM≥10, FDR≤ 0.05) and 83 up-regulated mRNAs (FPKM≥10, FDR≤ 0.05) (**Figure 12**, panel **A**). Interestingly, the mRNAs most up-regulated in TAC+AAV9-Control animals were also the transcripts most down-

regulated in the TAC+hsa-miR-665 group, supporting the ability of hsa-miR-665 to blunt the hypertrophic phenotype (**Figure 12**, panel **B**).

Among the mRNAs found to be the most down-regulated, we sought to identify those responsible for controlling CM cell size. We individually knocked down 43 of these mRNAs, for which short interfering RNAs were available, under conditions similar to those of the initial screening. Mouse CMs were prepared from P0 mice and reverse transfected with the library of selected siRNAs. After 52 hours, EdU was added and 20 hours later cells were fixed and stained for **α-actinin** and **EdU** (experimental scheme **Figure 12**, panel **C**). Five of these siRNAs (targeting Cdc42, RRP7A, Desmin, Enah and Smpd2) had an effect on cell size which was comparable (less than 2 standard deviations compared to has-miR-665) to that induced by hsa-miR-665 overexpression (**Figure 12**, panel **D**). Enah and Cdc42 were the only two genes that were also down-regulated more than 2 fold after the over-expression of has-miR-665 *in vivo* (**Figure 12**, panel **E**). In particular, Enah is a downstream effector of cdc42 and is necessary for cdc42/IRSp53-induced actin polymerization [200]. Moreover, Enah cooperates with N-Wasp and WAVE2 in promoting F-actin polymerization under the stimulation of IGF1, a known pro-hypertrophic stimulus [201] [202]. In addition, the cardiac overexpression of Enah leads to a marked hypertrophic phenotype [203].

Further analysis identified two additional genes (Xirp2 and Fhl1) that are not only known to play a role in cardiac hypertrophic but are also functionally connected to Enah. These genes were also strongly down-regulated in the mRNA-seq dataset (**Figure 12**, panel **E**) and the same results were obtained by confirmation experiment using qRT-PCR. When knocked-down individually, however, the siRNAs against *Xirp2* and *Fhl1* were individually inefficient at reducing cell size in vitro (**Figure 7**, panel **D**), suggesting that the effect of their down-regulation might become apparent only when other genes also simultaneously repressed.

3.6 Luciferase 3'-UTR reporter assay to validate direct targets of hsa-miR-665

We decided to focus our attention on three hits: Enah, Xirp2 and FHL1. All these transcripts encode for proteins that localize in the proximity of the intercalated discs. Here they integrate and transduce multiple mechanical stimuli, thereby promoting cardiac hypertrophic remodelling both at a transcriptional and a structural level [89, 203-205]. The question that we wanted to address was whether these transcripts are

direct targets of hsa-miR-665. Since the in vivo study and the subsequent mRNAseq on total heart was performed by overexpressing a human microRNA in a mouse background, we decided to analyse the predicted targets of both hsa-miR-665 and mmu-mir-665-3p (ortholog in mouse) in their respective species background. **Figure 13** panel **A** reports the result of the above-mentioned analysis run with the bioinformatic tool RNA22 (Computational Medicine Center of Thomas Jefferson University). We were able to identify positive matches for hsa-miR-665 in the human transcripts of all three candidates, however only the mouse transcript of Xirp2 scored positively also for mmu-miR-665-3p.

We are well aware of the poor predictive capacity of virtually any currently available software or software combination aimed at predicting microRNA targets. For this reason, and due to the discordance of the predictions obtained, we decided to manually check for canonical site types, such as:

- 8mer: match to microRNA positions 2–8 with an A opposite position 1 [206];
- 7mer-m8 site: position 2–8 match[206]
- 7mer-A1 site: position 2–7 match with an A opposite position 1 [206]
- 6mer: position 2–7 match [206] [207];
- offset-6mer: position 3–8 match [206] [207].

As reported in **Figure 13** panel **B**, we found that Fhl1 has three offset-6mer sites (two sites are present in the 3'UTR and 1 site in the 5'UTR), Enah has 4 offset-6mer sites in the 3'UTR while Xirp2, in accordance with the prediction, showed one 8mer match in the 5'UTR.

In order to validate these potential microRNA target sequences, four constructs were generated by cloning the complete sequence of the 3' UTR and 5'UTR of Fhl1, 5'UTR of Xirp2 and a portion of the 3'UTR of Enah into the reporter vector psiCHECK-2 (Promega) (**Figure 13**, panel **C**). In this construct the expression of Renilla-luciferase is modulated by the binding of the microRNA to its targets, while the expression of Firefly-luciferase is used as reference.

As reported in **Figure 14** panel **A**, we reverse transfected HeLa cells with hsa-miR-665 (50 nM final concentration) and, after 24 hours, the medium was changed and cells were transfected with one of the four different constructs. Forty-eight hours after, cells were lysed and both Renilla-luciferase and Firefly-luciferase activity were measured using the Dual-Glo luciferase assay system (Promega). The Renilla-luciferase expression

was then normalized on Firefly-luciferase for each of the samples and then expressed as fold change over MC1. The results of the assay (**Figure 14**, panel **C**) clearly indicate that hsa-miR-665 was able to target the 3'UTR of Fhl1, the 5'UTR of Xirp2 and the 3'UTR of Enah.

DISCUSSION

4.1 Discussion

In this research project, the screening of 875 microRNA mimics using a fluorescence-microscopy-based, high-throughput assay in NRVCMs led to the identification of a previously uncharacterized anti-hypertrophic microRNA, hsa-miR-665. Our experiments revealed that this microRNA is able to turn off the foetal cardiac gene program and to upregulate *Myh6*, *Ryr* and *Atp2a2* in NRVCMs upon stimulation with PE, a strong α_1-adrenergic receptor agonist, known to mimic the molecular signature of pathological cardiac hypertrophy. In particular, pathological cardiac hypertrophy is known to be associated with the upregulation of foetal genes, such as *Nppa*, *Nppb*, *Myh7* and *Acta-1* and the downregulation of *Atp2a2 Myh6* and *Ryr* (reviewed in ref. [11]). The switch in myosin isoforms is commonly considered a marker of the failing heart, nevertheless it represents an adaptive response to pathological stimuli, since βMHC, which is encoded by *Myh7*, is slower in catalysing ATP-hydrolysis, thus allowing a less powerful but more energy-saving contractile function [208] [209] [210]. The same concepts can be applied to the increased production of the natriuretic peptides ANP and BNP, encoded by *Nppa* and *Nppb* genes respectively. ANP and BNP are highly increased in the failing heart; clinically, plasma levels of BNP are used as diagnostic and prognostic markers for hypertrophy and HF in human patients [211]. Once released in the blood flow, these peptides exert a plethora of systemic effects aimed at unloading the failing heart, including antagonism of the renin-angiotensin system, increase in renal natriuresis and diuresis and vasodilatation (reviewed in ref. [212]).

The re-activation of foetal genes and the switch in contractile protein isoforms does not occur in physiological hypertrophy (mainly induced by exercise), despite a remarkable increase in protein production and consequent cellular growth (reviewed in ref. [11]). This evidence suggests that the contribution of this subset of foetal genes to the pathophysiology of cardiac hypertrophy is not well understood. Despite these uncertainties, it is broadly established that a prolonged condition of cardiac hypertrophy is characterized by the upregulation of *Nppa*, *Nppb*, *Myh7* and *Acta-1* and leads to a detrimental cardiac remodelling. The expression of these genes was normalized upon delivery of hsa-miR-665.

Our results also indicated that hsa-miR-665, formulated as an AAV9 vector, significantly blunted the hypertrophic phenotype in hearts submitted to chronic pressure overload (8 weeks of TAC), when the vector was administered simultaneously to aortic banding.

Treatment with AAV9-hsa-miR-665 increased animal survival during the 2 month follow up (data not shown) and effectively preserved cardiac function under chronic pressure overload. This was best seen by the echocardiographic analysis of left ventricular ejection fraction, which, 60 days after TAC, was 33% higher in microRNA-treated animals compared to controls.

In addition, hsa-miR-665 showed a remarkable therapeutic effect by blocking pathological cardiac remodelling and preventing heart failure in hearts submitted to chronic pressure overload (8 weeks of TAC). In this model, the microRNA was administered 15 days after aortic banding, again formulated as an AAV9 vector. The treatment with hsa-miR-665 was not able to revert the mild-hypertrophic phenotype developed during the first 15 days of pressure-overload but it effectively prevented the treated hearts from developing HF by blocking left ventricular dilation and preserving cardiac ejection fraction (after 8 weeks of TAC: LVEF scored 50% higher in treated animals compared to controls). The key message of the results of this rescue experiment is that hsa-miR-665 not only has to be considered as an anti-hypertrophic agent but also that its effect has the potential to extend to a broader range of pathological conditions, aiming at the improvement of cardiac function in the presence of pathological cardiac remodelling.

To understand the mechanisms of action of hsa-miR-665, we decided to assess the global mRNA expression changes after TAC in hearts transduced with the AAV9 expressing this microRNA or an AAV9-Control. Particular attention was paid to the genes that were downregulated, which should include all direct and indirect targets of the microRNA. Subsequently, the most downregulated mRNAs were individually silenced in NMVCMs and the cell size was automatically measured.

Understanding the mRNA targets of a given microRNA is commonly considered a very challenging task. In this respect, bioinformatics algorithms are of little help, since the capacity of these algorithms, even when used collectively, is relatively poor in predicting the mRNAs that are really downregulated in vivo by the microRNA. One powerful method to assess microRNA target function is to explore the changes of the transcriptome in response to cell treatment with the microRNA, focus on downregulated genes (which include direct targets, in addition to indirect ones), and then verify whether any of these targets, once downregulated by specific siRNAs, mimic the phenotype imparted by the microRNA itself.

When siRNAs against the genes downregulated by hsa-miR-655 treatment were individually tested, we observed that only five of these genes (*Cdc42*, *Enah*, *Des*, *Rrp7a* and *Smpd2*), when individually silenced, were able to mimic the effect of hsa-miR-665 in reducing cell size of NMVCMs. These genes were all downregulated in the transcriptome analysis even if only two (Cdc42 and Enah) scored less than -1Log_2 fold, which was the limit of statistical significance set for our analysis, considering a false discovery rate ≤0.05 and 3 replicates per condition. In contrast, the genes that resulted most downregulated by the over-expression of hsa-miR-665 (i.e. *Nppa*, *Ankrd1*, *Acta1*, *Xirp2* and *Fhl1*), when individually silenced, were either not or only slightly effective in reducing NMVCMs cell size.

At this point two possibilities were equally probable: 1) the most-down regulated transcripts were off-targets 2) hsa-miR-665 modulates biological processes that cannot be effectively measured in vitro, such as mechanosensing and CMs compliance to stretch, by an individual siRNA knockdown.

Further along the path of discovering functional hsa-miR-655 targets, we selected three candidates, namely Enah, Xirp2 and Fhl1.

ENAH localizes in IDs and is a down-stream effector of CDC42. Both these genes are involved in actin filament elongation, thus regulating cellular morphology and polarity [213]. The function of Cdc42 in cardiomyocytes is still debated, although the overexpression of Cdc42 was reported to enhance CM hypertrophy in vitro [214]; nevertheless in 2009 Maillet et al. reported a novel anti-hypertrophic signalling pathway due to the CDC42-dependent, JNK activation, which antagonizes calcineurin-NFAT activity, thus reducing pathological hypertrophic cardiac remodelling [215].

Only a few scientific reports describe the effect of Enah in the heart; the role of Cdc42 is equally unclear. On the one hand, Belmonte et al. have reported that the cardiac over-expression of Enah leads to cardiac hypertrophy and promotes HF [203]. On the other hand, altered levels of Enah (upon either its over-expression or silencing) are associated with impaired connexin-43 localization, conduction abnormalities and dilated cardiomyopathy [216] [217]. This evidence suggests that the levels of Enah have to be finely tuned and that extreme variations in both directions are equally detrimental. Interestingly, the mRNA levels of Enah are upregulated by TAC and are restored at basal levels by treatment with has-miR-665 (data reported in **Table 4** and **Figure 12** panel **G**).

Xirp2 is a member of the muscle-specific, actin-binding *Xin* gene family. Interestingly, the class of proteins encoded by this family of genes is expressed only in the four-chambered heart of vertebrates (reviewed in [218]). In particular, all the proteins that belong to this family are characterized by the presence, at their N-terminus, of multiple copies of a conserved repeating unit of 16 amino acid residues (reviewed in [218]). In humans, two Xin repeat-containing proteins have been identified so far, namely XIRP1 (Xin actin- binding repeat-containing protein 1) and XIRP2 (Xin actin- binding repeat-containing protein 2). These proteins are encoded by two different genes, which were first identified as genes associated with cardiomyopathies, respectively named as cardiomyopathies associated gene 1 (*CMYA1*) and cardiomyopathies associated gene 3 (*CMYA3*) [219] [220]. The orthologous genes in the mouse are *Xinα* and *Xinβ* respectively. The former codes for three different protein variants (XINA, XINB, XINC/XIRP1), while the latter codes for XIRP2 [221]. The common functional feature shared by the member of this class of proteins is the ability to bind actin filaments, hence the name XIRP. Moreover, both XIRP1 and XIRP2 were shown to selectively bind the SH3 domain of nebulette, which is known to be exposed and to actively recruit N-WASP during myofibril formation and elongation [222] [223]. In addition, in the mouse, XIRP1 directly interacts with F-Actin and recruits ENAH, which in turn promotes myofibril formation exerting its "anti-capping" activity [224]. Finally, McCalmon et al. showed that XIRP2 is upregulated in pressure overload-induced cardiac hypertrophy and that its expression is regulated by Mef2a, a known pro-hypertrophic transcription factor [225] [226].

Even if a direct interaction between XIRP2 and ENAH has not been described yet, the aforementioned evidence on the role of XIRP1 in recruiting ENAH on F-actin together with the known upregulation of both ENAH and XIRP2 during pathological cardiac remodelling, are consistent in indicating a pivotal role of these proteins in complex sarcomeric remodelling under cardiac stress-response.

FHL1 is a member of the four and a half LIM domain-only protein family, together with FHL2 and FHL3; expression of these proteins is particularly enriched in striated muscle [227]. These proteins are structurally characterized by four complete LIM domains and an N-terminal half LIM domain. LIM domain are protein-protein interaction domains, characterized by a cysteine rich motif that co-ordinately binds two zinc atoms and mediates protein-protein interactions [228]. Recent studies have shown that FHL1 is the only member of the FHL-protein family to be upregulated in mouse hearts after in vivo

pressure overload-induced hypertrophy as well as in the hearts of patients with hypertrophic cardiomyopathy, thus suggesting its involvement in pathological cardiac remodelling in both mouse and humans [229] [230]. Furthermore, work performed by Sheikh et al. led to the conclusion that FHL1 is a novel sensor of sarcomeric stretch. In particular, it was shown that FHL1 binds the N2B domain of titin and is responsible for stretch- or Gq-induced- activation of the MAPK cascade in pressure-overload-induced hypertrophy. FHL1 performs a scaffolding function, since direct interactions between FHL1 and Raf-mediated MAPK was shown to be fundamental in sustaining transduction of pro-hypertrophic stimuli [103]. Furthermore, FHL1 double KO mice showed increased LV-diastolic-compliance in TAC-induced hypertrophy, thus suggesting that, in the absence of FHL1, the N2B domain of titin adopts a more relaxed conformation [103].

Taking our results together with the available literature evidence, we suggest a model (**Figure 10**) by which hsa-miR-655 exerts a triple role in modulating cardiac hypertrophy: 1) hsa-miR-655-induced down-regulation of *Fhl1* eventually blocks transduction, into the nucleus, of pro-hypertrophic signals that rely on the Raf-mediated MAPK cascade - these signals can include pressure-overload induced hypertrophy; 2) down-regulation of *Fhl1* also eventually reduces ventricular wall-stress by the modulation of titin elasticity, thus protecting IDs morphology and preventing CM functional uncoupling; 3) hsa-miR-655-induced downregulation of *Xirp2* and *Enah* eventually reduces the recruitment of *Xirp2* and *Enah* to the IDs, where these proteins are known to promote myofibril formation. At this point, further experiments are needed in order to evaluate the global effect of hsa-miR-665 over-expression in the heart. In particular, on the one hand it will be crucial to elucidate the effects, on CM biology, of all the other genes whose mRNAs resulted strongly down-regulated ($\geq 2\text{Log}_2$ fold) by hsa-miR-665 overexpression, namely Gm4841, Art3, Ankrd1 and Tesk1. On the other hand, we need to understand what is the effect of hsa-miR-665 overexpression in the two main other cardiac cell types, namely cardiac fibroblasts and endothelial cells. In addition, differential proteomic analysis (SILAC) has to be performed in order to identify the effect that hsa-miR-665 may directly exert at the translational level, by identifying differentially downregulated proteins.

4.2 Conclusions and future perspectives

The results presented in this thesis indicate that hsa-miR-665 effectively reduces cell size of rat and mouse neonatal cardiomyocytes under strong pro-hypertrophic conditions and negatively regulates the expression of genes known to be associated with pathological cardiac remodelling *(Nppa*, *Nppb*, *Myh7* and *Acta-1*). Moreover, hsa-miR-665 blocks cardiac hypertrophy and pathological cardiac remodelling whilst increasing cardiac function, in a mouse model of left ventricular pressure overload. Finally, hsa-miR-665 acts therapeutically, in a mouse model of left ventricle pressure overload with established cardiac hypertrophy, by preventing left ventricular dilatation and heart failure thus increasing animals life span.

These results not only reveal an important regulator of cardiomyocyte response to external stress, but also suggests means and targets for therapeutic intervention. Direct delivery of hsa-miR-665, either as a modified mimic RNA or in the form of an AAV vector, might be considered as a possible therapeutic strategy for pathological hypertrophy and, in particular, for HFpEF, a condition in which modulation of cardiac elasticity and down-regulation of stiffness are expected to provide important benefit.

In addition to the direct use of hsa-miR-665 as a therapeutic molecule, this work has revealed a few targets of its action which could be exploited themselves for the generation of innovative small molecule therapeutics. Indeed, our results predict that the controlled, pharmacological inhibition of *Flh1*, *Enah* and *Xirp2* would provide benefit to conditions of pathological cardiac hypertrophy and, again, HFpEF. More in general, the discovery of the beneficial effect of the down-regulation of these genes is an example of the powerful use of microRNAs as therapeutic tool in the treatment of cardiovascular disease.

FIGURES

FIGURE 1. The heart structure

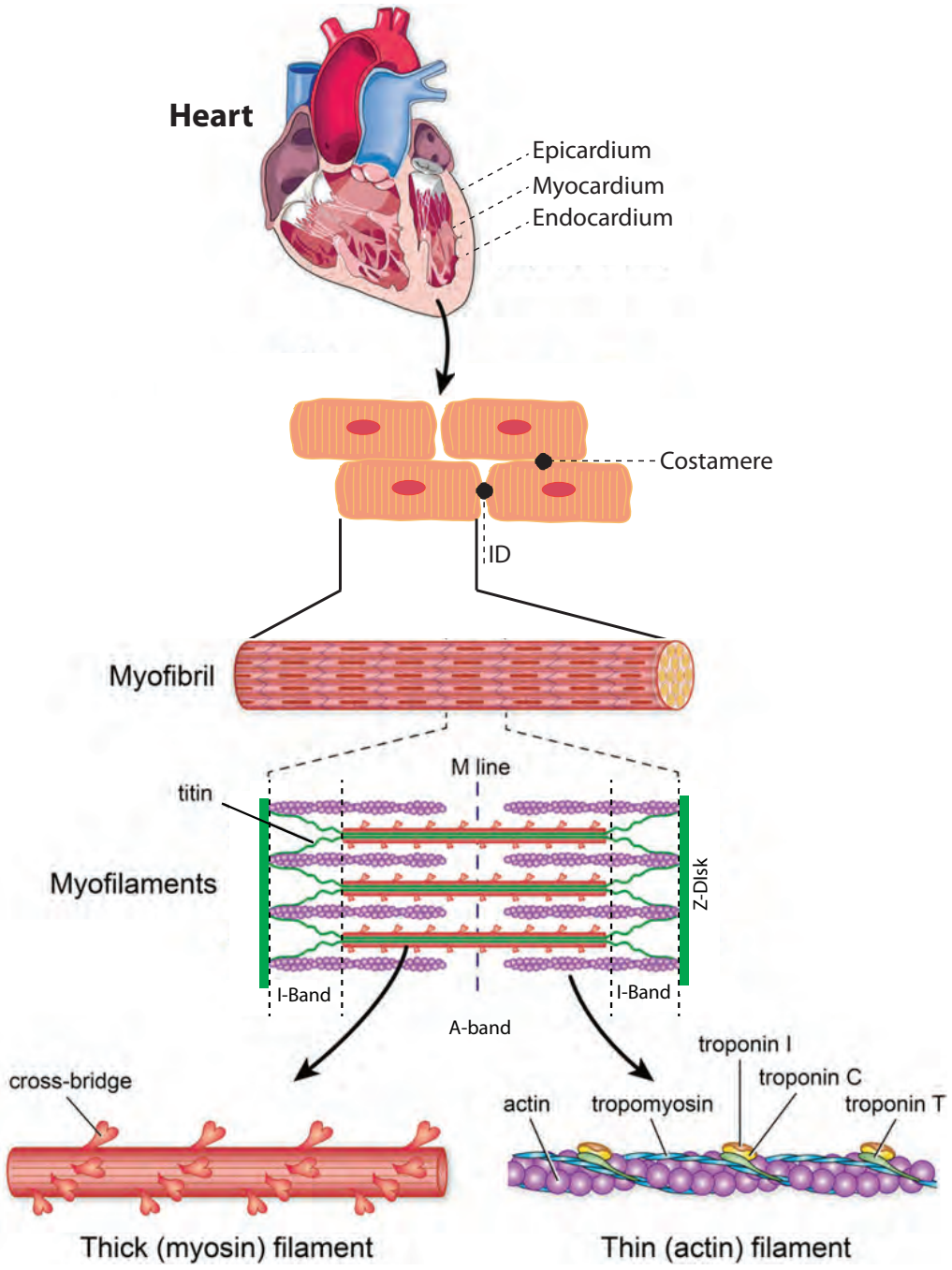

FIGURE 2. Pathological and physiological cardiac hypertrophy

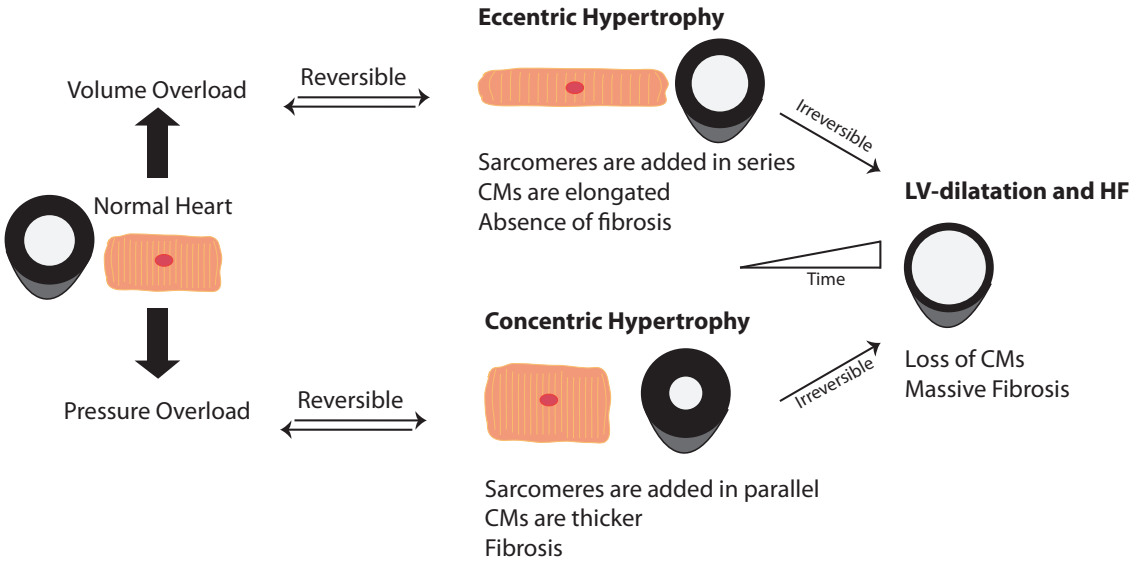

FIGURE 3. Main pathways involved in cardiac hypertrophy

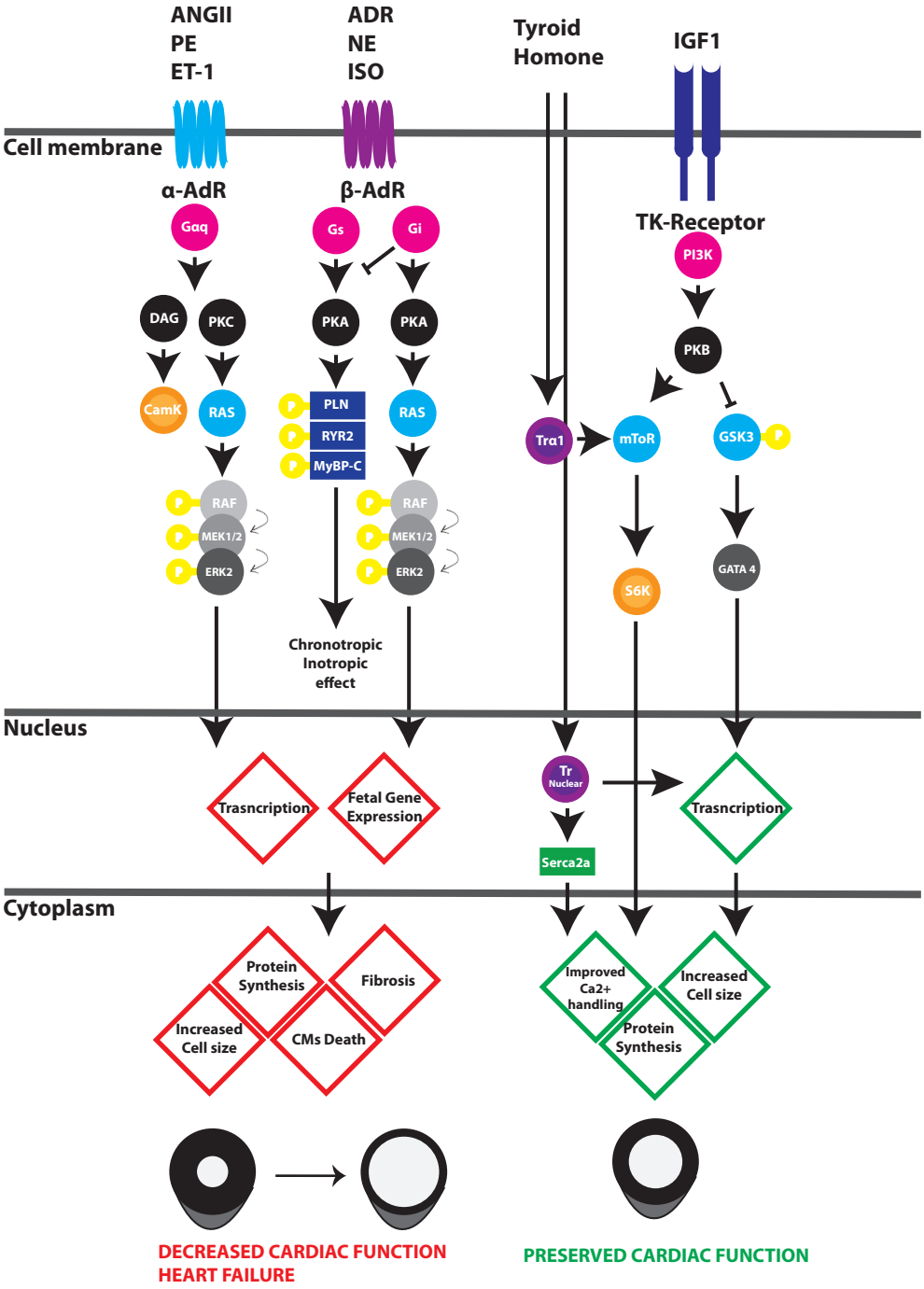

FIGURE 4. MicroRNA biogenesis

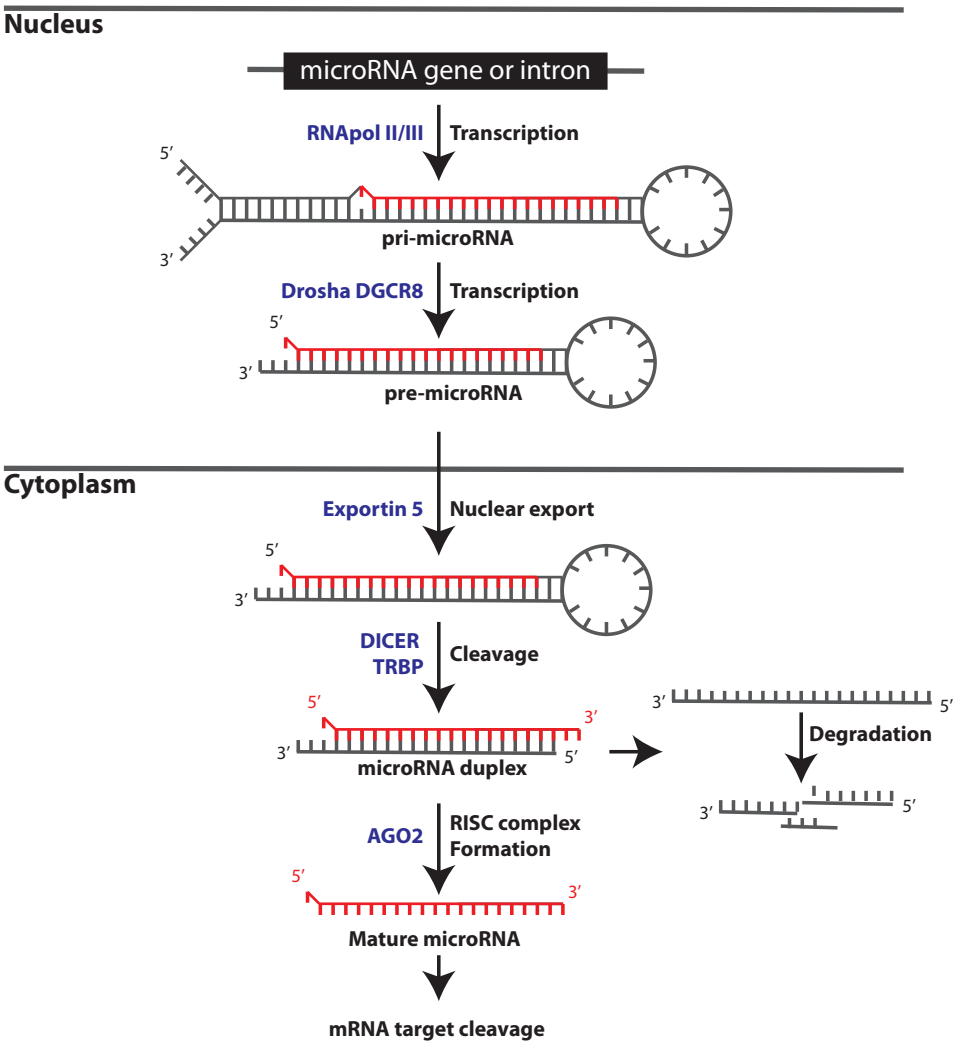

FIGURE 5. Adeno associated virus.

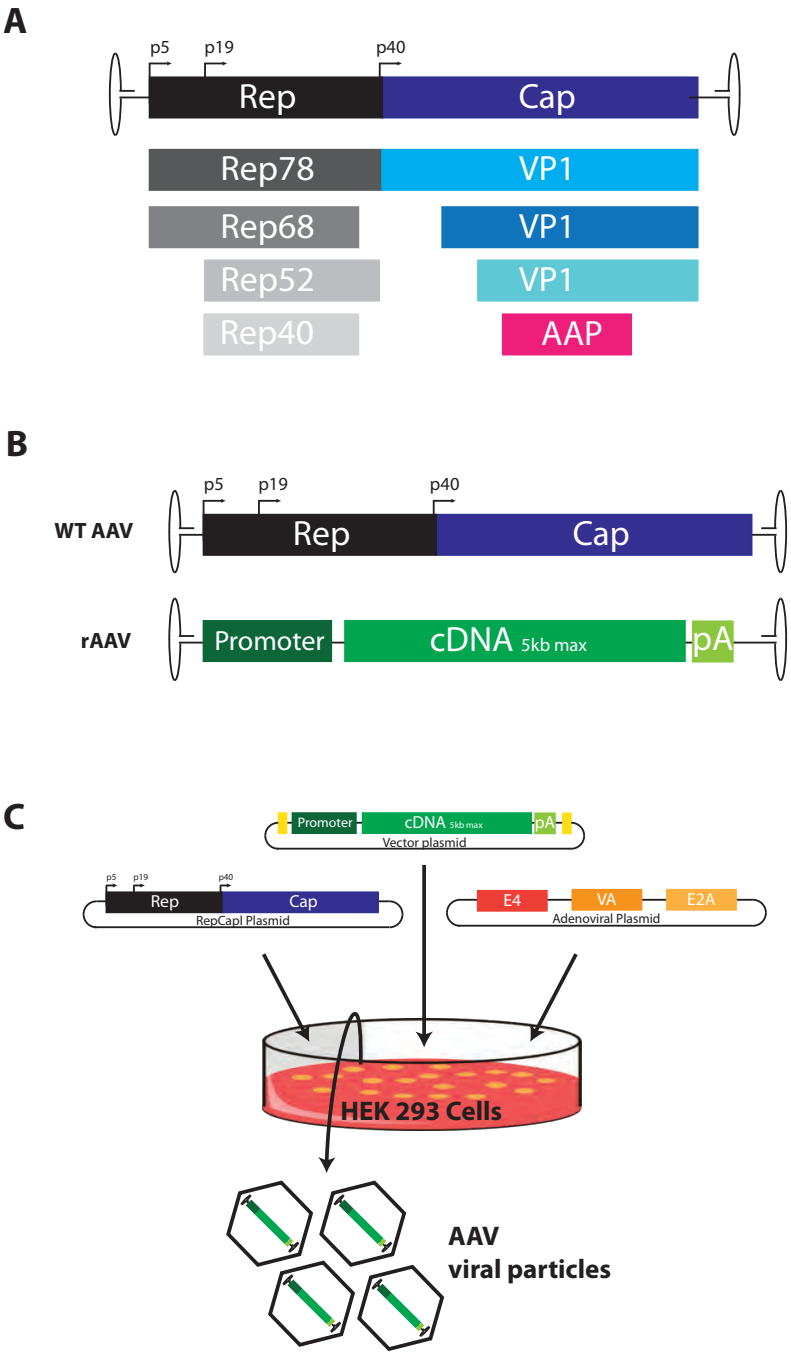

FIGURE 6 High-content screening for microRNAs regulating cardiomyocyte cell size

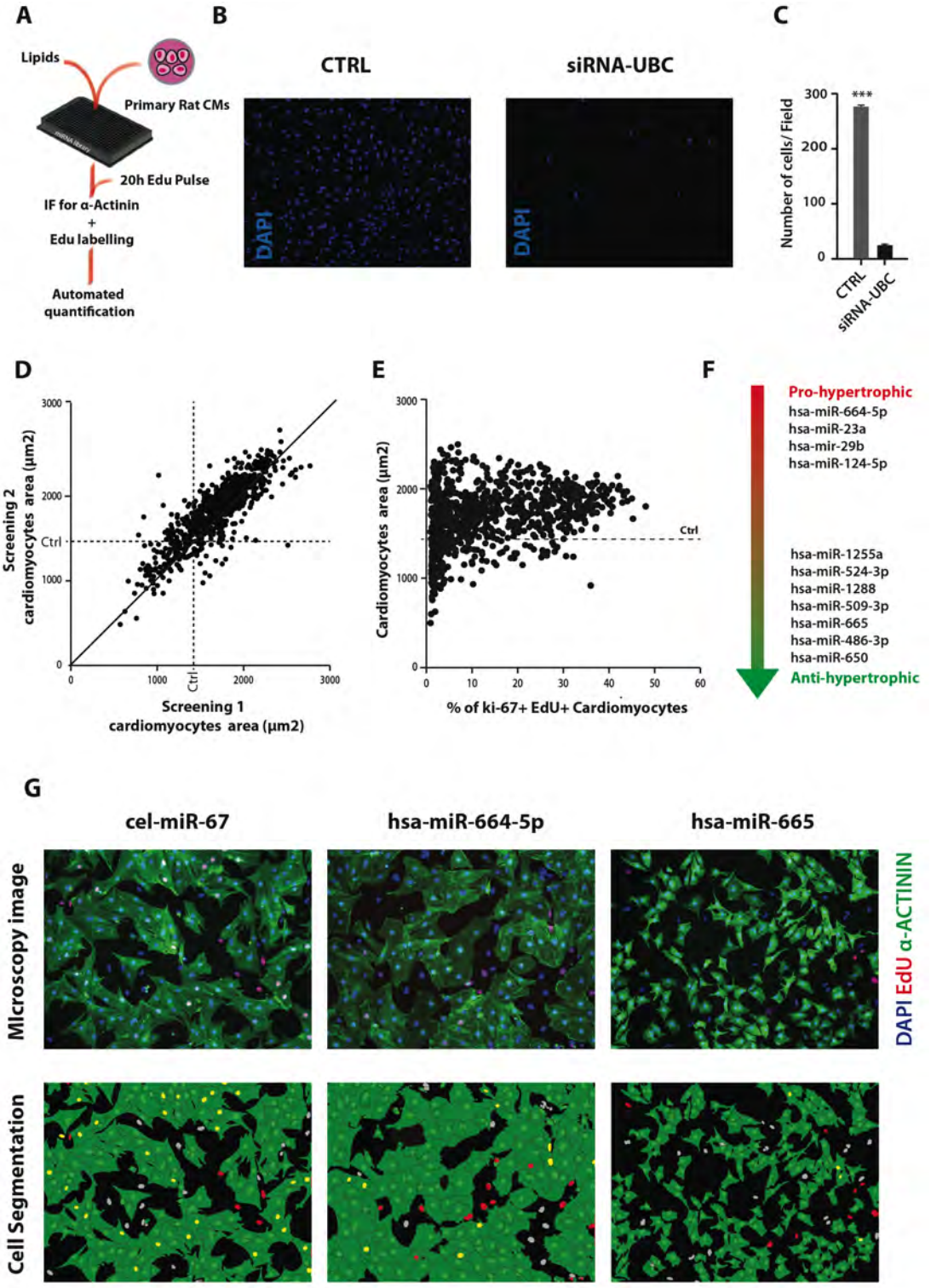

FIGURE 7. Validation of selected microRNAs in rat CMs

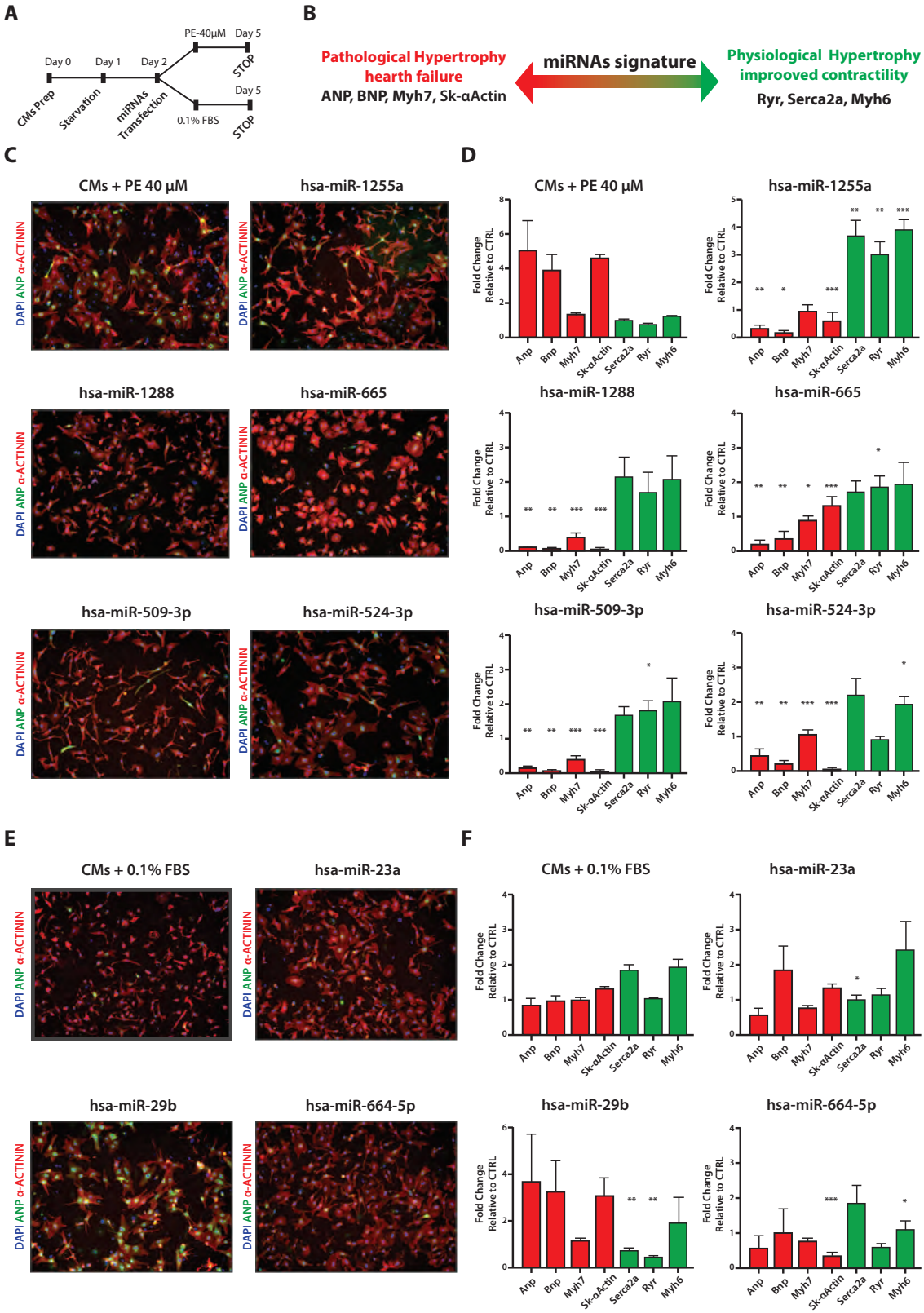

FIGURE 8. Validation of selected anti-hypertrophic microRNAs in mouse CMs

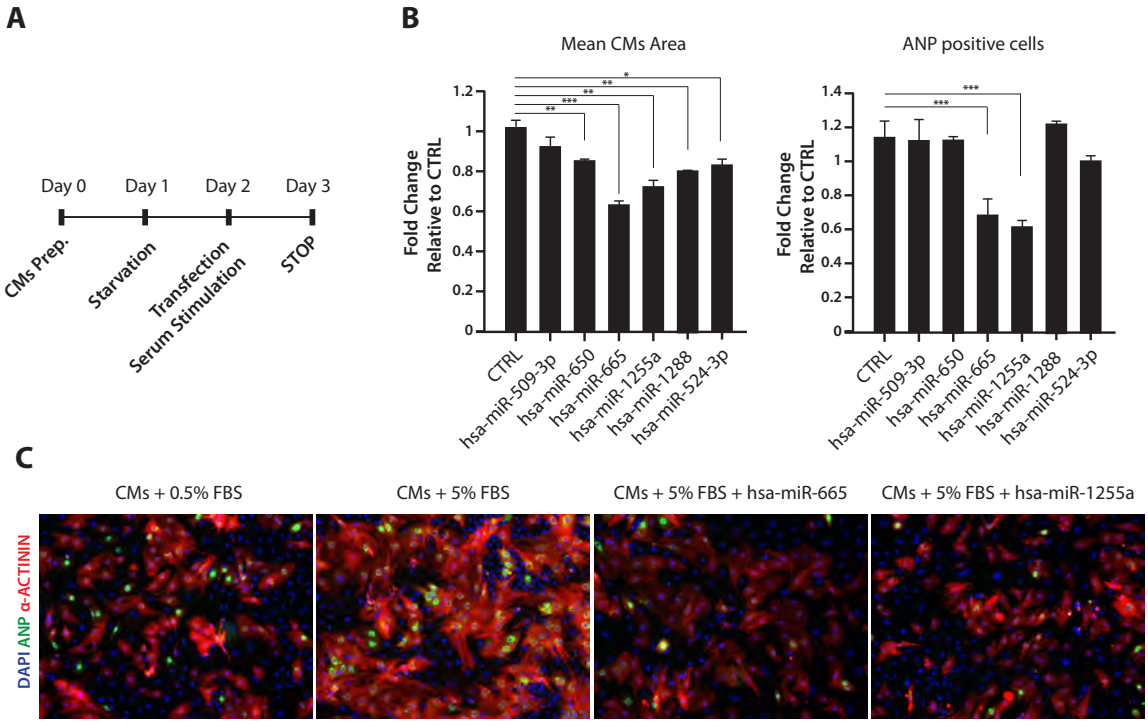

FIGURE 9. Overexpression of hsa-miR-665 in a TAC model of chronic pressure overload

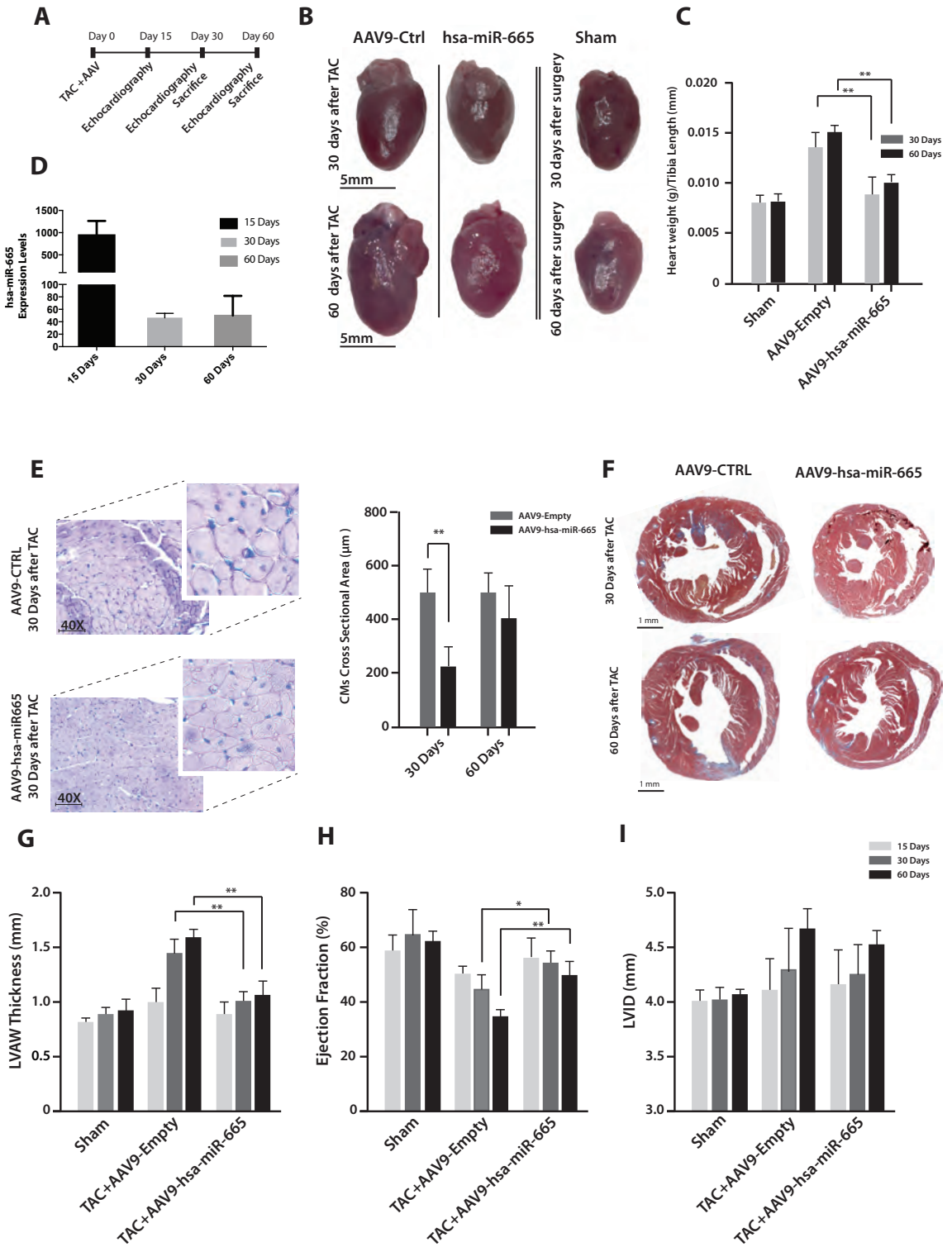
A
Day 0
Day 15
Day 30
Day 60
TAC+AAV
Echocardiography
Echocardiography
Sacrifice
Echocardiography
Sacrifice
B
AAV9-Ctrl
hsa-miR-665
Sham
30 days after TAC
60 days after TAC
30 days after surgery
60 days after surgery
5mm
5mm
C
Heart weight (g)/Tibia Length (mm)
0.020
0.015
0.010
0.005
0
**
**
30 Days
60 Days
Sham
AAV9-Empty
AAV9-hsa-miR-665
D
hsa-miR-665 Expression Levels
1500
1000
500
100
80
60
40
20
0
15 Days
30 Days
60 Days
15 Days
30 Days
60 Days
E
AAV9-CTRL
30 Days after TAC
40X
AAV9-hsa-miR665
30 Days after TAC
40X
CMs Cross Sectional Area (µm)
800
600
400
200
0
**
AAV9-Empty
AAV9-hsa-miR-665
30 Days
60 Days
F
AAV9-CTRL
AAV9-hsa-miR-665
30 Days after TAC
60 Days after TAC
1 mm
1 mm
G
LVAW Thickness (mm)
2.0
1.5
1.0
0.5
0
**
**
Sham
TAC+AAV9-Empty
TAC+AAV9-hsa-miR-665
H
Ejection Fraction (%)
80
60
40
20
0
*
**
Sham
TAC+AAV9-Empty
TAC+AAV9-hsa-miR-665
I
15 Days
30 Days
60 Days
LVID (mm)
5.0
4.5
4.0
3.5
3.0
Sham
TAC+AAV9-Empty
TAC+AAV9-hsa-miR-665

FIGURE 10. Overexpression of hsa-miR-665 on established hypertrophic phenotype

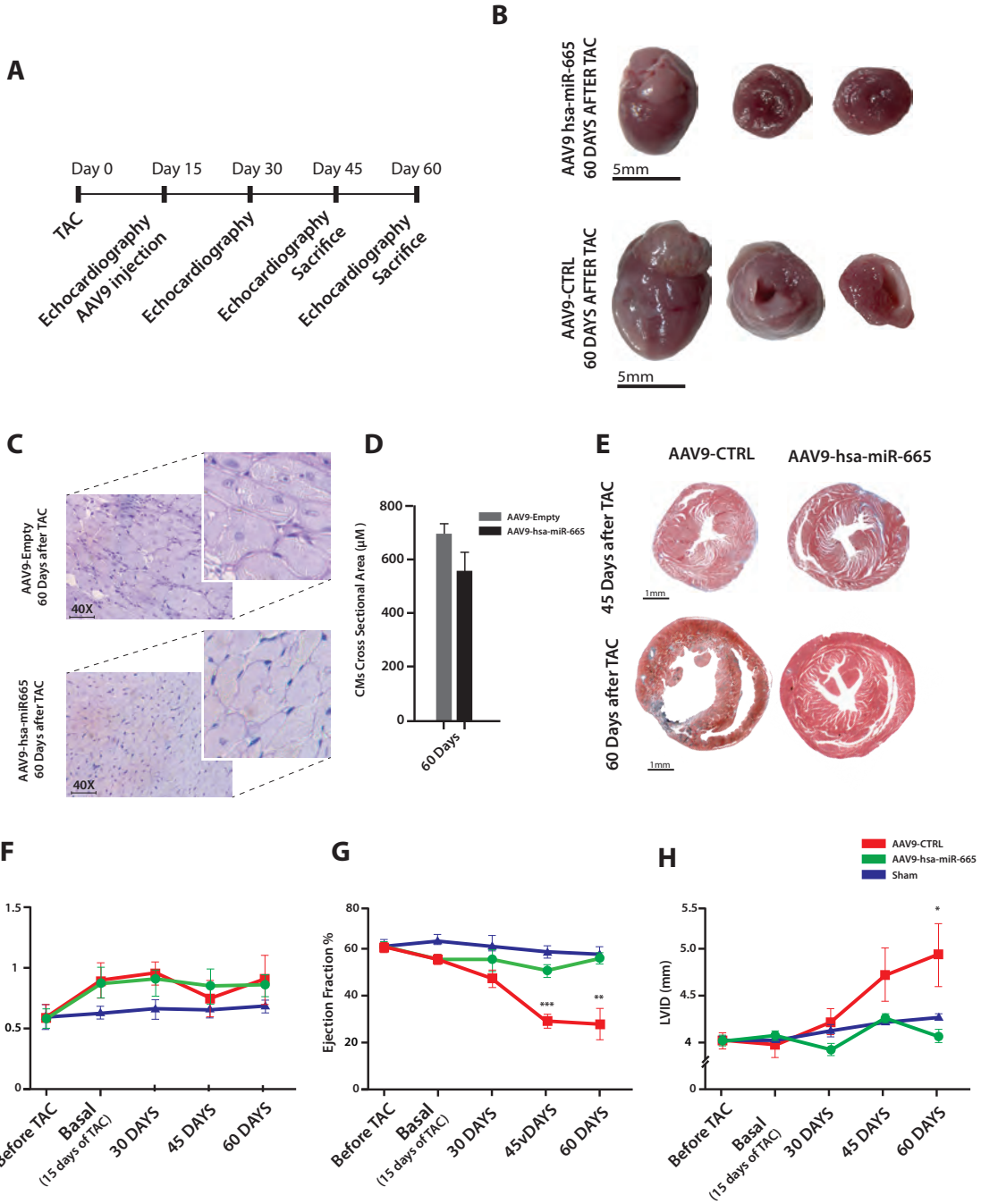

FIGURE 11. mRNAseq analysis

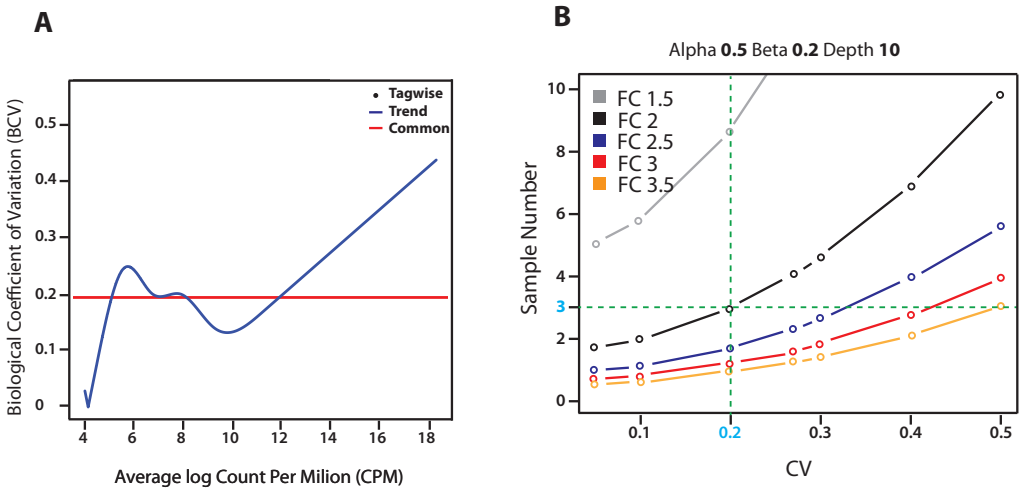

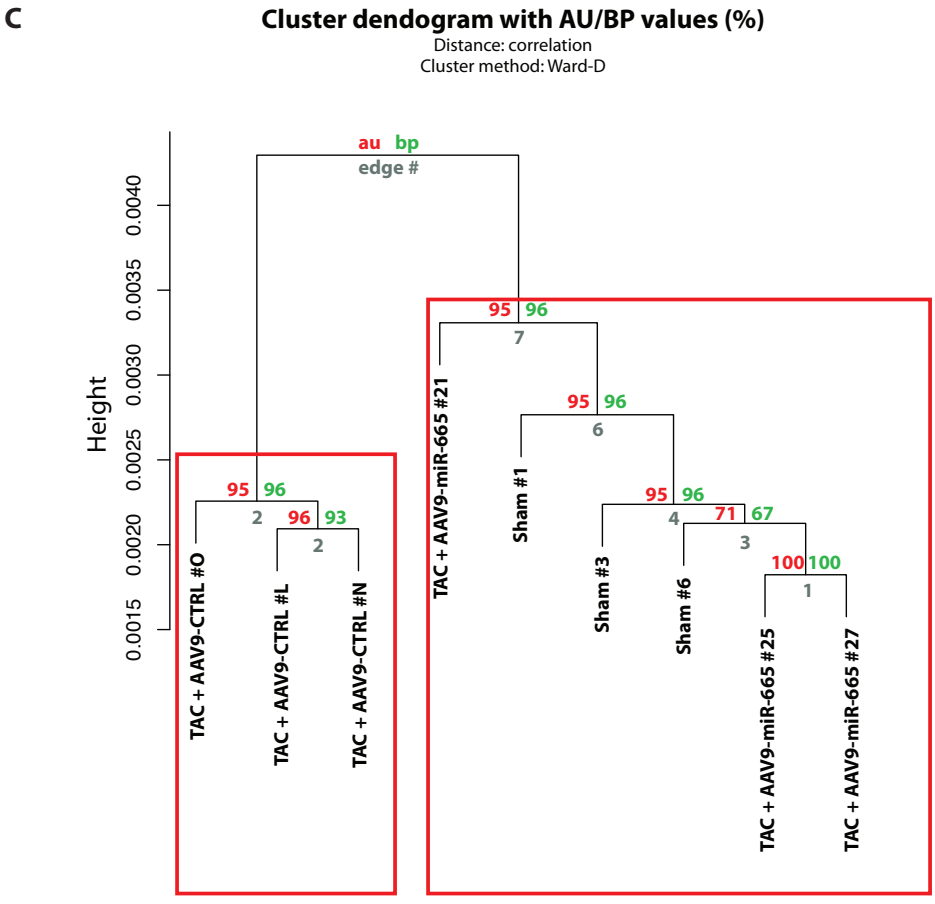

FIGURE 12. The molecular signature of hsa-miR-665

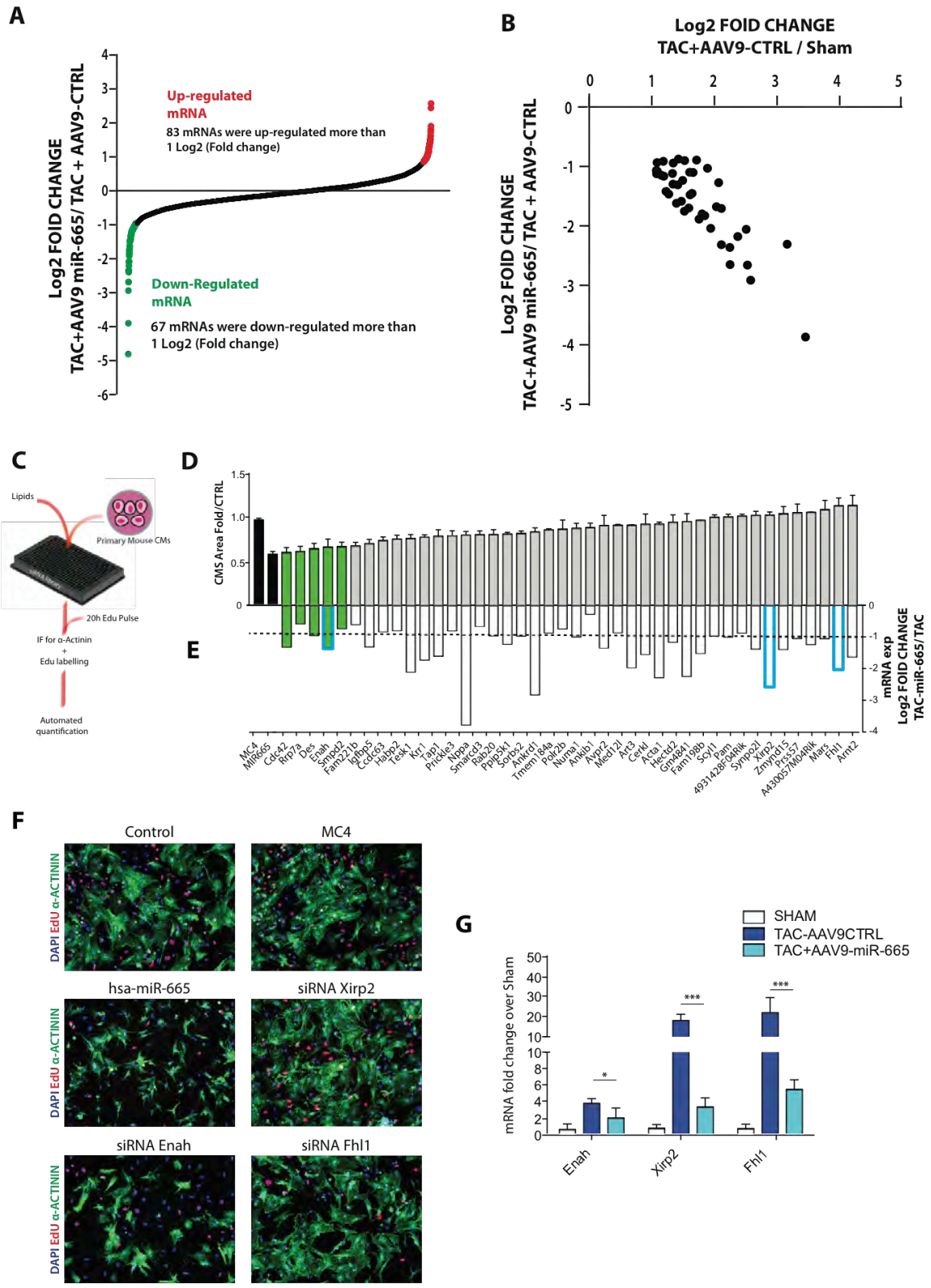

FIGURE 13. Generation of luciferase reporter constructs for 3'UTR binding assay

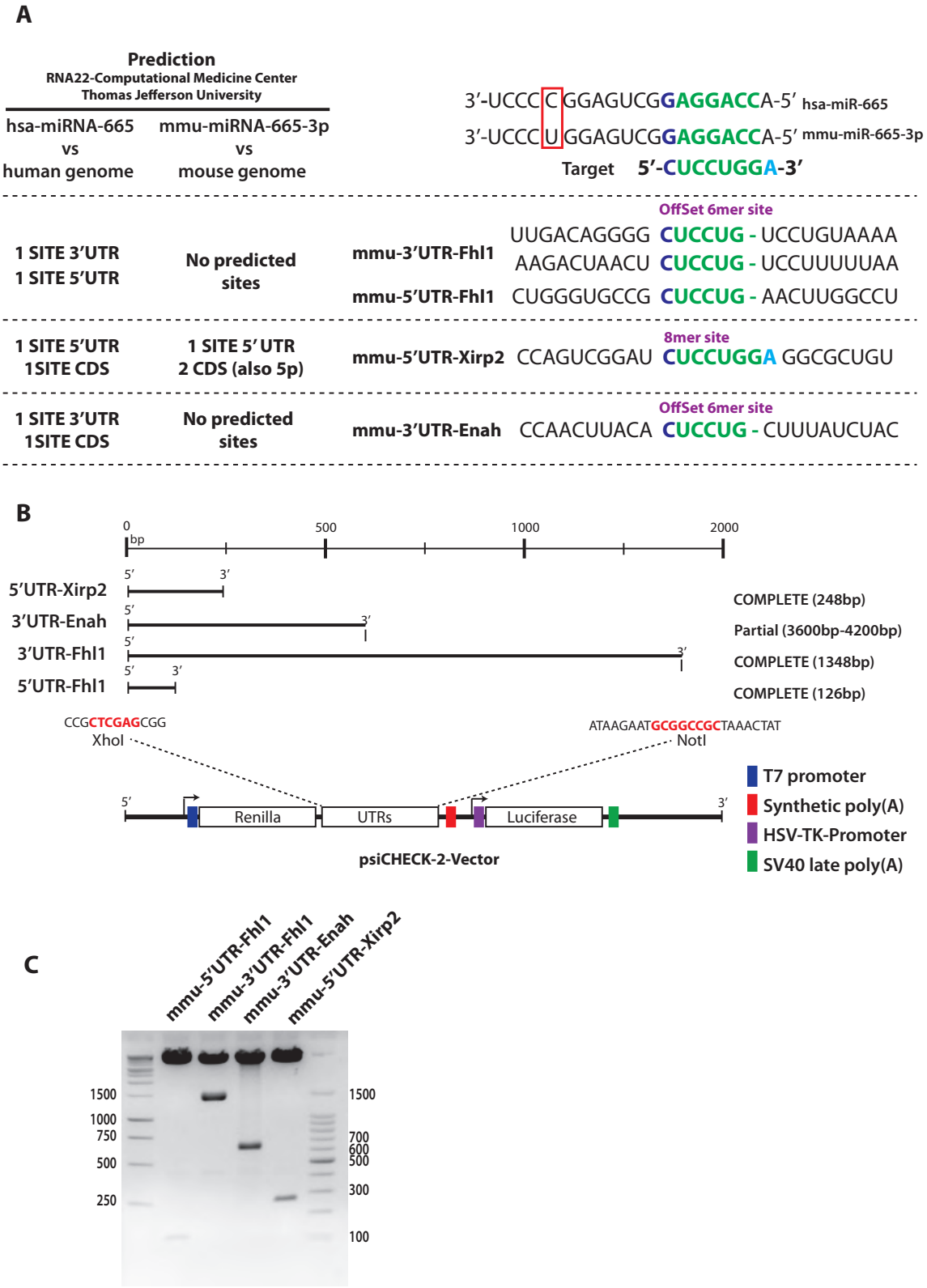

FIGURE 14. Fhl1, Enah and Xirp2 are direct targets of has-miR-665.

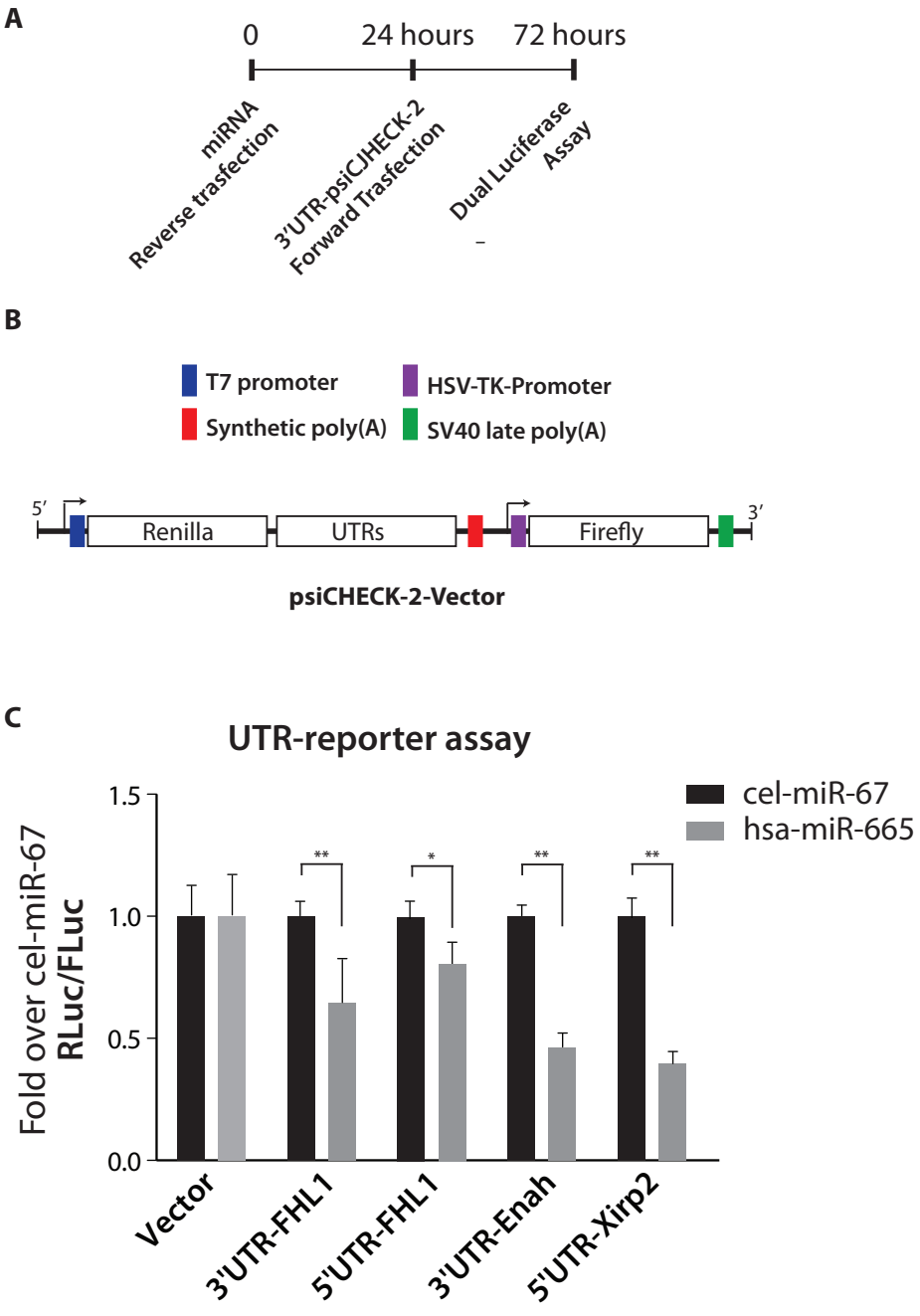

FIGURE 15. The proposed mechanism of action for hsa-miR-665

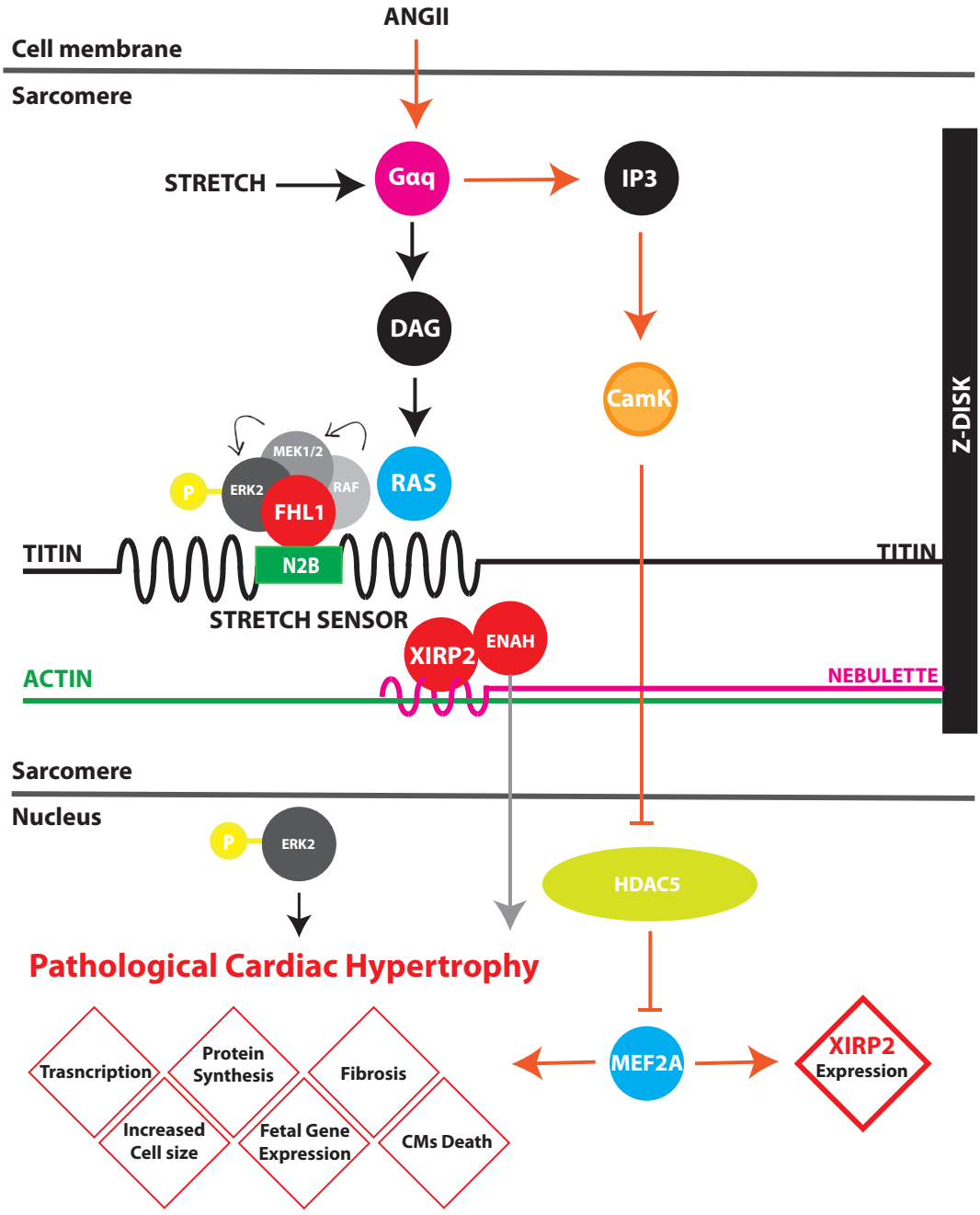

FIGURE LEGENDS

Figure 1. **The structure of the heart**. The heart is a muscular organ that pumps blood through the circulatory system. In mammals, it is composed of four chambers: upper left and right atria; and lower left and right ventricles. Myocardium is the contractile portion of the heart and it is mainly composed of CMs. The contractile activity of CM is based on sarcomeres, which can be defined as highly ordered arrays of thick- and thin-filaments. The sarcomere can shorten its length, under increased level of cytoplasmic Ca^{2+}, thus allowing the CMs to undergo cycles of contraction and relaxation in a Ca^{2+} dependent manner. IDs, which couple CMs activity, permit a coordinated and efficient contraction. (adaoted from [231])

Figure 2. Concentric and eccentric hypertrophy Pressure overload induces concentric hypertrophy by the thickening of the left ventricle wall. Volume overload induces an increase in muscle mass via the addition of sarcomeres in series, leading to eccentric hypertrophy. Both concentric and eccentric hypertrophy are in the beginning to be considered as adaptive and, if the stimulation is prolonged, both induces pathological cardiac remodelling and heart failure (adapted from [11]).

Figure 3. Main pathways involved in cardiac hypertrophy.

A schematic and simplified representation of the major signalling pathways involved in pathological and physiological cardiac hypertrophy. It has to be considered that the molecular mechanism at the basis of cardiac hypertrophy are relying on the integration of multiple signalling cascades and due to their intrinsic complexity is difficult to generate an all encompassing scheme.

Figure 4. The microRNA processing pathway. This figure reports a schematic representation of the microRNA processing pathway. Into the nucleus, primary microRNA are transcribed by RNA polymerase II or III and cleaved by the microprocessor complex Drosha–DGCR8 (Pasha), thus generating a pre-microRNA. The pre-microRNA, is transported by Exportin-5 from the nucleus into the cytoplasm, where the RNase Dicer in complex with TRBP cleaves the hairpin and generates a dsRNA of 20-22 nucleotide termed as mature microRNA. The functional strand of the mature microRNA is loaded

together with Ago2 into the RISC complex. Once loaded, it targets the RISC complex to silence specific transcripts.

Figure 5. Adeno Associated Virus. A, genome structure. **B**, Schematic representation of wt-AAV and r-AAV genome structure. **C**, Schematic representation of the strategy used for the production of rAAV vectors expressing a given gene.

Figure 6. **High-content screening for microRNAs regulating CM cell size**. **A**, Screening workflow; **B-C**, reverse transfection efficiency of rat CMs. Rat CMs were reverse transfected with a toxic siRNA (siRNA targeting Ubiquitin C), and fixed 72 hours later. Nuclei were stained with Hoechst and quantified automatically; **D**, CM area in μm^2 following transfection with 875 microRNAs; approximately 2500 cells were analysed per microRNA/replicate, Ctrl dashed line correspond to CMs transfected with MC4; Correlation between two screening replicates: Spearman coefficient 0.84; **E**, Correlation between CM size and percentage of proliferating cells following treatment with the 875 microRNAs, Ctrl dashed line correspond to CMs transfected with MC4; **F**, list of selected microRNAs modulating CM cell size; **G**, Microscopy images (**α-actinin, EdU, Nuclei**) and image reconstruction of rat CMs treated with control MC4, hsa-miR-665 and has-miR-664-5p. Values show mean±SD of two independent screenings conducted on two independent mouse CM preparations.

Figure 7. Validation of selected microRNAs in rat CMs. **A**, Experimental model; **B**, Known molecular signature of pathological vs physiological hypertrophy; **C**, Immunostaining (**α-actinin, ANP, Nuclei**) of rat CMs treated with selected anti-hypertrophic microRNAs stimulated with 40 μ M PE; **D**. qRT-PCR results of rat CMs treated with selected anti-hypertrophic microRNAs stimulated with 40 μ M PE; **E**, Immunostaining (**α-actinin, ANP, Nuclei**) of rat CMs treated with selected pro-hypertrophic microRNAs; **F**. qRT-PCR results of rat CMs treated with selected anti-hypertrophic microRNAs stimulated with 40μM PE. Values show mean±SD of three independent experiments conducted on three independent mouse CM preparations.

. All conditions were compared to PE-treated CMs using unpaired t-test. *P<0.05, **P<0.01, ***P<0.001

Figure 8. Validation of selected anti-hypertrophic microRNAs in mouse CMs. **A**, Experimental model; **B**, CM area and ANP positive cells, fold change over CTRL (control microRNA#4) following treatment with the selected anti-hypertrophic microRNAs, approximately 2500 cells were analysed per microRNA/replicate; **C**, Immunostaining (**α-actinin, ANP, Nuclei**) of mouse CMs treated with MC4, hsa-miR-665 and hsa-miR-1255a. Values show mean±SD of three independent experiments conducted on three independent mouse CM preparations. All conditions were compared to CTRL using unpaired t-test. *P<0.05, **P<0.01, ***P<0.001

Figure 9. Overexpression of hsa-miR-665 in a TAC model of chronic pressure overload. **A**, sham surgery or thoracic aortic constriction (TAC) was performed in 10 weeks old female CD1 mice. At the same time mice (n=8), which received TAC surgery, were injected with AAV9-hsa-miR-665 or an AAV9 control (1×1011 vg/animal). Heart function was analysed by echocardiography at 15, 30 and 60 days post-TAC, and mice were sacrificed at days 30 or 60 post-TAC for histological analysis. **B**, Whole heart images for sham, AAV9-Empty, AAV9-hsa-miR-665 30 and 60 days after TAC**. C**, Heart mass, reported as ratio of heart weight to tibia length for sham, AAV9-Empty, AAV9-hsa-miR-665, 30 and 60 days after TAC.**D**, qRT-PCR on premiR-hsa-665 expression levels expressed as absolute number of molecules. **E**, Periodic acid–Schiff (PAS) staining of heart sections from mice with the same treatment as in panel B (scale bar, 50 μm). Graphs at right show quantification of cell size as cell surface area. **F**, Masson trichromic staining of heart sections from mice treated as in panel B. Echocardiography measurement of LVAWd - Left Ventricle Anterior Wall thickness during Diastole (**G**), EF - Ejection Fraction (**H**), LVID - Left Ventricle Internal Diameter (**I**) at 30, 45 and 60 days after AAV-control or AAV-miR-665 intra-cardiac injection (1×10^{11} vg/animal). Values represent a mean±SD; n=8animals/group. Two-way ANOVA, Tukey's post-hoc comparison tests *P<0.05, **P<0.01, ***P<0.001..

Figure 10. Overexpression of hsa-miR-665 on established hypertrophic phenotype. **A**, sham surgery or thoracic aortic constriction (TAC) was performed in 10 weeks old female CD1 mice. 15 days after TAC mice (n=8), which received TAC surgery,

were injected with AAV9-hsa-miR-665 or an AAV9 control. heart function was analyzed by echocardiography at 30, 45 and 60 days post-TAC, and mice were sacrificed at days 45 or 60 post-TAC for histological analysis. **B**, Whole heart images for AAV9-Empty and AAV9-hsa-miR-665 60 days after TAC (n=8 per group). **C** , PAS staining of heart sections from mice treated with AAV9-Empty and AAV9-hsa-miR-665 45 and 60 days after TAC (scale bar,50 µm). Graphs at right show quantification of cell size as cell surface area (**D**). **E**, Masson tricromic staining of heart section from mice treated as in panel C. Echocardiography measurement of LVAWd - Left Ventricle Anterior Wall thickness during Diastole (**F**), EF - Ejection Fraction (**G**), LVID - Left Ventricle Internal Diameter (**H**) at 30, 45 and 60 days after AAV-control or AAV-miR-665 intra-cardiac injection (1×10^{11} vg/animal). Values represent a mean±SD; n=8animals/group. Two-way ANOVA, Tukey's post-hoc comparison tests *P<0.05, **P<0.01, ***P<0.001.

Figure 11. mRNAseq. **A**. Determination of the coefficient of variation across replicates. **B**, Rnapower analysis with the biological coefficient of variation. y-axis is reports the number of replicates per group, x-axis reports the coeeficient of variation. Green dashed line indicates the number of replicates used (n=3) and the estimated BCV of 0.2. **C**, Hierarchical cluster analysis using Ward-D method: in red boxes are the samples that resulted in significant clustering (AU≥95%).

Figure 12. The molecular signature of hsa miR-665. A, Log2 Fold change of mRNA **up**/**down** regulated in TAC-mice injected with AAV9-hsa-miR-665 (n=3) over TAC-mice injected with AAV9-Ctrl (n°=3); **B**, The mRNA most upregulated in TAC-mice injected with AAV9-Ctrl (n=3) are the most down-regulated following overexpression of AAV9-hsa-miR-665; **C** siRNA screening workflow; **D**, Effect on mouse CM cell size of selected siRNAs. **F**, **Alpha-actinin** and **EdU** staining of mouse primary CMs treated with hsa-miR-665 and selected siRNAs: Enah, Fhl1 and XIrp2; **G**, Validation of the mRNA level of expression of Enah, Fhl1 and Xirp2 by qRT-PCR, same experimental condition as in A.

Values represent a mean±SD; n=3 animals/group. Two-way ANOVA, Tukey's post-hoc comparison tests *P<0.05, **P<0.01, ***P<0.001.

Figure 13. Generation of luciferase reporter constructs for 3'UTR binding assay. **A,** Comparison between the predicted sequences (RNA22 computational tool by the Computational medicine centre of Thomas Jefferson University) targeted either by hsa-miR-665 or mmu-miR-665-3p in the UTRs of Fhl1, Xirp2 and Enah; **B**, Seed sequences of hsa-miR-665 and mmu-miR-665-3p, and the list of matches found in the UTRs of the selected candidate targets; **C,** UTR cloning strategy into psi-CHECK2-Vector (Promega); **D**, Gel electrophoresis (1.5 % agarose) of the reporter constructs generated as in panel **C** and digested with XhoI and NotI in order to verify correct cloning.

Figure 14. Fhl1, Enah and Xirp2 are direct targets of has-miR-665. **A,** Experimental scheme. **B**, Reporter vector. **C,** 3'-UTR luciferase reporter assays performed in HeLa cells transfected with MC1(cel-miR-67) or hsa-miR-665. Results are shown for the 3'-UTRs of Fhl1, Enah and for the 5'UTRs of Fhl1 and Xirp2, as well as for the empty vector (Vector); Renilla luciferase activity was normalized to that of firefly luciferase. Values represent a mean±SD of three independent experiments. All conditions were compared to cel-miR-67 using unpaired t-test. *P<0.05, **P<0.01, ***P<0.001

Figure 15. The proposed mechanism of action for hsa-miR-665

The hsa-miR-655-induced downregulation of *Fhl1* blocks the pro-hypertrophic signals (i.e. pressure-overload induced hypertrophy or ANGII induced hypertrophy) that rely on phosphorylated ERK2. The downregulation of *Fhl1* increases titin elasticity, thus reducing ventricular wall-stress and consequently protecting IDs morphology and CM functional coupling. The hsa-miR-655-induced downregulation of *Xirp2* and *Enah* reduces the recruitment of *Xirp2* and *Enah* to the IDs, where these proteins are known to promote myofibril formation during cardiac hypertrophic remodelling.

TABLES

Table 1. List of reagents

List of reagents	Supplier
Anti alpha-actinin antibody	Abcam
iQ Supermix	BIO-RAD
Masson's trichrome staining kit	BioOptica
Anti connexin-43 antibody	
35 mm primaria tissue culture dishes	CORNING
100 mm primaria tissue culture dishes	CORNING
microRNAs mimic	Dharmacon
siRNAs smart pool	Dharmacon
siRNA/microRNA resuspension buffer	Dharmacon
Transparent 96 multiwell tissue cultured plates	Falcon
T75 tissue cultured flasks	Falcon
T175 tissue cultured flasks	Falcon
DMEM, low glucose, GlutaMAX™ Supplement, pyruvate	Gibco
DMEM, high glucose, GlutaMAX[a] Supplement, pyruvate	Gibco
Foetal calf serum	Gibco
Primer and Oligos	Integrated DNA Technology
gBLOCKs	Integrated DNA Technology
RNAiMax	Invitrogen
TRIZOL	Invitrogen
Hoechst 33342	Life Technologies
Nucleobond Xra Maxi	Machery Nagel
Anti ANP antibody	Millipore
100 mm tissue cultured dishes	NEST
Restriction Enzymes	NewEnglandBiolabs
ViewPlate-96 Black, Optically Clear Bottom, Tissue Culture Treated, Sterile	PerkynElmer
CellCarrier-384, Black, Ultra Microplates, Collagen type 1-coated, Sterile	PerkynElmer
OptiPlate-96, White Opaque 96-well Microplate	PerkynElmer
FuGENE HD	Promega
Dual-Glo Luciferase Assay System	Promega
Wizard SV MiniPrep system	Promega
RNeasy mini kits	Quiagen
bovine serum albumin (BSA)	Roche
Vitamin B12	Sigma
Trypsin	Sigma
penicillin/streptomycin	Sigma
Phenyephryne	Sigma
PARAFORMALDEHYDE	Sigma
Tryton X-100	Sigma
PAS staining kit	Sigma
Eukitt mounting medium	Sigma
Eukitt mounting medium	Sigma
Ethanol	Sigma
Chloroform	Sigma
Taqman probes for qRT-PCR	Thermo Fisher
Click-IT EdU 594 Imaging kit	ThermoFIsher
EdU	ThermoFIsher
ALEXA-594-α-mouse	ThermoFIsher
ALEXA-488-α-mouse	ThermoFIsher
ALEXA-594-α-Rabbit	ThermoFIsher

Table 2. List of TaqMan probes

Gene	Probe
NPPA	(FAM)-RN00664637_g1
NPPB	(FAM)-RN00676450_g1
MYH7	(FAM)-RN001488777_g1
ACTA-1	(FAM)-RN00570060_g1
ATP2A2	(FAM)-RN00568762_m1
MYH6	(FAM)-RN01489272_g1
RYR	(FAM)-RN01470303_m1
FHL1	(FAM)-Mm04204611_g1
XIRP2	(FAM)-Mm01335343_m1
ENAH	(FAM)-Mm00468746_m1
GAPDH	(FAM)-Rn99999916_s1

Table 3. List and sequences of cherry picked mouse siRNAs

Gene Symbol	Gene Id	Sequence
1110014J01RIK	74778	GAAGUAGACGCAUUCAUGG
1110014J01RIK	74778	GCGGAAUUCACAAGUGGAU
1110014J01RIK	74778	GCUUUCAGGUAGCUUAUGU
1110014J01RIK	74778	UAAAUUCCGACCCUACUGA
1110032E23RIK	68659	CGAGAGAGCAACAUUAGGA
1110032E23RIK	68659	GCGAAGAUAACUUAAACUU
1110032E23RIK	68659	GGACUCAUCUCUAGCAUCU
1110032E23RIK	68659	GGGCUAGAGUAUUACCUAU
4921511C16	330188	CGCAGGAAGCGGACAUUUA
4921511C16	330188	GGACACAAGAGGCCAAUAA
4921511C16	330188	UAACGACCGCUCUGAAUUU
4921511C16	330188	UUAAGAAGAUCAACUGCGA
4930412F15RIK	242408	CAGCCAAUAUCCCAGAGUA
4930412F15RIK	242408	CCAGACAGGUAUCUACAUU
4930412F15RIK	242408	GGACAUUUGUUGAGAGAAC
4930412F15RIK	242408	GUAAACACACUCACGAAGA
4931428F04Rik	74356	AAGCGAGGACAGACGGAUA
4931428F04Rik	74356	GGUUAUAGACAGACGCUCU
4931428F04Rik	74356	CGCAGUACGUGCAGGACGA
4931428F04Rik	74356	AUAGUGUGCUGUUUCGAAA
6720401E04RIK	101706	CAGCUACGCUCCUUUCUUG
6720401E04RIK	101706	GAACGGAGCCGCUUUGAAG
6720401E04RIK	101706	GGACGGCCAUUCUCUAGUA
6720401E04RIK	101706	GGACUUAAGUAUUGACAGC
A430057M04RIK	319486	CGUACGACAGGAAGGAAGA
A430057M04RIK	319486	CUUCAAUGCUACUGCGCUA
A430057M04RIK	319486	GAACUGCGUCGGGUGAAAU
A430057M04RIK	319486	GGUCACGUGUGCUGGAGUA
ACTA1	11459	CAGCCUUCCUUUAUCGGUA
ACTA1	11459	CAGCUGAACGUGAGAUUGU
ACTA1	11459	CGGGAGAAGAUGACUCAAA
ACTA1	11459	GCAAUGAGCGUUUCCGUUG
Ankib1	70797	GGAGUAUGCUGCCUUAGAC
Ankib1	70797	GACAAACGAUACCUACAGU
Ankib1	70797	GUCUGUGGCUGUUAACUAA
Ankib1	70797	GCCAUAGGCUCAUCUUUAC
ANKRD1	107765	CCACCGAGCAUGCUUAGAA
ANKRD1	107765	CGUCUGCGAUGAGUAUAAA
ANKRD1	107765	GAACCGCUAUAAGAUGAUU
ANKRD1	107765	UCGCAUAGCUACAUUCUGA
ARNT2	11864	CAACGGGACAGAACAUAUC
ARNT2	11864	GGAAUGGACUUCGAUGACG
ARNT2	11864	GGAGAUGGCGUCAGACAUA
ARNT2	11864	GUGAAGGUCCCAGUAAAUU
ART3	109979	CGAAGACGGUACAUCUAUA
ART3	109979	CGACAGCGUUGUUUUAAUA
ART3	109979	GAACGCGUUUGACGACGAA

Gene Symbol	Gene Id	Sequence
ART3	109979	GAGACGACCUUGCGAGAAA
AVPR2	12000	CAUCUUUGCUCAACGUGAU
AVPR2	12000	GCAGAUGGUGGGCAUGUAU
AVPR2	12000	GGAGUUGCGUAGCCUGCUU
AVPR2	12000	UGACCGAGACCCGCUGUUA
AW111922	60440	CAAGAUAUAUUCAGGAGUU
AW111922	60440	CUCAAGAGAUCCUCAAUUU
AW111922	60440	GGAUUUGGCUGGAAGGAUU
AW111922	60440	UAUCACAGAUUCAGUCAUU
B430315C20RIK	327655	GAAGGGUGCUCCAUGGUAC
B430315C20RIK	327655	GAGCGUGACUUUCGACAAA
B430315C20RIK	327655	GGUCACUUCUCAGGUAUUA
B430315C20RIK	327655	UAAAUGAACCUGUGGAGAA
BC019731	231832	GACCUUGUGCUUCCAAUAU
BC019731	231832	GAGAAACGCAUGCUGAUUC
BC019731	231832	GAGGAAUGCGUCAGGGUUU
BC019731	231832	UAAGAAGAGUCGCAACAUA
CDC42	12540	CGGAAUAUGUACCAACUGU
CDC42	12540	GACUACGACCGCUAAGUUA
CDC42	12540	GCAGUCACAGUUAUGAUUG
CDC42	12540	UCUAGUAUGUUUCUCAGUG
Cerkl	228094	GAAUGUAGAUGGUGACUUA
Cerkl	228094	GCUUGAAGGAGCAACGGAA
Cerkl	228094	CCCAAAGAGUAAUAGCAAU
Cerkl	228094	AAGCAUGGCUCUUAGGGUU
DES	13346	CAACUUGGCUGCCUUCCGA
DES	13346	GGAGAUCGCGUUCCUUAAG
DES	13346	GUGACAACCUGAUAGACGA
DES	13346	UGACUCAGGCAGCCAAUAA
ENAH	13800	GACAGAAGGCCUUGACUAU
ENAH	13800	GAGAACGACUAGAACGAGA
ENAH	13800	GCACUAAUUUGCGAUGUAU
ENAH	13800	GCAGAAAGAUUCAAGACCA
FHL1	14199	CGGAGAAGUUCGACUGUCA
FHL1	14199	GAGACCAGAACGUGGAGUA
FHL1	14199	GCAAGAUCCUGUGCAACAA
FHL1	14199	GGAGGUGCAUUAUAAGAAU
Gm4841	225594	CUUUAUACUAGCCGAUCUA
Gm4841	225594	UGUUGAAAUGUAAGGAGGA
Gm4841	225594	GCCAGUAGUAGUAGAAUAA
Gm4841	225594	GCGAGAAGGAUGUAGUAGU
HABP2	226243	AGACGGAGAUCCAGGUUUA
HABP2	226243	GCAAAUACCCUUACACGGG
HABP2	226243	GCAGGAGACUUAUAACAUG
HABP2	226243	GUAAGACAGUCAACCAGAA
HECTD2	226098	GACGACUUGUGCCAGGUUA
HECTD2	226098	GAUCAGAGUACACCAGUAG
HECTD2	226098	GUAUUGAAGGGAAUCAUUA
HECTD2	226098	UCAUGGGACUAGCUGUUUA

Gene Symbol	Gene Id	Sequence
HRB2	52705	CGAAAUACCGCGAGGCUUA
HRB2	52705	CGGAGGAAGUUAAGCUCAA
HRB2	52705	CUACCGAAACUAAGAUUGA
HRB2	52705	UGAACAGGCAGUACGGAUA
IGFBP5	16011	AAGAAGGACCGCAGAAAGA
IGFBP5	16011	CGCAAAGGAUUCUACAAGA
IGFBP5	16011	GAUGAGACAGGAAUCCGAA
IGFBP5	16011	UUUCCGAGCUGAAGGCUGA
LMO6	54630	CAGGACACCUCAACCGAAA
LMO6	54630	CCACACCGCUCACAACUUC
LMO6	54630	CGGAGCAGGUUUACCAGUU
LMO6	54630	GCACAUGGGUCACUUCUGC
Mars	216443	CGGGAUGCCUUGCGCAGUA
Mars	216443	GGCCUAACCCCACGGGAAA
Mars	216443	AGUGCAAUCUGCCGAUAUU
Mars	216443	GAGCCCUGGAAACGGAUUA
Med12l	329650	CAGCAUAUUGGCCGAGAAA
Med12l	329650	CCAAGAUCGGUGCGUAUUU
Med12l	329650	AGGAAUGUUUGACACGGUA
Med12l	329650	UCGCAAAGGCAACGAUAGA
Nppa	230899	ACACAGAUCUGAUGGAUUU
Nppa	230899	CGAUAGAUCUGCCCUCUUG
Nppa	230899	CCUCGGAGCCUACGAAGAU
Nppa	230899	GGGUAGGAUUGACAGGAUU
PAM	18484	CAAUGCAUGUGUUUGCCUA
PAM	18484	GAUGGAAAUUAUUGGGUCA
PAM	18484	GCAAGUUCGUUUACCAACA
PAM	18484	GCGGGCAUGUACCUUAUGA
POLR2B	231329	GCGCAGAAGUUUAUUGAUC
POLR2B	231329	GGACGAUGACGGUUUGAUA
POLR2B	231329	GGGCAGAUCUCGUGAUGGU
POLR2B	231329	GUUAAGAAAUCUCACGUAU
Prss57	73106	CAGCAGACAUUUAGCAUUG
Prss57	73106	AACGAUAUCUGCCUGCUAA
Prss57	73106	UCAUGUGGCUCCCUGGUUG
Prss57	73106	CUGUGAGGCUAUUACGAUU
RAB20	19332	CCGCUAUCAUCCUUACAUA
RAB20	19332	GCAGUGGCGUUCCUUCAAC
RAB20	19332	GGUGGUACCUAUGAUCAUG
RAB20	19332	UGCCAAGACUGGAUACAAU
SCYL1	78891	CCAAAUCCCUGGUGACCCA
SCYL1	78891	CUUCGUGUAUGAUGUGAAA
SCYL1	78891	GAAGAUUUCUGUCGACACA
SCYL1	78891	GAGCUGAGCAAGAGUCUAG
SMARCD3	66993	CAGAGGGACUUCAUGCUAA
SMARCD3	66993	CAUCAAUGGCGACAAGUAU
SMARCD3	66993	GAUCAAACCAUCAUGCGGA
SMARCD3	66993	GCCGCUACUUCUACUGUAA
SMPD2	20598	CAGCAUGUCUACAGUCUGA

Gene Symbol	Gene Id	Sequence
SMPD2	20598	CCCAAGAACUGCUACGUCA
SMPD2	20598	CUACGUGACUCAUCUACAU
SMPD2	20598	GAUGCACACUACUUCAGAA
Sorbs2	234214	CUACAGACCUCUUUCGAAA
Sorbs2	234214	GAAAGACAUUUGCGACCAA
Sorbs2	234214	CAGAAGUGCAUCACGGGAA
Sorbs2	234214	GCUUCUUACACUCGAUUUA
SYNPO2L	68760	AGACAGAUAGUGAUGUUGA
SYNPO2L	68760	CAGCUAUGCUUAAUGGGCA
SYNPO2L	68760	GAAAUACUCACCCAACAUC
SYNPO2L	68760	GGUACCACCUCAGUGAUUU
TAP1	21354	CCGCAUCACUGACUGGAUU
TAP1	21354	GACAAGAGCCGCUGCUAUU
TAP1	21354	GUGCAGGAGUCUCUAGCAA
TAP1	21354	UGAAAGGCCUUGUGGAGUU
TESK1	21754	GACCUCCCCUCAACAAUAA
TESK1	21754	GGAGAGCUGUAUGAUGAGA
TESK1	21754	GGGAAAUGACUGUCCGCUA
TESK1	21754	GUUCCACCAUCACCACUUA
Xirp2	241431	GUAAAGAACUACACUCAUA
Xirp2	241431	GAGAGGAGCUUAUGCAAAU
Xirp2	241431	GCAUAUCCAUCCAGAGUUA
Xirp2	241431	GGAAAGGCGUGCAAAGAAA
Zmynd15	574428	GCAAGGAAUUCGAUCUCGU
Zmynd15	574428	GAAGACUGAUUGUCGGAAC
Zmynd15	574428	CUGGAUACCGAGACGAGUU
Zmynd15	574428	GCCCAAGGCUCUCAGCGUU

Table 4. RNAseq data

ID	hgnc_symbol	Entrez ID	log2FoldChange hsa-miR-665 vs Ctrl	pvalue
ENSMUSG00000014837.11	4931428F04Rik	74356	-0.864829	1.06E-04
ENSMUSG00000090564.5	A430057M04Rik	NA	-1.2309023	9.35E-08
ENSMUSG00000031972.4	Acta1	11459	-2.2855283	7.23E-12
ENSMUSG00000040351.8	Ankib1	70797	-0.2675715	5.74E-01
ENSMUSG00000024803.8	Ankrd1	107765	-2.8310012	7.57E-29
ENSMUSG00000015709.8	Arnt2	11864	-1.6305396	1.47E-05
ENSMUSG00000034842.13	Art3	109979	-1.9655713	1.18E-05
ENSMUSG00000031390.8	Avpr2	12000	-1.3408918	9.13E-05
ENSMUSG00000043036.10	Ccdc63	330188	-0.8242056	2.50E-04
ENSMUSG00000006699.14	Cdc42	12540	-1.3171401	8.90E-04
ENSMUSG00000075256.6	Cerkl	228094	-1.5412429	5.37E-05
ENSMUSG00000026208.9	Des	13346	-0.9472144	1.89E-04
ENSMUSG00000022995.13	Enah	13800	-1.3645253	1.71E-04
ENSMUSG00000027955.13	Fam198b	68659	-1.5108667	6.96E-05
ENSMUSG00000043633.6	Fam221b	242408	-0.5971324	5.78E-05
ENSMUSG00000023092.13	Fhl1	14199	-2.0311443	1.19E-12
ENSMUSG00000068606.5	Gm4841	225594	-2.2443904	2.51E-06
ENSMUSG00000025075.11	Habp2	226243	-0.7896597	2.12E-04
ENSMUSG00000041180.10	Hectd2	226098	-1.1561911	1.60E-05
ENSMUSG00000026185.8	Igfbp5	16011	-1.3097495	4.48E-06
ENSMUSG00000063334.13	Krr1	52705	-1.7243245	7.69E-05
ENSMUSG00000040354.11	Mars	216443	-1.0467266	2.56E-04
ENSMUSG00000056476.10	Med12l	329650	-0.8566621	2.89E-04
ENSMUSG00000041616.9	Nppa	230899	-3.7894475	6.42E-34
ENSMUSG00000066306.9	Numa1	101706	-0.9891489	1.45E-03
ENSMUSG00000026335.13	Pam	18484	-0.9936884	1.22E-04
ENSMUSG00000029250.5	Polr2b	231329	-0.7333303	7.18E-04
ENSMUSG00000033526.13	Ppip5k1	327655	-1.2198184	3.55E-04
ENSMUSG00000031145.12	Prickle3	54630	-0.7954645	8.64E-05
ENSMUSG00000020323.11	Prss57	73106	-1.0416156	1.54E-06
ENSMUSG00000031504.5	Rab20	19332	-0.9538548	3.58E-04
ENSMUSG00000018040.6	Rrp7a	74778	-0.5738517	2.33E-04
ENSMUSG00000024941.8	Scyl1	78891	-0.9593912	3.14E-05
ENSMUSG00000028949.10	Smarcd3	66993	-0.6519333	1.30E-04
ENSMUSG00000019822.9	Smpd2	20598	-0.7261175	1.77E-04
ENSMUSG00000031626.13	Sorbs2	234214	-0.9637293	1.48E-03
ENSMUSG00000039376.10	Synpo2l	68760	-1.3764994	1.51E-03
ENSMUSG00000037321.14	Tap1	21354	-1.6035044	4.34E-04
ENSMUSG00000028458.9	Tesk1	21754	-2.1044271	6.29E-06
ENSMUSG00000036687.10	Tmem184a	231832	-0.8635794	3.81E-05
ENSMUSG00000027022.10	Xirp2	241431	-2.5783339	9.97E-24
ENSMUSG00000040829.11	Zmynd15	574428	-1.388588	1.97E-04

BIBLIOGRAPHY

Citations

1. Venes, D. and C.W. Taber, *Taber's cyclopedic medical dictionary*. 2017, [Place of publication not identified]: F A Davis.
2. Moorman, A., et al., *Development of the heart: (1) formation of the cardiac chambers and arterial trunks.* Heart, 2003. **89**(7): p. 806-14.
3. Bettex, D.A., R. Pretre, and P.G. Chassot, *Is our heart a well-designed pump? The heart along animal evolution.* Eur Heart J, 2014. **35**(34): p. 2322-32.
4. Moore, K.L., A.F. Dalley, and A.M.R. Agur, *Clinically oriented anatomy*. 2014.
5. Ehler, E., *Cardiac cytoarchitecture - why the "hardware" is important for heart function!* Biochim Biophys Acta, 2016. **1863**(7 Pt B): p. 1857-63.
6. Vermij, S.H., H. Abriel, and T.A. van Veen, *Refining the molecular organization of the cardiac intercalated disc.* Cardiovasc Res, 2017.
7. LeWinter, M.M., et al., *Cardiac titin: structure, functions and role in disease.* Clin Chim Acta, 2007. **375**(1-2): p. 1-9.
8. Anderson, R.H., et al., *The anatomy of the cardiac conduction system.* Clin Anat, 2009. **22**(1): p. 99-113.
9. Olson, E.N., *A decade of discoveries in cardiac biology.* Nat Med, 2004. **10**(5): p. 467-74.
10. Berenji, K., et al., *Does load-induced ventricular hypertrophy progress to systolic heart failure?* Am J Physiol Heart Circ Physiol, 2005. **289**(1): p. H8-H16.
11. Bernardo, B.C., et al., *Molecular distinction between physiological and pathological cardiac hypertrophy: experimental findings and therapeutic strategies.* Pharmacol Ther, 2010. **128**(1): p. 191-227.
12. Haider, A.W., et al., *Increased left ventricular mass and hypertrophy are associated with increased risk for sudden death.* J Am Coll Cardiol, 1998. **32**(5): p. 1454-9.
13. Ahuja, P., P. Sdek, and W.R. MacLellan, *Cardiac myocyte cell cycle control in development, disease, and regeneration.* Physiol Rev, 2007. **87**(2): p. 521-44.
14. Maillet, M., J.H. van Berlo, and J.D. Molkentin, *Molecular basis of physiological heart growth: fundamental concepts and new players.* Nat Rev Mol Cell Biol, 2013. **14**(1): p. 38-48.
15. Maron, B.J. and A. Pelliccia, *The heart of trained athletes: cardiac remodeling and the risks of sports, including sudden death.* Circulation, 2006. **114**(15): p. 1633-44.
16. Eghbali, M., et al., *Heart hypertrophy during pregnancy: a better functioning heart?* Trends Cardiovasc Med, 2006. **16**(8): p. 285-91.
17. Frey, N. and E.N. Olson, *Cardiac hypertrophy: the good, the bad, and the ugly.* Annu Rev Physiol, 2003. **65**: p. 45-79.
18. Iemitsu, M., et al., *Physiological and pathological cardiac hypertrophy induce different molecular phenotypes in the rat.* Am J Physiol Regul Integr Comp Physiol, 2001. **281**(6): p. R2029-36.

19. Garciarena, C.D., et al., *Endurance training in the spontaneously hypertensive rat: conversion of pathological into physiological cardiac hypertrophy.* Hypertension, 2009. **53**(4): p. 708-14.
20. van Bilsen, M., F.A. van Nieuwenhoven, and G.J. van der Vusse, *Metabolic remodelling of the failing heart: beneficial or detrimental?* Cardiovasc Res, 2009. **81**(3): p. 420-8.
21. Weiner, R.B. and A.L. Baggish, *Exercise-induced cardiac remodeling.* Prog Cardiovasc Dis, 2012. **54**(5): p. 380-6.
22. Hefti, M.A., et al., *Signaling pathways in cardiac myocyte hypertrophy.* J Mol Cell Cardiol, 1997. **29**(11): p. 2873-92.
23. Wettschureck, N., et al., *Absence of pressure overload induced myocardial hypertrophy after conditional inactivation of Galphaq/Galpha11 in cardiomyocytes.* Nat Med, 2001. **7**(11): p. 1236-40.
24. Nicol, R.L., N. Frey, and E.N. Olson, *From the sarcomere to the nucleus: role of genetics and signaling in structural heart disease.* Annu Rev Genomics Hum Genet, 2000. **1**: p. 179-223.
25. Zimmerman, B.G. and E.W. Dunham, *Tissue renin-angiotensin system: a site of drug action?* Annu Rev Pharmacol Toxicol, 1997. **37**: p. 53-69.
26. Lorell, B.H., *Role of angiotensin AT1, and AT2 receptors in cardiac hypertrophy and disease.* Am J Cardiol, 1999. **83**(12A): p. 48H-52H.
27. Paradis, P., et al., *Overexpression of angiotensin II type I receptor in cardiomyocytes induces cardiac hypertrophy and remodeling.* Proc Natl Acad Sci U S A, 2000. **97**(2): p. 931-6.
28. Masaki, H., et al., *Cardiac-specific overexpression of angiotensin II AT2 receptor causes attenuated response to AT1 receptor-mediated pressor and chronotropic effects.* J Clin Invest, 1998. **101**(3): p. 527-35.
29. Zou, Y., et al., *Mechanical stress activates angiotensin II type 1 receptor without the involvement of angiotensin II.* Nat Cell Biol, 2004. **6**(6): p. 499-506.
30. Gu, X. and S.P. Bishop, *Increased protein kinase C and isozyme redistribution in pressure-overload cardiac hypertrophy in the rat.* Circ Res, 1994. **75**(5): p. 926-31.
31. Inagaki, K., et al., *Tissue angiotensin II during progression or ventricular hypertrophy to heart failure in hypertensive rats; differential effects on PKC epsilon and PKC beta.* J Mol Cell Cardiol, 2002. **34**(10): p. 1377-85.
32. Pass, J.M., et al., *PKCepsilon activation induces dichotomous cardiac phenotypes and modulates PKCepsilon-RACK interactions and RACK expression.* Am J Physiol Heart Circ Physiol, 2001. **280**(3): p. H946-55.
33. Takeishi, Y., et al., *Transgenic overexpression of constitutively active protein kinase C epsilon causes concentric cardiac hypertrophy.* Circ Res, 2000. **86**(12): p. 1218-23.
34. Wakasaki, H., et al., *Targeted overexpression of protein kinase C beta2 isoform in myocardium causes cardiomyopathy.* Proc Natl Acad Sci U S A, 1997. **94**(17): p. 9320-5.
35. Rolfe, M., et al., *Activation of protein synthesis in cardiomyocytes by the hypertrophic agent phenylephrine requires the activation of ERK and involves phosphorylation of tuberous sclerosis complex 2 (TSC2).* Biochem J, 2005. **388**(Pt 3): p. 973-84.
36. Rundqvist, B., et al., *Increased cardiac adrenergic drive precedes generalized sympathetic activation in human heart failure.* Circulation, 1997. **95**(1): p. 169-75.
37. Hall, S.A., et al., *Time course of improvement in left ventricular function, mass and geometry in patients with congestive heart failure treated with beta-adrenergic blockade.* J Am Coll Cardiol, 1995. **25**(5): p. 1154-61.

38. Eichhorn, E.J. and M.R. Bristow, *Medical therapy can improve the biological properties of the chronically failing heart. A new era in the treatment of heart failure.* Circulation, 1996. **94**(9): p. 2285-96.
39. Molenaar, P., et al., *Both beta(2)- and beta(1)-adrenergic receptors mediate hastened relaxation and phosphorylation of phospholamban and troponin I in ventricular myocardium of Fallot infants, consistent with selective coupling of beta(2)-adrenergic receptors to G(s)-protein.* Circulation, 2000. **102**(15): p. 1814-21.
40. Miyashita, Y., et al., *Redistribution of intracellular Ca2+ stores after beta-adrenergic stimulation of rat tail artery SMC.* Am J Physiol, 1997. **272**(1 Pt 2): p. H244-55.
41. Meszaros, J.G., et al., *Identification of G protein-coupled signaling pathways in cardiac fibroblasts: cross talk between G(q) and G(s).* Am J Physiol Cell Physiol, 2000. **278**(1): p. C154-62.
42. Kuschel, M., et al., *beta2-adrenergic cAMP signaling is uncoupled from phosphorylation of cytoplasmic proteins in canine heart.* Circulation, 1999. **99**(18): p. 2458-65.
43. Xiao, R.P., et al., *Beta 2-adrenergic receptor-stimulated increase in cAMP in rat heart cells is not coupled to changes in Ca2+ dynamics, contractility, or phospholamban phosphorylation.* J Biol Chem, 1994. **269**(29): p. 19151-6.
44. Rybin, V.O., et al., *Differential targeting of beta -adrenergic receptor subtypes and adenylyl cyclase to cardiomyocyte caveolae. A mechanism to functionally regulate the cAMP signaling pathway.* J Biol Chem, 2000. **275**(52): p. 41447-57.
45. Jurevicius, J. and R. Fischmeister, *cAMP compartmentation is responsible for a local activation of cardiac Ca2+ channels by beta-adrenergic agonists.* Proc Natl Acad Sci U S A, 1996. **93**(1): p. 295-9.
46. Xiao, R.P., X. Ji, and E.G. Lakatta, *Functional coupling of the beta 2-adrenoceptor to a pertussis toxin-sensitive G protein in cardiac myocytes.* Mol Pharmacol, 1995. **47**(2): p. 322-9.
47. Engelhardt, S., et al., *Progressive hypertrophy and heart failure in beta1-adrenergic receptor transgenic mice.* Proc Natl Acad Sci U S A, 1999. **96**(12): p. 7059-64.
48. Au, D.H., et al., *Risk of mortality and heart failure exacerbations associated with inhaled beta-adrenoceptor agonists among patients with known left ventricular systolic dysfunction.* Chest, 2003. **123**(6): p. 1964-9.
49. Hawkins, N.M., et al., *Baseline characteristics and outcomes of patients with heart failure receiving bronchodilators in the CHARM programme.* Eur J Heart Fail, 2010. **12**(6): p. 557-65.
50. Eschenhagen, T., et al., *Increased messenger RNA level of the inhibitory G protein alpha subunit Gi alpha-2 in human end-stage heart failure.* Circ Res, 1992. **70**(4): p. 688-96.
51. Ruan, H., et al., *Gi alpha 1-mediated cardiac electrophysiological remodeling and arrhythmia in hypertrophic cardiomyopathy.* Circulation, 2007. **116**(6): p. 596-605.
52. McCloskey, D.T., et al., *Expression of a Gi-coupled receptor in the heart causes impaired Ca2+ handling, myofilament injury, and dilated cardiomyopathy.* Am J Physiol Heart Circ Physiol, 2008. **294**(1): p. H205-12.
53. Klee, C.B., T.H. Crouch, and M.H. Krinks, *Calcineurin: a calcium- and calmodulin-binding protein of the nervous system.* Proc Natl Acad Sci U S A, 1979. **76**(12): p. 6270-3.
54. Heineke, J. and J.D. Molkentin, *Regulation of cardiac hypertrophy by intracellular signalling pathways.* Nat Rev Mol Cell Biol, 2006. **7**(8): p. 589-600.
55. Molkentin, J.D., et al., *A calcineurin-dependent transcriptional pathway for cardiac hypertrophy.* Cell, 1998. **93**(2): p. 215-28.

56. Sussman, M.A., et al., *Prevention of cardiac hypertrophy in mice by calcineurin inhibition.* Science, 1998. **281**(5383): p. 1690-3.
57. Kee, H.J. and H. Kook, *Roles and targets of class I and IIa histone deacetylases in cardiac hypertrophy.* J Biomed Biotechnol, 2011. **2011**: p. 928326.
58. Johnson, C.A. and B.M. Turner, *Histone deacetylases: complex transducers of nuclear signals.* Semin Cell Dev Biol, 1999. **10**(2): p. 179-88.
59. Zhang, C.L., et al., *Class II histone deacetylases act as signal-responsive repressors of cardiac hypertrophy.* Cell, 2002. **110**(4): p. 479-88.
60. Zhang, Y., et al., *Receptor-independent protein kinase C alpha (PKCalpha) signaling by calpain-generated free catalytic domains induces HDAC5 nuclear export and regulates cardiac transcription.* J Biol Chem, 2011. **286**(30): p. 26943-51.
61. Monovich, L., et al., *A novel kinase inhibitor establishes a predominant role for protein kinase D as a cardiac class IIa histone deacetylase kinase.* FEBS Lett, 2010. **584**(3): p. 631-7.
62. Kee, H.J., et al., *Inhibition of histone deacetylation blocks cardiac hypertrophy induced by angiotensin II infusion and aortic banding.* Circulation, 2006. **113**(1): p. 51-9.
63. Adams, T.E., et al., *Structure and function of the type 1 insulin-like growth factor receptor.* Cell Mol Life Sci, 2000. **57**(7): p. 1050-93.
64. Toker, A. and L.C. Cantley, *Signalling through the lipid products of phosphoinositide-3-OH kinase.* Nature, 1997. **387**(6634): p. 673-6.
65. Delaughter, M.C., et al., *Local insulin-like growth factor I expression induces physiologic, then pathologic, cardiac hypertrophy in transgenic mice.* FASEB J, 1999. **13**(14): p. 1923-9.
66. McMullen, J.R., et al., *The insulin-like growth factor 1 receptor induces physiological heart growth via the phosphoinositide 3-kinase(p110alpha) pathway.* J Biol Chem, 2004. **279**(6): p. 4782-93.
67. Shioi, T., et al., *The conserved phosphoinositide 3-kinase pathway determines heart size in mice.* EMBO J, 2000. **19**(11): p. 2537-48.
68. Luo, J., et al., *Class IA phosphoinositide 3-kinase regulates heart size and physiological cardiac hypertrophy.* Mol Cell Biol, 2005. **25**(21): p. 9491-502.
69. Lu, Z., et al., *Loss of cardiac phosphoinositide 3-kinase p110 alpha results in contractile dysfunction.* Circulation, 2009. **120**(4): p. 318-25.
70. Kim, J., et al., *Insulin-like growth factor I receptor signaling is required for exercise-induced cardiac hypertrophy.* Mol Endocrinol, 2008. **22**(11): p. 2531-43.
71. Jones, P.F., et al., *Molecular cloning and identification of a serine/threonine protein kinase of the second-messenger subfamily.* Proc Natl Acad Sci U S A, 1991. **88**(10): p. 4171-5.
72. DeBosch, B., et al., *Akt2 regulates cardiac metabolism and cardiomyocyte survival.* J Biol Chem, 2006. **281**(43): p. 32841-51.
73. McMullen, J.R., et al., *Phosphoinositide 3-kinase(p110alpha) plays a critical role for the induction of physiological, but not pathological, cardiac hypertrophy.* Proc Natl Acad Sci U S A, 2003. **100**(21): p. 12355-60.
74. DeBosch, B., et al., *Akt1 is required for physiological cardiac growth.* Circulation, 2006. **113**(17): p. 2097-104.
75. Condorelli, G., et al., *Akt induces enhanced myocardial contractility and cell size in vivo in transgenic mice.* Proc Natl Acad Sci U S A, 2002. **99**(19): p. 12333-8.
76. Zhai, P., et al., *Glycogen synthase kinase-3alpha reduces cardiac growth and pressure overload-induced cardiac hypertrophy by inhibition of extracellular signal-regulated kinases.* J Biol Chem, 2007. **282**(45): p. 33181-91.

77. Matsuda, T., et al., *Distinct roles of GSK-3alpha and GSK-3beta phosphorylation in the heart under pressure overload.* Proc Natl Acad Sci U S A, 2008. **105**(52): p. 20900-5.
78. Jabbar, A., et al., *Thyroid hormones and cardiovascular disease.* Nat Rev Cardiol, 2017. **14**(1): p. 39-55.
79. He, H., et al., *Overexpression of the rat sarcoplasmic reticulum Ca2+ ATPase gene in the heart of transgenic mice accelerates calcium transients and cardiac relaxation.* J Clin Invest, 1997. **100**(2): p. 380-9.
80. Rohrer, D.K., R. Hartong, and W.H. Dillmann, *Influence of thyroid hormone and retinoic acid on slow sarcoplasmic reticulum Ca2+ ATPase and myosin heavy chain alpha gene expression in cardiac myocytes. Delineation of cis-active DNA elements that confer responsiveness to thyroid hormone but not to retinoic acid.* J Biol Chem, 1991. **266**(13): p. 8638-46.
81. Kiss, E., et al., *Thyroid hormone-induced alterations in phospholamban protein expression. Regulatory effects on sarcoplasmic reticulum Ca2+ transport and myocardial relaxation.* Circ Res, 1994. **75**(2): p. 245-51.
82. Kahaly, G.J. and W.H. Dillmann, *Thyroid hormone action in the heart.* Endocr Rev, 2005. **26**(5): p. 704-28.
83. Kenessey, A. and K. Ojamaa, *Thyroid hormone stimulates protein synthesis in the cardiomyocyte by activating the Akt-mTOR and p70S6K pathways.* J Biol Chem, 2006. **281**(30): p. 20666-72.
84. Kim, S., et al., *Angiotensin II induces cardiac phenotypic modulation and remodeling in vivo in rats.* Hypertension, 1995. **25**(6): p. 1252-9.
85. Ruf, S., M. Piper, and K.D. Schluter, *Specific role for the extracellular signal-regulated kinase pathway in angiotensin II- but not phenylephrine-induced cardiac hypertrophy in vitro.* Pflugers Arch, 2002. **443**(3): p. 483-90.
86. Rosenkranz, S., *TGF-beta1 and angiotensin networking in cardiac remodeling.* Cardiovasc Res, 2004. **63**(3): p. 423-32.
87. Rockman, H.A., et al., *Segregation of atrial-specific and inducible expression of an atrial natriuretic factor transgene in an in vivo murine model of cardiac hypertrophy.* Proc Natl Acad Sci U S A, 1991. **88**(18): p. 8277-81.
88. Tarnavski, O., et al., *Mouse cardiac surgery: comprehensive techniques for the generation of mouse models of human diseases and their application for genomic studies.* Physiol Genomics, 2004. **16**(3): p. 349-60.
89. Kebir, S., et al., *Sarcomeric lesions and remodeling proximal to intercalated disks in overload-induced cardiac hypertrophy.* Exp Cell Res, 2016. **348**(1): p. 95-105.
90. Wang, Y., U. Wisloff, and O.J. Kemi, *Animal models in the study of exercise-induced cardiac hypertrophy.* Physiol Res, 2010. **59**(5): p. 633-44.
91. Hunt, S.A., C. American College of, and G. American Heart Association Task Force on Practice, *ACC/AHA 2005 guideline update for the diagnosis and management of chronic heart failure in the adult: a report of the American College of Cardiology/American Heart Association Task Force on Practice Guidelines (Writing Committee to Update the 2001 Guidelines for the Evaluation and Management of Heart Failure).* J Am Coll Cardiol, 2005. **46**(6): p. e1-82.
92. Jessup, M., et al., *2009 focused update: ACCF/AHA Guidelines for the Diagnosis and Management of Heart Failure in Adults: a report of the American College of Cardiology Foundation/American Heart Association Task Force on Practice Guidelines: developed in collaboration with the International Society for Heart and Lung Transplantation.* Circulation, 2009. **119**(14): p. 1977-2016.

93. Ambrosy, A.P., et al., *The global health and economic burden of hospitalizations for heart failure: lessons learned from hospitalized heart failure registries.* J Am Coll Cardiol, 2014. **63**(12): p. 1123-33.
94. Reddy, Y.N. and B.A. Borlaug, *Heart Failure With Preserved Ejection Fraction.* Curr Probl Cardiol, 2016. **41**(4): p. 145-88.
95. Fukuta, H., et al., *Statin therapy may be associated with lower mortality in patients with diastolic heart failure: a preliminary report.* Circulation, 2005. **112**(3): p. 357-63.
96. Kitzman, D.W., et al., *Pathophysiological characterization of isolated diastolic heart failure in comparison to systolic heart failure.* JAMA, 2002. **288**(17): p. 2144-50.
97. Bursi, F., et al., *Systolic and diastolic heart failure in the community.* JAMA, 2006. **296**(18): p. 2209-16.
98. Gladden, J.D., W.A. Linke, and M.M. Redfield, *Heart failure with preserved ejection fraction.* Pflugers Arch, 2014. **466**(6): p. 1037-53.
99. Writing Committee, M., et al., *2013 ACCF/AHA guideline for the management of heart failure: a report of the American College of Cardiology Foundation/American Heart Association Task Force on practice guidelines.* Circulation, 2013. **128**(16): p. e240-327.
100. Paulus, W.J. and C. Tschope, *A novel paradigm for heart failure with preserved ejection fraction: comorbidities drive myocardial dysfunction and remodeling through coronary microvascular endothelial inflammation.* J Am Coll Cardiol, 2013. **62**(4): p. 263-71.
101. Hidalgo, C., et al., *PKC phosphorylation of titin's PEVK element: a novel and conserved pathway for modulating myocardial stiffness.* Circ Res, 2009. **105**(7): p. 631-8, 17 p following 638.
102. Yamasaki, R., et al., *Protein kinase A phosphorylates titin's cardiac-specific N2B domain and reduces passive tension in rat cardiac myocytes.* Circ Res, 2002. **90**(11): p. 1181-8.
103. Sheikh, F., et al., *An FHL1-containing complex within the cardiomyocyte sarcomere mediates hypertrophic biomechanical stress responses in mice.* J Clin Invest, 2008. **118**(12): p. 3870-80.
104. Rapp, J.P. and H. Dene, *Development and characteristics of inbred strains of Dahl salt-sensitive and salt-resistant rats.* Hypertension, 1985. **7**(3 Pt 1): p. 340-9.
105. Doi, R., et al., *Development of different phenotypes of hypertensive heart failure: systolic versus diastolic failure in Dahl salt-sensitive rats.* J Hypertens, 2000. **18**(1): p. 111-20.
106. Klotz, S., et al., *Development of heart failure in chronic hypertensive Dahl rats: focus on heart failure with preserved ejection fraction.* Hypertension, 2006. **47**(5): p. 901-11.
107. Murase, T., et al., *Cardiac remodeling and diastolic dysfunction in DahlS.Z-Lepr(fa)/Lepr(fa) rats: a new animal model of metabolic syndrome.* Hypertens Res, 2012. **35**(2): p. 186-93.
108. Xu, Z., et al., *Pravastatin attenuates left ventricular remodeling and diastolic dysfunction in angiotensin II-induced hypertensive mice.* J Cardiovasc Pharmacol, 2008. **51**(1): p. 62-70.
109. Mori, J., et al., *Agonist-induced hypertrophy and diastolic dysfunction are associated with selective reduction in glucose oxidation: a metabolic contribution to heart failure with normal ejection fraction.* Circ Heart Fail, 2012. **5**(4): p. 493-503.
110. Bartel, D.P., *MicroRNAs: target recognition and regulatory functions.* Cell, 2009. **136**(2): p. 215-33.

111. Van Wynsberghe, P.M., et al., *Analysis of microRNA expression and function.* Methods Cell Biol, 2011. **106**: p. 219-52.
112. Grosshans, H. and F.J. Slack, *Micro-RNAs: small is plentiful.* J Cell Biol, 2002. **156**(1): p. 17-21.
113. Yekta, S., I.H. Shih, and D.P. Bartel, *MicroRNA-directed cleavage of HOXB8 mRNA.* Science, 2004. **304**(5670): p. 594-6.
114. Mallory, A.C. and H. Vaucheret, *MicroRNAs: something important between the genes.* Curr Opin Plant Biol, 2004. **7**(2): p. 120-5.
115. Tuschl, T., et al., *Targeted mRNA degradation by double-stranded RNA in vitro.* Genes Dev, 1999. **13**(24): p. 3191-7.
116. Llave, C., et al., *Endogenous and silencing-associated small RNAs in plants.* Plant Cell, 2002. **14**(7): p. 1605-19.
117. Liu, J., et al., *Argonaute2 is the catalytic engine of mammalian RNAi.* Science, 2004. **305**(5689): p. 1437-41.
118. Bagga, S., et al., *Regulation by let-7 and lin-4 miRNAs results in target mRNA degradation.* Cell, 2005. **122**(4): p. 553-63.
119. Liu, J., et al., *MicroRNA-dependent localization of targeted mRNAs to mammalian P-bodies.* Nat Cell Biol, 2005. **7**(7): p. 719-23.
120. Cougot, N., S. Babajko, and B. Seraphin, *Cytoplasmic foci are sites of mRNA decay in human cells.* J Cell Biol, 2004. **165**(1): p. 31-40.
121. Lee, R.C., R.L. Feinbaum, and V. Ambros, *The C. elegans heterochronic gene lin-4 encodes small RNAs with antisense complementarity to lin-14.* Cell, 1993. **75**(5): p. 843-54.
122. Brennecke, J., et al., *bantam encodes a developmentally regulated microRNA that controls cell proliferation and regulates the proapoptotic gene hid in Drosophila.* Cell, 2003. **113**(1): p. 25-36.
123. Cimmino, A., et al., *miR-15 and miR-16 induce apoptosis by targeting BCL2.* Proc Natl Acad Sci U S A, 2005. **102**(39): p. 13944-9.
124. Chen, X., *A microRNA as a translational repressor of APETALA2 in Arabidopsis flower development.* Science, 2004. **303**(5666): p. 2022-5.
125. Pillai, R.S., et al., *Inhibition of translational initiation by Let-7 MicroRNA in human cells.* Science, 2005. **309**(5740): p. 1573-6.
126. Thomson, D.W., C.P. Bracken, and G.J. Goodall, *Experimental strategies for microRNA target identification.* Nucleic Acids Res, 2011. **39**(16): p. 6845-53.
127. Barwari, T., A. Joshi, and M. Mayr, *MicroRNAs in Cardiovascular Disease.* J Am Coll Cardiol, 2016. **68**(23): p. 2577-2584.
128. Hata, A., *Functions of microRNAs in cardiovascular biology and disease.* Annu Rev Physiol, 2013. **75**: p. 69-93.
129. Creemers, E.E., A.J. Tijsen, and Y.M. Pinto, *Circulating microRNAs: novel biomarkers and extracellular communicators in cardiovascular disease?* Circ Res, 2012. **110**(3): p. 483-95.
130. Bernardo, B.C., et al., *miRNA therapeutics: a new class of drugs with potential therapeutic applications in the heart.* Future Med Chem, 2015. **7**(13): p. 1771-92.
131. Zhao, Y., et al., *Dysregulation of cardiogenesis, cardiac conduction, and cell cycle in mice lacking miRNA-1-2.* Cell, 2007. **129**(2): p. 303-17.
132. Liu, N., et al., *microRNA-133a regulates cardiomyocyte proliferation and suppresses smooth muscle gene expression in the heart.* Genes Dev, 2008. **22**(23): p. 3242-54.
133. Eulalio, A., et al., *Functional screening identifies miRNAs inducing cardiac regeneration.* Nature, 2012. **492**(7429): p. 376-81.

134. Li, Q., et al., *Attenuation of microRNA-1 derepresses the cytoskeleton regulatory protein twinfilin-1 to provoke cardiac hypertrophy.* J Cell Sci, 2010. **123**(Pt 14): p. 2444-52.
135. Care, A., et al., *MicroRNA-133 controls cardiac hypertrophy.* Nat Med, 2007. **13**(5): p. 613-8.
136. van Rooij, E., et al., *A signature pattern of stress-responsive microRNAs that can evoke cardiac hypertrophy and heart failure.* Proc Natl Acad Sci U S A, 2006. **103**(48): p. 18255-60.
137. da Costa Martins, P.A., et al., *MicroRNA-199b targets the nuclear kinase Dyrk1a in an auto-amplification loop promoting calcineurin/NFAT signalling.* Nat Cell Biol, 2010. **12**(12): p. 1220-7.
138. Ucar, A., et al., *The miRNA-212/132 family regulates both cardiac hypertrophy and cardiomyocyte autophagy.* Nat Commun, 2012. **3**: p. 1078.
139. Nagalingam, R.S., et al., *A cardiac-enriched microRNA, miR-378, blocks cardiac hypertrophy by targeting Ras signaling.* J Biol Chem, 2013. **288**(16): p. 11216-32.
140. Gladka, M.M., P.A. da Costa Martins, and L.J. De Windt, *Small changes can make a big difference - microRNA regulation of cardiac hypertrophy.* J Mol Cell Cardiol, 2012. **52**(1): p. 74-82.
141. van Rooij, E., et al., *Dysregulation of microRNAs after myocardial infarction reveals a role of miR-29 in cardiac fibrosis.* Proc Natl Acad Sci U S A, 2008. **105**(35): p. 13027-32.
142. Thum, T., et al., *MicroRNA-21 contributes to myocardial disease by stimulating MAP kinase signalling in fibroblasts.* Nature, 2008. **456**(7224): p. 980-4.
143. van Rooij, E., et al., *Control of stress-dependent cardiac growth and gene expression by a microRNA.* Science, 2007. **316**(5824): p. 575-9.
144. Montgomery, R.L., et al., *Therapeutic inhibition of miR-208a improves cardiac function and survival during heart failure.* Circulation, 2011. **124**(14): p. 1537-47.
145. McCarthy, J.J., *MicroRNA-206: the skeletal muscle-specific myomiR.* Biochim Biophys Acta, 2008. **1779**(11): p. 682-91.
146. Ikeda, S., et al., *MicroRNA-1 negatively regulates expression of the hypertrophy-associated calmodulin and Mef2a genes.* Mol Cell Biol, 2009. **29**(8): p. 2193-204.
147. Dong, D.L., et al., *Reciprocal repression between microRNA-133 and calcineurin regulates cardiac hypertrophy: a novel mechanism for progressive cardiac hypertrophy.* Hypertension, 2010. **55**(4): p. 946-52.
148. Luo, X., et al., *Down-regulation of miR-1/miR-133 contributes to re-expression of pacemaker channel genes HCN2 and HCN4 in hypertrophic heart.* J Biol Chem, 2008. **283**(29): p. 20045-52.
149. Wang, D., et al., *Activation of cardiac gene expression by myocardin, a transcriptional cofactor for serum response factor.* Cell, 2001. **105**(7): p. 851-62.
150. Wang, K., et al., *miR-9 and NFATc3 regulate myocardin in cardiac hypertrophy.* J Biol Chem, 2010. **285**(16): p. 11903-12.
151. Porrello, E.R., et al., *MiR-15 family regulates postnatal mitotic arrest of cardiomyocytes.* Circ Res, 2011. **109**(6): p. 670-9.
152. Busk, P.K. and S. Cirera, *MicroRNA profiling in early hypertrophic growth of the left ventricle in rats.* Biochem Biophys Res Commun, 2010. **396**(4): p. 989-93.
153. Atchison, R.W., B.C. Casto, and W.M. Hammon, *Adenovirus-Associated Defective Virus Particles.* Science, 1965. **149**(3685): p. 754-6.
154. Kotin, R.M., et al., *Site-specific integration by adeno-associated virus.* Proc Natl Acad Sci U S A, 1990. **87**(6): p. 2211-5.
155. Srivastava, A., E.W. Lusby, and K.I. Berns, *Nucleotide sequence and organization of the adeno-associated virus 2 genome.* J Virol, 1983. **45**(2): p. 555-64.

156. Sonntag, F., K. Schmidt, and J.A. Kleinschmidt, *A viral assembly factor promotes AAV2 capsid formation in the nucleolus.* Proc Natl Acad Sci U S A, 2010. **107**(22): p. 10220-5.
157. Wu, Z., A. Asokan, and R.J. Samulski, *Adeno-associated virus serotypes: vector toolkit for human gene therapy.* Mol Ther, 2006. **14**(3): p. 316-27.
158. Girod, A., et al., *The VP1 capsid protein of adeno-associated virus type 2 is carrying a phospholipase A2 domain required for virus infectivity.* J Gen Virol, 2002. **83**(Pt 5): p. 973-8.
159. Bohenzky, R.A., R.B. LeFebvre, and K.I. Berns, *Sequence and symmetry requirements within the internal palindromic sequences of the adeno-associated virus terminal repeat.* Virology, 1988. **166**(2): p. 316-27.
160. Ni, T.H., et al., *Cellular proteins required for adeno-associated virus DNA replication in the absence of adenovirus coinfection.* J Virol, 1998. **72**(4): p. 2777-87.
161. Summerford, C. and R.J. Samulski, *Membrane-associated heparan sulfate proteoglycan is a receptor for adeno-associated virus type 2 virions.* J Virol, 1998. **72**(2): p. 1438-45.
162. Summerford, C., J.S. Bartlett, and R.J. Samulski, *AlphaVbeta5 integrin: a co-receptor for adeno-associated virus type 2 infection.* Nat Med, 1999. **5**(1): p. 78-82.
163. Qing, K., et al., *Human fibroblast growth factor receptor 1 is a co-receptor for infection by adeno-associated virus 2.* Nat Med, 1999. **5**(1): p. 71-7.
164. Kashiwakura, Y., et al., *Hepatocyte growth factor receptor is a coreceptor for adeno-associated virus type 2 infection.* J Virol, 2005. **79**(1): p. 609-14.
165. Asokan, A., et al., *Adeno-associated virus type 2 contains an integrin alpha5beta1 binding domain essential for viral cell entry.* J Virol, 2006. **80**(18): p. 8961-9.
166. Akache, B., et al., *The 37/67-kilodalton laminin receptor is a receptor for adeno-associated virus serotypes 8, 2, 3, and 9.* J Virol, 2006. **80**(19): p. 9831-6.
167. Nicolson, S.C. and R.J. Samulski, *Recombinant adeno-associated virus utilizes host cell nuclear import machinery to enter the nucleus.* J Virol, 2014. **88**(8): p. 4132-44.
168. Stahnke, S., et al., *Intrinsic phospholipase A2 activity of adeno-associated virus is involved in endosomal escape of incoming particles.* Virology, 2011. **409**(1): p. 77-83.
169. Harbison, C.E., J.A. Chiorini, and C.R. Parrish, *The parvovirus capsid odyssey: from the cell surface to the nucleus.* Trends Microbiol, 2008. **16**(5): p. 208-14.
170. Cohen, S., et al., *Parvoviral nuclear import: bypassing the host nuclear-transport machinery.* J Gen Virol, 2006. **87**(Pt 11): p. 3209-13.
171. Seisenberger, G., et al., *Real-time single-molecule imaging of the infection pathway of an adeno-associated virus.* Science, 2001. **294**(5548): p. 1929-32.
172. Lux, K., et al., *Green fluorescent protein-tagged adeno-associated virus particles allow the study of cytosolic and nuclear trafficking.* J Virol, 2005. **79**(18): p. 11776-87.
173. Johnson, J.S. and R.J. Samulski, *Enhancement of adeno-associated virus infection by mobilizing capsids into and out of the nucleolus.* J Virol, 2009. **83**(6): p. 2632-44.
174. Sonntag, F., et al., *Adeno-associated virus type 2 capsids with externalized VP1/VP2 trafficking domains are generated prior to passage through the cytoplasm and are maintained until uncoating occurs in the nucleus.* J Virol, 2006. **80**(22): p. 11040-54.
175. Russell, D.W., I.E. Alexander, and A.D. Miller, *DNA synthesis and topoisomerase inhibitors increase transduction by adeno-associated virus vectors.* Proc Natl Acad Sci U S A, 1995. **92**(12): p. 5719-23.
176. Nakai, H., T.A. Storm, and M.A. Kay, *Increasing the size of rAAV-mediated expression cassettes in vivo by intermolecular joining of two complementary vectors.* Nat Biotechnol, 2000. **18**(5): p. 527-32.

177. Tratschin, J.D., et al., *A human parvovirus, adeno-associated virus, as a eucaryotic vector: transient expression and encapsidation of the procaryotic gene for chloramphenicol acetyltransferase.* Mol Cell Biol, 1984. **4**(10): p. 2072-81.
178. Nakai, H., et al., *Extrachromosomal recombinant adeno-associated virus vector genomes are primarily responsible for stable liver transduction in vivo.* J Virol, 2001. **75**(15): p. 6969-76.
179. Inagaki, K., et al., *Robust systemic transduction with AAV9 vectors in mice: efficient global cardiac gene transfer superior to that of AAV8.* Mol Ther, 2006. **14**(1): p. 45-53.
180. Zincarelli, C., et al., *Comparative cardiac gene delivery of adeno-associated virus serotypes 1-9 reveals that AAV6 mediates the most efficient transduction in mouse heart.* Clin Transl Sci, 2010. **3**(3): p. 81-9.
181. Mussolino, C., et al., *AAV-mediated photoreceptor transduction of the pig cone-enriched retina.* Gene Ther, 2011. **18**(7): p. 637-45.
182. Louboutin, J.P., L. Wang, and J.M. Wilson, *Gene transfer into skeletal muscle using novel AAV serotypes.* J Gene Med, 2005. **7**(4): p. 442-51.
183. Blankinship, M.J., et al., *Efficient transduction of skeletal muscle using vectors based on adeno-associated virus serotype 6.* Mol Ther, 2004. **10**(4): p. 671-8.
184. Sands, M.S., *AAV-mediated liver-directed gene therapy.* Methods Mol Biol, 2011. **807**: p. 141-57.
185. Wang, Z., et al., *Widespread and stable pancreatic gene transfer by adeno-associated virus vectors via different routes.* Diabetes, 2006. **55**(4): p. 875-84.
186. Mingozzi, F. and K.A. High, *Therapeutic in vivo gene transfer for genetic disease using AAV: progress and challenges.* Nat Rev Genet, 2011. **12**(5): p. 341-55.
187. Manno, C.S., et al., *AAV-mediated factor IX gene transfer to skeletal muscle in patients with severe hemophilia B.* Blood, 2003. **101**(8): p. 2963-72.
188. Mendell, J.R., et al., *Dystrophin immunity in Duchenne's muscular dystrophy.* N Engl J Med, 2010. **363**(15): p. 1429-37.
189. Gaudet, D., et al., *Efficacy and long-term safety of alipogene tiparvovec (AAV1-LPLS447X) gene therapy for lipoprotein lipase deficiency: an open-label trial.* Gene Ther, 2013. **20**(4): p. 361-9.
190. Jessup, M., et al., *Calcium Upregulation by Percutaneous Administration of Gene Therapy in Cardiac Disease (CUPID): a phase 2 trial of intracoronary gene therapy of sarcoplasmic reticulum Ca2+-ATPase in patients with advanced heart failure.* Circulation, 2011. **124**(3): p. 304-13.
191. Hulot, J.S., et al., *Effect of intracoronary administration of AAV1/SERCA2a on ventricular remodelling in patients with advanced systolic heart failure: results from the AGENT-HF randomized phase 2 trial.* Eur J Heart Fail, 2017.
192. Stiles, S. *HF Gene-Therapy Trial CUPID-2 Fails to Meet Primary End Point: Top-Line Results*. Medscape 2015 April 29; Available from: http://www.medscape.com/viewarticle/843901.
193. Dobin, A., et al., *STAR: ultrafast universal RNA-seq aligner.* Bioinformatics, 2013. **29**(1): p. 15-21.
194. Love, M.I., W. Huber, and S. Anders, *Moderated estimation of fold change and dispersion for RNA-seq data with DESeq2.* Genome Biol, 2014. **15**(12): p. 550.
195. McCarthy, D.J., Y. Chen, and G.K. Smyth, *Differential expression analysis of multifactor RNA-Seq experiments with respect to biological variation.* Nucleic Acids Res, 2012. **40**(10): p. 4288-97.
196. Benjamini, Y. and Y. Hochberg, *Controlling the False Discovery Rate: A Practical and Powerful Approach to Multiple Testing.* Journal of the Royal Statistical Society. Series B (Methodological), 1995. **57**(1): p. 289-300.

197. Hart, S.N., et al., *Calculating sample size estimates for RNA sequencing data.* J Comput Biol, 2013. **20**(12): p. 970-8.
198. deAlmeida, A.C., R.J. van Oort, and X.H. Wehrens, *Transverse aortic constriction in mice.* J Vis Exp, 2010(38).
199. Bass, G.T., et al., *Automated image analysis identifies signaling pathways regulating distinct signatures of cardiac myocyte hypertrophy.* J Mol Cell Cardiol, 2012. **52**(5): p. 923-30.
200. Krugmann, S., et al., *Cdc42 induces filopodia by promoting the formation of an IRSp53:Mena complex.* Curr Biol, 2001. **11**(21): p. 1645-55.
201. Takano, K., et al., *Nebulin and N-WASP cooperate to cause IGF-1-induced sarcomeric actin filament formation.* Science, 2010. **330**(6010): p. 1536-40.
202. Takahashi, K. and K. Suzuki, *WAVE2, N-WASP, and Mena facilitate cell invasion via phosphatidylinositol 3-kinase-dependent local accumulation of actin filaments.* J Cell Biochem, 2011. **112**(11): p. 3421-9.
203. Belmonte, S.L., et al., *Cardiac overexpression of Mammalian enabled (Mena) exacerbates heart failure in mice.* Am J Physiol Heart Circ Physiol, 2013. **305**(6): p. H875-84.
204. Raskin, A., et al., *A novel mechanism involving four-and-a-half LIM domain protein-1 and extracellular signal-regulated kinase-2 regulates titin phosphorylation and mechanics.* J Biol Chem, 2012. **287**(35): p. 29273-84.
205. van der Ven, P.F., et al., *Unusual splicing events result in distinct Xin isoforms that associate differentially with filamin c and Mena/VASP.* Exp Cell Res, 2006. **312**(11): p. 2154-67.
206. Lewis, B.P., C.B. Burge, and D.P. Bartel, *Conserved seed pairing, often flanked by adenosines, indicates that thousands of human genes are microRNA targets.* Cell, 2005. **120**(1): p. 15-20.
207. Friedman, R.C., et al., *Most mammalian mRNAs are conserved targets of microRNAs.* Genome Res, 2009. **19**(1): p. 92-105.
208. Korte, F.S., et al., *Power output is linearly related to MyHC content in rat skinned myocytes and isolated working hearts.* Am J Physiol Heart Circ Physiol, 2005. **289**(2): p. H801-12.
209. Barany, M., *ATPase activity of myosin correlated with speed of muscle shortening.* J Gen Physiol, 1967. **50**(6): p. Suppl:197-218.
210. Krenz, M. and J. Robbins, *Impact of beta-myosin heavy chain expression on cardiac function during stress.* J Am Coll Cardiol, 2004. **44**(12): p. 2390-7.
211. Battistoni, A., S. Rubattu, and M. Volpe, *Circulating biomarkers with preventive, diagnostic and prognostic implications in cardiovascular diseases.* Int J Cardiol, 2012. **157**(2): p. 160-8.
212. Woods, R.L., *Cardioprotective functions of atrial natriuretic peptide and B-type natriuretic peptide: a brief review.* Clin Exp Pharmacol Physiol, 2004. **31**(11): p. 791-4.
213. Disanza, A., et al., *CDC42 switches IRSp53 from inhibition of actin growth to elongation by clustering of VASP.* EMBO J, 2013. **32**(20): p. 2735-50.
214. Nagai, T., et al., *Cdc42 plays a critical role in assembly of sarcomere units in series of cardiac myocytes.* Biochem Biophys Res Commun, 2003. **305**(4): p. 806-10.
215. Maillet, M., et al., *Cdc42 is an antihypertrophic molecular switch in the mouse heart.* J Clin Invest, 2009. **119**(10): p. 3079-88.
216. Ram, R., et al., *Mena associates with Rac1 and modulates connexin 43 remodeling in cardiomyocytes.* Am J Physiol Heart Circ Physiol, 2014. **306**(1): p. H154-9.

217. Benz, P.M., et al., *Mena/VASP and alphaII-Spectrin complexes regulate cytoplasmic actin networks in cardiomyocytes and protect from conduction abnormalities and dilated cardiomyopathy*. Cell Commun Signal, 2013. **11**: p. 56.
218. Wang, Q., et al., *New insights into the roles of Xin repeat-containing proteins in cardiac development, function, and disease*. Int Rev Cell Mol Biol, 2014. **310**: p. 89-128.
219. Duka, A., et al., *A novel gene (Cmya3) induced in the heart by angiotensin II-dependent but not salt-dependent hypertension in mice*. Am J Hypertens, 2006. **19**(3): p. 275-81.
220. Wang, D.Z., et al., *Requirement of a novel gene, Xin, in cardiac morphogenesis*. Development, 1999. **126**(6): p. 1281-94.
221. Jung-Ching Lin, J., et al., *Structure, Expression, and Function of a Novel Intercalated Disc Protein, Xin*. J Med Sci, 2005. **25**(5): p. 215-222.
222. Chen, M.J., C.L. Shih, and K. Wang, *Nebulin as an actin zipper. A two-module nebulin fragment promotes actin nucleation and stabilizes actin filaments*. J Biol Chem, 1993. **268**(27): p. 20327-34.
223. Eulitz, S., et al., *Identification of Xin-repeat proteins as novel ligands of the SH3 domains of nebulin and nebulette and analysis of their interaction during myofibril formation and remodeling*. Mol Biol Cell, 2013. **24**(20): p. 3215-26.
224. Bear, J.E., et al., *Antagonism between Ena/VASP proteins and actin filament capping regulates fibroblast motility*. Cell, 2002. **109**(4): p. 509-21.
225. Kolodziejczyk, S.M., et al., *MEF2 is upregulated during cardiac hypertrophy and is required for normal post-natal growth of the myocardium*. Curr Biol, 1999. **9**(20): p. 1203-6.
226. McCalmon, S.A., et al., *Modulation of angiotensin II-mediated cardiac remodeling by the MEF2A target gene Xirp2*. Circ Res, 2010. **106**(5): p. 952-60.
227. Lee, S.M., et al., *Chromosomal mapping, tissue distribution and cDNA sequence of four-and-a-half LIM domain protein 1 (FHL1)*. Gene, 1998. **216**(1): p. 163-70.
228. Way, J.C. and M. Chalfie, *mec-3, a homeobox-containing gene that specifies differentiation of the touch receptor neurons in C. elegans*. Cell, 1988. **54**(1): p. 5-16.
229. Hwang, D.M., et al., *A genome-based resource for molecular cardiovascular medicine: toward a compendium of cardiovascular genes*. Circulation, 1997. **96**(12): p. 4146-203.
230. Lim, D.S., R. Roberts, and A.J. Marian, *Expression profiling of cardiac genes in human hypertrophic cardiomyopathy: insight into the pathogenesis of phenotypes*. J Am Coll Cardiol, 2001. **38**(4): p. 1175-80.
231. Golob, M., R.L. Moss, and N.C. Chesler, *Cardiac tissue structure, properties, and performance: a materials science perspective*. Ann Biomed Eng, 2014. **42**(10): p. 2003-13.